Title
Discovering regulators of ER autophagy using CRISPR screening

Author
Lingeman, Emily A

Publication Date
2019

Peer reviewed|Thesis/dissertation

Discovering regulators of ER autophagy using CRISPR screening

By

Emily A Lingeman

A dissertation submitted in partial satisfaction of the

requirements for the degree of

Doctor of Philosophy

in

Molecular and Cell Biology

in the

Graduate Division

of the

University of California, Berkeley

Committee in charge:

Professor Jacob Corn, Chair
Professor James Olzmann
Professor Jeffrey Cox
Professor David Drubin

Spring 2019

Abstract

Discovering regulators of ER autophagy using CRISPR screening

by

Emily A Lingeman

Doctor of Philosophy in Molecular and Cell Biology

University of California, Berkeley

Professor Jacob Corn, Chair

Autophagy, the process by which cellular contents are degraded via the lysosome, is critical for cellular homeostasis and regulation. ER autophagy (ER-phagy) is the process by which pieces of the endoplasmic reticulum (ER) are degraded by the lysosome. This process was only recently discovered to occur in mammalian cells, and it has been suggested that mis-regulation manifests in neuropathy conditions. In order to understand this process, we developed genome-editing tools to aid in uncovering regulators of ER autophagy (ER-phagy).

We developed and improved multiple genome-editing tools. In chapter 2, I describe how to use CasRNPs (ribonucleotide proteins) to genome edit cell lines. This protocol is ideal for individual desired edits or to genome-edit in arrayed screening fashion. This chapter details how to make single guide RNAs (sgRNAs), how to purify Cas proteins, and how to use those reagents to edit a cell line.

In chapter 3, we used various genome-editing tools (including the protocols described in chapter 2) to uncover regulators of ER autophagy. We conducted a genome-wide screen to identify factors that inhibit or enhance ER-phagy when knocked down. Our screen yielded 200 high-confidence hits. We mechanistically followed up on two pathways: mitochondrial oxidative phosphorylation (OXPHOS) and ER-localized DDRGK1 and UFMylation. This work advances our understanding of the regulatory mechanisms of ER-phagy, and my hope is that the CRISPR tools and ER-phagy tools we generated will allow the ER-phagy field to progress quickly.

Dedication

This dissertation is dedicated to my parents, Mary Kay Peterson and Steven Lingeman, for supporting my sense of curiosity and interest in biology.

The dissertation is also dedicated to my grandmothers, JoAnn Hanaway and Ann Lingeman, who both modeled what it means to be a strong and intelligent woman.

Acknowledgements

I would like to acknowledge Jacob Corn for his support and mentorship during my PhD. In addition, thank you to Amos Liang for being the best hands-on mentor and support a grad student could ask for. I would also like to acknowledge my Corn Lab co-workers who provided me guidance, mentorship, and friendship during my PhD: Alan Wang, Mandy Boontanrart, Jenny Shin, Ron Baik, Shaheen Kabir, Stacia Wyman, Market Dewitt, Benjamin Gowen, Elena Zelin, Chris Richardson, and Beeke Wienert. Thank you to Tracie Luong for allowing me to practice my mentorship skills.

I would also like to acknowledge James Olzmann and the Olzmann Lab members for taking me in mid-fifth year and being so welcoming.

I would like to thank the friends, both near and far, who supported me during this endeavor. My classmates were truly outstanding and supportive. Shout out to my roommates who supported me during my PhD: Ashley Thelen, Natalie Wolf, and Sally Winkler.

I want to acknowledge Imm Thai and delicious Pad Se Ew. I know it's not a person, but it provided me so many delicious lunches.

I want to acknowledge my partner, Jordan Rein, for supporting me from Wisconsin.

The biggest acknowledgement of all goes to my parents – Mary Kay Peterson and Steven Lingeman – who convinced me to complete my PhD despite strong considerations to leave.

Table of Contents

List of Figures

List of Tables

1 Introduction

1.1 Autophagy

Macroautophagy (hereafter referred to as autophagy) is the process by which cellular proteins and organelles are degraded via the lysosome. Autophagy allows unneeded or damaged proteins, lipids, carbohydrates, and even entire organelles to be degraded into component parts and be recycled. This process can be either non-selective or selective. In autophagy, a double-membrane structure (known as the phagophore) engulfs the autophagic cargo, forming the autophagosome. The autophagosome fuses with the lysosome, leading to the formation of autolysosomes, where the cargo is degraded (Figure 1A).

In the early 1990s, Yoshinori Ohsumi's laboratory conducted a screen in yeast to identify proteins required to deliver cargo to the vacuole, which is similar to the lysosome in human cells. The screen identified 15 autophagy-related proteins (ATGs) and the field of autophagy subsequently exploded (Tsukada and Ohsumi, 1993).

Autophagy begins at phagophore assembly sites (PAS) where the double membrane structure expands and begins to form. Numerous organelles have been identified as sites of PAS nucleation, including the endoplasmic reticulum (ER) (Axe et al., 2008; Graef et al., 2013), mitochondria (Hailey et al., 2010), ER-mitochondria contact sites (Hamasaki et al., 2013), ER-plasma membrane contact sites (Hamasaki et al., 2013; Nascimbeni et al., 2017), recycling endosomes (Puri et al., 2014), and the Golgi (van der Vaart and Reggiori, 2010). It is unclear whether all of these locations are true PASs, or if so many organelles have been identified due to experimental limitations used to identify the originating organelle. Furthermore, it is quite possible that the PAS location may be cell type and context dependent.

ULK1 (unc-51-like kinase 1), a serine/threonine kinase, is central to initiating autophagy. ULK1 functions in complex with FIP200, ATG13, and ATG101 (Figure 1B) (Ganley et al., 2009; Hara et al., 2008; Hosokawa et al., 2009b, 2009a; Jung et al., 2009; Mercer et al., 2009). Upon its activation, the ULK1 complex triggers nucleation of the phagophore by phosphorylating and activating components of the PI3KC3 Complex I (Russell et al., 2013).

The PI3KC3 complex I is comprised of VSP34, Beclin-1, ATG14, and AMBRA1 (Itakura et al., 2008; Matsunaga et al., 2009; Rostislavleva et al., 2015; Stack et al., 1993; Zeng et al., 2006; Zhong et al., 2009). PI3KC3 complex I is activated by ULK1 through phosphorylation of Beclin-1 and ATG14 (Russell et al., 2013). VPS34 is the catalytic component of this complex and it converts the lipid PI (phosphatidylinositol) into PI3P (phosphatidylinositol 3-phosphate) (Schu et al., 1993). PI3P recruits PI3P effector proteins, including WIPI2 (Polson et al., 2010). The function of WIPI2 is described in later paragraphs, and it is used to bring specific protein complexes to the autophagosome membrane.

Phagophore membrane expansion relies upon ATG9 and two ubiquitin-like (Ubl) conjugation systems. ATG9 is the only transmembrane core ATG that has been identified. ATG9 delivers lipid vesicles to the growing membrane to allow further expansion (Orsi et al., 2012; Yamamoto et al., 2012), and ATG9 is regulated by ULK1 (Papinski et al., 2014; Young et al., 2006).

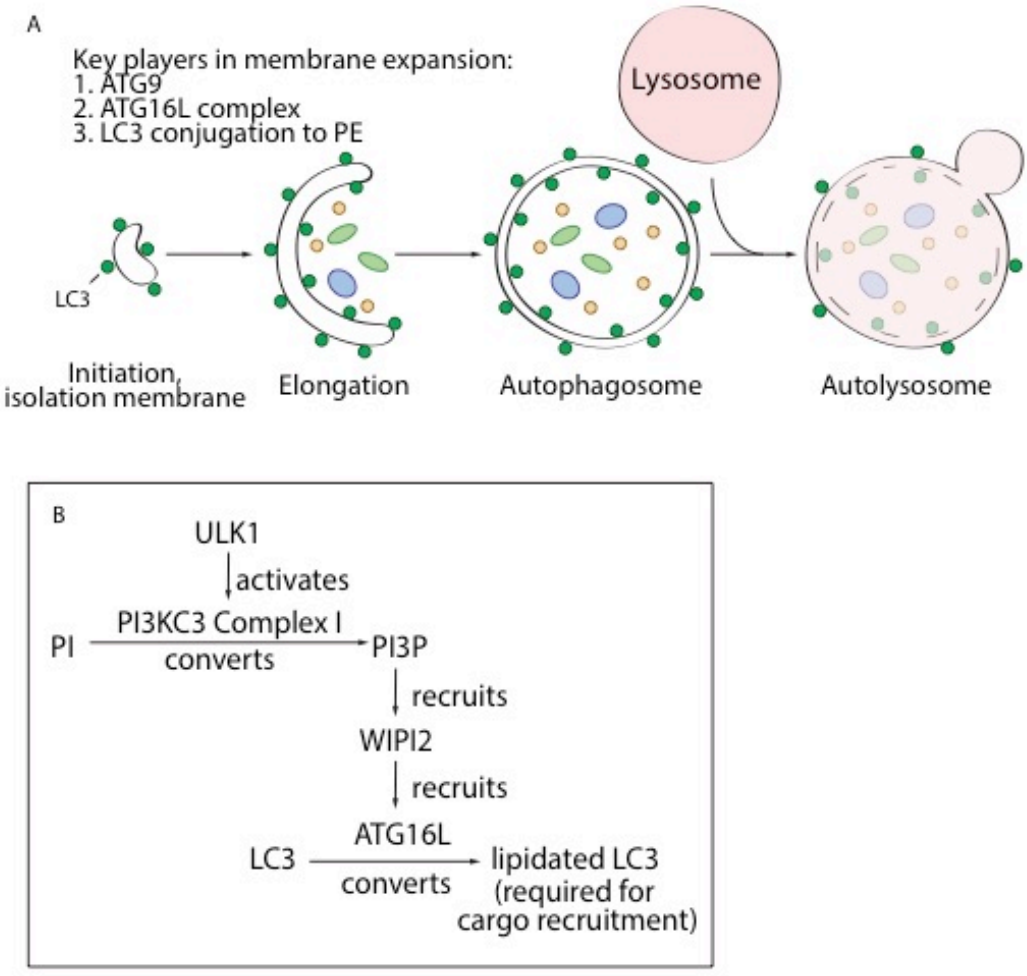

Figure 1: Overview of autophagy
(A) The high-level overview of autophagy initiation, membrane expansion, and fusion with the lysosome is depicted. In addition, three key players in membrane expansion are called out: ATG9, ATG16L complex, and LC3. (B) Simplified depiction of proteins involved in autophagy initiation and membrane expansion.

Ubiquitin-like conjugation systems (Ubls) are protein conjugation systems analogous to the ubiquitin pathway. Ubiquitin, a small protein modifier, is added to a target protein with the aid of three enzymes. The enzymes are as follows: ubiquitin-activating enzyme, ubiquitin-conjugating enzyme, and ubiquitin ligase. These proteins are known as E1s, E2s, and E3s respectively. Interestingly, biology as adopted a similar enzyme cascade system to other situations with other proteins that are structurally homologous to ubiquitin. These conjugation systems are known as ubiquitin-like systems, or Ubls (Geng and Klionsky, 2008).

In the first Ubl conjugation system, Atg12 is conjugated to Atg5 by the E1/E2-like enzymes Atg7 and Atg10 (Mizushima et al., 1998; Shintani et al., 1999). The Atg12-Atg5 complex interacts with Atg16L, forming a structure known as the Atg16L complex (Kuma et al., 2002). Recent work revealed that ATG16L directly binds WIPI2, bringing this Ubl conjugation system to the growing membrane (Dooley et al., 2014).

The second ubiquitin-like conjugation system is the conjugation of ubiquitin-like ATG8 family members. ATG8 family members include the light chain 3 (LC3) subfamily. LC3 is processed at the C terminus by ATG4, allowing LC3 conjugation to phosphatidylethanolamine (PE) (Ichimura et al., 2000; Kirisako et al., 2000). LC3 is conjugated to PE by Atg7 (an E1-like protein), Atg3 (an E2-like protein), and Atg5-Atg12-Atg16L complex (E3-like) (Ichimura et al., 2000). The conjugated LC3 promotes phagophore expansion and aids in recruiting the appropriate cargo into the autophagosome (which will be discussed in a later discussion).

Eventually, the phagopore closes, creating the autophagosome. In the final step, the autophagosome fuses with the lysosome, creating the autolysosome. The internal cargo is degraded.

1.1.1 AMPK and mTORC1 regulation of ULK1 and autophagy

There are two important kinase proteins that sense nutrient and energy levels in cells and control ULK1 activity: AMPK and mTORC1.

The mechanistic target of rapamycin (mTOR), a serine/threonine kinase, is part of two protein complexes: mTORC1 and mTORC2. mTORC1 regulates cell growth, including autophagy, while mTORC2 regulates survival and proliferation (Saxton and Sabatini, 2017).

mTORC1 is the "nutrient sensor" of the cell and responds to cellular levels of oxygen, growth factors, and amino acids (Saxton and Sabatini, 2017). In nutrient-rich conditions, the ULK1-Atg13-FIP200 complex is bound to mTORC1, and ULK1 and ATG13 are phosphorylated by mTORC1, preventing ULK1 activity (Hosokawa et al., 2009a). In nutrient-depleted conditions, these proteins are no longer phosphorylated and bound to mTORC1. ULK1 becomes active through dissociation from mTORC1, autophosphorylation, and the ULK1 complex is active after ULK1 phosphorylates ATG13 and FIP200 (Hosokawa et al., 2009a; Jung et al., 2009).

5' AMP-activated protein kinase (AMPK) is the "energy sensor" of the cell and senses the levels of AMP within a cell, which is an indirect readout of ATP levels. AMPK is activated when threonine 172 (T172) is phosphorylated (Hawley et al., 1996; Sanders et al., 2007; Suter et al., 2006). This occurs under conditions of higher ratios of AMP/ATP and ADP/ATP (Davies et al., 1995; Rajamohan et al., 2016; Ross et al., 2016; Sanders et al., 2007; Suter et al., 2006). Broadly, activation of AMPK leads to an increase in ATP production by increasing cellular catabolism pathways and turning off biosynthesis pathways.

AMPK directly regulates both mTORC1 and ULK1. AMPK phosphorylates and activates ULK1, VSP34, and Beclin-1, thereby bypassing mTORC1 inhibition of ULK1 (Kim et al., 2011; Lin and Hurley, 2016). Thus, the activity ULK1 is balanced by competing phosphorylation sites. In addition, AMPK inhibits mTORC1 directly by phosphorylating Raptor, one protein in mTORC1 (Gwinn et al., 2008), as well as indirectly by activating TSC2 via phosphorylation, which eventually leads to mTORC1 inactivation (Huang and Manning, 2009; Inoki et al., 2003).

1.2 Selective autophagy

Autophagy was initially thought by researchers to engulf cytosolic contents indiscriminately. However, in the decades since autophagy was discovered, researchers have discovered many processes where specific cargo is targeted, including proteins or organelles. Broadly, selective autophagy can be broken down into two categories: ubiquitin-dependent and

ubiquitin-independent selective autophagy. Perhaps the most famous example of ubiquitin-dependent selective autophagy is Parkin-mediated mitophagy. On the other hand, published examples of ER-phagy are ubiquitin-independent where the autophagy adaptor is on the cargo itself. There is more detail about both these types of selective autophagy in the following sections.

In ubiquitin-dependent autophagy, ubiquitin, a small protein modifier, is added to the cargo of interest by an E3 ubiquitin ligase. Then, receptors connect the ubiquitinated cargo to LC3 on the growing phagophore. These receptors bind LC3 with LIR (LC3-interacting regions) domains and bind ubiquitin with a UBD (ubiquitin binding domain). There are five commonly studied autophagy receptors that contain LIRs and ubiquitin-binding domains: p62, NBR1, Optineurin (OPTN), NDP52, and TAX1BP1 (Khaminets et al., 2016).

In ubiquitin-independent selective autophagy, a resident protein of the target cargo contains an LIR. When this LIR is exposed, the cargo is directly connected to the autophagy machinery and is degraded via autophagy (Khaminets et al., 2016).

Numerous organelles undergo organelle autophagy (organellophagy), including the mitochondria (mitophagy), endoplasmic reticulum (ER-phagy), and lysosome (lysophagy) (Ding and Yin, 2012; Khaminets et al., 2015; Otomo and Yoshimori, 2017). Below, I will expand on the most studied organellophagy, mitophagy, and then delve deep into the main topic of this dissertation: ER autophagy (ER-phagy).

1.2.1 Mitophagy

Mitophagy is the most-studied form of organelle autophagy. This is due to the link between mutations in key mitophagy genes (PINK1 and Parkin) and familial Parkinsonism (Kitada et al., 1998; Valente et al., 2004). Mitophagy in mammalian cells is recognized as either ubiquitin mediated or ubiquitin independent.

In ubiquitin-mediated mitophagy, depolarized or damage mitochondria accumulate PINK1 (PTEN-induced kinase 1) on the surface (Narendra et al., 2010). In healthy mitochondria, PINK1 is imported to the inner mitochondrial membrane (IMM) due to the mitochondrial transmembrane membrane potential. PINK1 is cleaved by proteases at the IMM making PINK1 a substrate for proteasome degradation (Deas et al., 2011; Greene et al., 2012; Jin et al., 2010; Meissner et al., 2011; Yamano and Youle, 2013). Therefore, this process continuously removes PINK1 when the mitochondria are healthy. When the mitochondria are damaged, PINK1 accumulates on the mitochondria surface where it autophosphorylates. The accumulated PINK1 recruits the E3 ubiquitin ligase Parkin to ubiquitinate a variety of substrates on the mitochondria and signal the mitochondria for autophagy (Jin and Youle, 2013; Matsuda et al., 2010). Interestingly, it was found that PINK1 phosphorylates ubiquitin, which further activates Parkin, creating a positive feedback loop that quickly amplifies signal on damaged mitochondria (Koyano et al., 2014).

Parkin activity results in a coating of ubiquitin around the targeted mitochondria. Two proteins ubiquitinated by Parkin are mitofusion 1 and mitofusion 2 (Gegg et al., 2010). The mitofusion proteins enable mitochondrial fusion, and the ubiquitination and subsequent degradation of mitofusions prevents the re-fusion of damage mitochondria (Tanaka et al., 2010). In addition, a paper published from the Youle Group showed that Optineurin (OPTN) and NDP52 are the receptors that connect ubiquitinated mitochondria to the autophagy machinery (Lazarou et al., 2015).

A mitochondrial-localized deubiquitinase, USP30, counteracts Parkin and maintains basal homeostasis at the mitochondria (Bingol et al., 2014; Cunningham et al., 2015; Liang et al., 2015). The balance towards heavy mitochondria ubiquitination (and then mitophagy) is shifted after depolarization of the mitochondria, accumulation of PINK1/Parkin at the mitochondrial surface, and Parkin-mediated degradation of USP30.

In ubiquitin-independent mitophagy, an autophagy receptor localized to the mitochondria directly connects the organelle with the autophagy machinery. Numerous examples have been identified, including NIX, BNIP3, FUNDC1, and Atg32 (Hanna et al., 2012; Kanki et al., 2009; Liu et al., 2012; Novak et al., 2010; Okamoto et al., 2009; Quinsay et al., 2010).

It is unclear why both ubiquitin-dependent and ubiquitin-independent mitophagy processes exist. These different pathways may play predominant roles in different cell types or in response to different cellular stressors

Initially, our lab hypothesized that ER-phagy would be analogous to ubiquitin-mediated mitophagy. However, our work, combined with other recent publications, reveals that ER-phagy is an ubiquitin-independent process.

1.2.2 ER-phagy

In the context of ER-phagy, we are considering two main morphologies of the ER: sheets and tubules. Sheets are flat structures and can be divided into smooth ER and rough ER. The rough ER is the site of protein synthesis via ribosomes. ER tubules are very dynamic in nature and function in lipid synthesis, calcium signaling, and contacts with other organelles (Schwarz and Blower, 2016). The cortical ER is a mix of ER sheets and tubules, and is considered intermediate ER structure (Schwarz and Blower, 2016).

Autophagy of the ER (or ER-phagy) is only beginning to be understood. The earliest evidence of ER-phagy dates back to the 1950s when ER pieces were found in a lysosome-rich fraction from rat liver using electron microscopy (Novikoff, 1956). However, at that point, the term “autophagy” did not even exist.

In 2005, ER-phagy was ‘rediscovered’ when pieces of the ER were found in a lysosome-rich fraction in *S. cerevisiae* (Hamasaki et al., 2005). In that paper, the Ohsumi group showed ER-phagy occurs in yeast with rapamycin treatment (inhibitor of mTOR) or with carbon or nitrogen starvation. Furthermore, the effect of starvation appeared to be specific to the ER as fragments of the Golgi apparatus did not appear in the vacuole (Hamasaki et al., 2005).

In the past couple of years, numerous research groups have started studying ER-phagy in mammalian cells. A majority of the mammalian ER-phagy factors that have been identified are autophagy adaptors (which means they directly connect the ER to the autophagy machinery). Thus far, all identified ER-phagy is ubiquitin-independent selective autophagy.

FAM134B was the first mammalian ER-phagy factor identified (Khaminets et al., 2015). The Dikic lab identified FAM134B as an ER autophagy adaptor that targets the ER to the autophagosome. Stable knockout of FAM134B leads to expansion of the ER. Furthermore, *Fam134b*$^{-/-}$ mice showed a sensory neuropathy phenotype, and this was the first instance where the biological relevance of ER-phagy was demonstrated experimentally (Khaminets et al., 2015). Simultaneously, the Nakatogawa lab identified Atg39 and Atg40 in *S. cerevisiae* and showed that the proteins serve as adaptor proteins to regulate autophagy of the ER and nuclear envelope. Atg40 localizes to the cortical ER and is predicted to be the functional counterpart to FAM134B (Mochida et al., 2015).

After the discovery of FAM134B's role in ER-phagy, the Dikic lab went on to explore another ER-phagy adaptor: RTN3L (Grumati et al., 2017). RTN3L, which is localized to ER tubules, is a reticulon domain-containing protein. The Dikic lab showed that RTN3L over-expression induces ER fragmentation during starvation. Furthermore, RTN3L is suggested to be an autophagy adaptor via direct interaction with LC3 (Grumati et al., 2017).

Sec62 is a unique autophagy adaptor that was identified to function after ER stress during the ER-recovery process where excess ER is removed (Fumagalli et al., 2016). The authors showed that after induction of the unfolded protein response by treatment with cyclopiazonic acid (CPA), there is an ER recovery phase mediated by Sec62 (Fumagalli et al., 2016). However, no other reports of ER-phagy have shown a similar process where ER-phagy occurs after acute ER stress. It remains to be seen whether this induction of ER-phagy is truly robust.

CCPG1 is an ER-localized protein that binds directly to the autophagy machinery (Smith et al., 2018). In this regard, it is similar to FAM134B, RTN3, and Sec62 where is can directly link the ER to LC3. Upon persistent ER stress via the unfolded protein response, CCPG1 expression is increased (Smith et al., 2018). That increased expression leads to ER-phagy suggests that ER-phagy may in fact be a response to ER stress when other ER quality control mechanisms are not sufficient. Those who study ER-phagy have been interested in the connection between other ER quality control mechanisms and ER-phagy, so this provides an intriguing result as other cell biologists study this connection further.

In addition, our lab identified Atlastin proteins as regulators of ER-phagy (Liang et al., 2018). Atlastins are resident ER GTPases and use catalysis of the nucleotide GTP to remodel the ER membrane morphology. Our lab showed that knockout of Atlastins inhibits ER-phagy during starvation conditions. We hypothesize that Atlastins are required to separate pieces of the ER membrane that are targeted for ER-phagy by FAM134B. This paper begins to shed light on upstream processes required for ER-phagy to occur.

1.3 CRISPR-Cas9

The previous sections focused on a particular cellular process. Behind all cell biology discoveries are tools and methodologies that make these discoveries possible – such as PCR, confocal microscopy, and Western blots. In 2012 and 2013, a major technology –CRISPR/Cas9- was introduced to cell biologists and has quickly become an important tool in a cell biologist's tool kit. Our lab is interested in harnessing this tool, developing the technology, and applying it to cell biology questions.

Clustered regularly interspaced short palindromic repeats (CRISPR)/CRISPR-associated (Cas) is a bacterial immune system allowing bacteria to defend against foreign viruses or plasmids (Bhaya et al., 2011; Terns and Terns, 2011; Wiedenheft et al., 2012). Once the mechanism for this process was discovered, it was quickly adapted by researchers to make edits in human cell lines and model organisms (Cong et al., 2013; Jinek et al., 2012, 2013; Mali et al., 2013). *Streptococcus pyogenes* Cas9, one protein in the cas family, has two domains (HNH and RuvC-like domains) that allow the protein to make a double-stranded break in DNA (Jinek et al., 2012; Sapranauskas et al., 2011). Cas9 is directed by a tracRNA and crRNA that contains a 20-nucleotide protospacer sequence that complexes to the targeted region of DNA (Jinek et al., 2012). The two separate RNAs were simplified into a single guide RNA (sgRNA) by researchers for ease of use (Jinek et al., 2012).

The double stranded break in the DNA is repaired by non-homologous end joining (NHEJ) or homology-directed repair (HDR). NHEJ leads to insertions or deletions (indels) in the sequencing, leading to a frame shift mutation and a non-functional protein. This ultimately creates cell lines that have the targeted gene knocked out. HDR allows researchers to change the DNA sequence in a directed fashion with a donor DNA containing the desired sequence.

1.3.1 Pooled library CRISPR screens

CRISPR-Cas9 was quickly adapted to be used for high-throughput pooled screens (Gilbert et al., 2014; Koike-Yusa et al., 2014; Shalem et al., 2014; Wang et al., 2014; Zhou et al., 2014). The different screening technologies can be broadly categorized into two categories: CRISPR cutting screens and CRISPR activation/inhibition screens. In CRISPR-Cas9 cutting screens, genes are knocked out using an active cas9 protein. In CRISPR activation/inhibition screens, an inactive cas9 protein (known as dead cas9, or dcas9) is attached to a transcription inhibitor (such as KRAB) or a transcription activator (such as VP64) (Gilbert et al., 2013).

1.4 CRISPR tools and their implications for studying autophagy

CRISPR-Cas9 is a powerful tool that will change numerous fields of biology. Relevant to this dissertation, CRISPR-Cas9 will impact the autophagy field dramatically. In the short term, CRISRP-Cas9 will accelerate basic scientific discovery. In the long term, the tool may be used in clinical applications to treat patients when autophagy processes go awry.

The near-term advantage of genome editing tools to the autophagy field is the ability to screen for regulators of autophagy pathways. This dissertation aims to make significant progress in the area as the first genome-wide screen for ER-phagy regulators. It will be very informative if similar ER-phagy screens are conducted in other cell lines, as different regulators may be more or less important in different contexts. Furthermore, as screening technology improves, more players involved in ER-phagy will show up as screen hits. More broadly, similar screens can be conducted for all types of autophagy.

In the long-term, genome editing may be used as a therapy for patients with mutations in autophagy pathways. However, this type of treatment will rely on targeting the affected area and reaching enough cells in the patient. Significant advances in delivery of genome editing reagents to the affected area will have to be made.

1.5 Long future ahead for ER-phagy

There are many more scientific discoveries to be had in the ER-phagy field. Very little is currently understood. Beyond knowing the specific regulators involved, which CRISPR-Cas9 technologies will play a role in, the larger context of ER-phagy remains a mystery.

Specifically, these are the unanswered questions: Why, and under what physiological conditions, does ER-phagy occur in mammalian cells? What diseases are caused by the mis-regulation of ER-phagy?

The disease implications of ER-phagy mis-regulation will likely be understood after more of the molecular factors are discovered. For example, once more ER-phagy regulators are discovered, GWAS analysis can be used to identify patients with SNPs in ER-phagy regulators and link those SNPs to specific diseases. Inhibition of ER-phagy has been linked to sensory

neuropathy phenotypes in mice (Khaminets et al., 2015), but that evidence supporting that connection is sparse. In addition, there may be diseases that have not yet been linked to ER-phagy, but will be in the future.

The field of ER-phagy has a long way to go, but my hope is that this dissertation and associated publications provides one step forward.

2 Production of Purified CasRNPs for Efficacious Genome Editing

A version of the material in this chapter was previously published as

Lingeman, E., Jeans, C., and Corn, J.E. (2017). Production of purified CasRNPs for efficacious genome editing. Current Protocols in Molecular Biology. *120* 31.10.1-31.10.19.

The work has been adapted here with permission from all co-authors.

2.1 Connection to overall dissertation

Given the importance of genome-editing to the autophagy field (described in the introduction), we set out to write a clear step-by-step protocol that would be accessible to any cell or molecular biology lab. This is incredibly useful for the field as other labs can apply leading knowledge of their field and integrate genome-editing technology into their standard lab protocols.

Furthermore, we used this protocol to learn more about ER-phagy itself. Chapter 3 highlights my work on ER-phagy, and the protocol detailed in this chapter was used to make specific cell lines to answer scientific questions that we couldn't answer any other way. This helped us make more definitive conclusions, and this protocol will help other cell biology labs in the same way.

2.2 Introduction

Prokaryotes defend against viral invasion using the combined action of Clustered Regularly Interspaced Short Palindromic Repeats (CRISPR) and the CRISPR Associated System (Cas) proteins. CRISPR-Cas systems induce a targeted double-stranded DNA break and have been co-opted as popular systems for genome editing. A mature complex includes Cas9 (or other Cas effector) protein with a tracrRNA and crRNA, which are often coupled with a linker loop to make a single guide RNA for ease of use in the laboratory (Jinek et al., 2012). After Cas9 introduces a DNA double-strand break, host cell DNA repair induces the formation of insertions and deletions (indels) or templated homology dependent repair (HDR). Indels can be used to disrupt a functional sequence (e.g., knockout a gene), while HDR can be used to insert new information or program a change (e.g., alter a SNP).

CRISPR-Cas nucleases have become popular for genome editing due to their ease in reprogramming and efficacy in a wide variety of cell types and organisms, from plants to animals. Initial protocols for using this system involved transfection of plasmids expressing the various components needed for editing. But these efforts often required optimization of parameters for expression of the Cas effector and gRNA in each cellular or organismal context, including promoter identity and base composition.

Recent work has shown that genome-editing using purified recombinant Cas effector proteins and synthetic or in vitro transcribed gRNAs can be highly efficacious. These Cas ribonucleoprotein complexes (CasRNPs) avoid the need to optimize host expression and offer several benefits. In comparison to plasmid transfections, CasRNPs typically introduce edits with higher efficacy than plasmid-based editing while simultaneously reducing off-target effects.

Furthermore, CasRNP delivery is particularly useful in hard to-transfect cell lines, such as fibroblasts and pluripotent stem cells (Kim et al., 2014). Human cells, a variety of agricultural crops, and even model- and non-model insects and animals have been edited using CasRNPs (Aida et al., 2015; Burger et al., 2016; Chen et al., 2016; Cho et al., 2013; Kouranova et al., 2016; Richardson et al., 2016a; Sung et al., 2014).

Here we outline the steps to make a Cas9 RNP and perform genome editing in human cell culture (Figure 2). This protocol is highly scalable and can be used by a single graduate student to make several hundred CasRNPs in less than a week. This scale allows one to rapidly test the efficacy of multiple guides, reducing reliance on the accuracy of computational predictions for guide efficacy and stringency. We first outline the production of a purified Cas9 protein, and in vitro transcription of the gRNA. Production of the gRNA comprises assembling a DNA template from short oligonucleotides by PCR, in vitro T7 transcription to produce the RNA, and purification of the gRNA using homemade SPRI (solid phase reverse immobilization) beads, which allow efficient selection of gRNAs away from free nucleotides or IVT transcription products of incorrect sizes. Bead purification enables the gRNA clean-up to be scaled easily to a 96-well plate format. We also include an alternate protocol to purify individual gRNAs using an RNA column. A final protocol outlines formation of the CasRNP complex and its introduction to mammalian cells by electroporation. Analysis of the efficacy of genome editing (e.g., by T7E1 assay) is not included here, but detailed protocols can be found online at https://www.protocols.io/groups/igi.

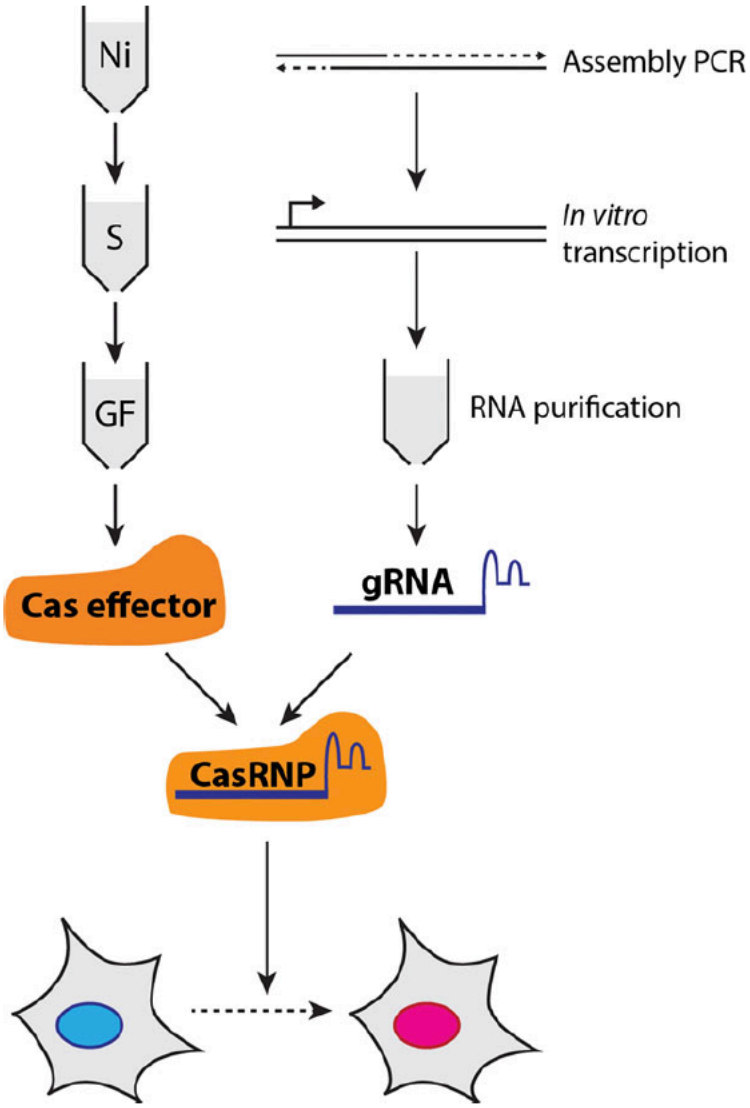

Figure 2: Overview of the preparation of CasRNPs
Hexahistidine-tagged Cas9 or other Cas effector is purified through a series of chromatographic steps. Guide RNA templates are made with assembly PCR and then in vitro T7 transcribed. Combining the Cas effector and guide RNA yields a CasRNP, which can be introduced into cells or organisms with methods such as electroporation or microinjection.

2.3 Strategic Planning

The protocol described here is scalable to hundreds of different CasRNPs. Guide assembly and in vitro transcription can be performed in 96-well plates using a thermocycler. The gRNA purification protocol using magnetic SPRI beads can also be done in 96-well format with an appropriate magnet (Thermo Fisher, AM10027). CasRNPs are introduced by electroporation, which is typically the rate-limiting step. Electroporation of individual CasRNPs is efficacious, but very slow when working with many CasRNPs. For high throughput, we use a Lonza 4D

nucleofector, which offers both 96-well and 384-well plate shuttles that can be connected to the main unit.

2.4 Cas9 Protein Bacterial Expression

The first component of a CasRNP is the Cas effector protein. Cas effectors are bacterial proteins, and despite their large size can be recombinantly expressed with high yield in a typical DE3 *E. coli* system. Here *S. pyogenes* Cas9 is expressed as a hexahistidinemaltose binding protein fusion with a TEV-protease cleavable linker, enabling simple purification in 2.5 Cas9 Purification.

2.4.1 Materials

- Rosetta2(DE3)pLysS competent cells (Novagen, cat. no. 71403)
- Ice
- Cas9 expression plasmid: pMJ915, Addgene, plasmid #69090
- 2×YT liquid medium (without antibiotics)
- LB-agar plate containing 100 μg/ml carbenicillin and 33 μg/ml chloramphenicol
- Sterile glass beads (3 mm)
- 10% bleach
- 2×YT liquid media containing 100 μg/ml carbenicillin and 33 μg/ml chloramphenicol
- Isopropyl β-D-1-thiogalactopyranoside (IPTG; 1 M in water)
- Pepstatin A (1 mg/ml in methanol)
- Leupeptin (1 mg/ml in water)
- Phenylmethylsulfonyl fluoride (PMSF, 100 mM in 95% ethanol)
- Nickel Buffer A (ice-cold, see recipe below)
- Heated water bath (42°C)
- Incubator (37°C) with rotating platform
- Sterile pipette tips or toothpicks
- 250-ml and 2.5-liters baffled culture flasks (e.g., Thompson Instrument Company, cat. nos. 931144 and 931136-B)
- Refrigerated shaking incubator (e.g., Certomat BS-1)
- 25-ml serological pipette
- Cell density meter (e.g., GE Lifesciences Ultrospec 10) or UV-vis spectrometer
- Centrifuge for 1-liter bottles (Beckman Coulter Avanti J26-XP) and 1-liter bottles (Beckman Coulter, cat. no. 363676)

2.4.2 Transformation of cells

1. Thaw a 100-μl aliquot of Rosetta2(DE3)pLysS competent cells on ice.
2. Add 1 μl Cas9 expression plasmid (10 to 100 ng/μl). Flick the tube a few times to mix. The plasmid used here is an excellent starting point for reliable purifications and good yields. Many other vectors are available, and this protocol may be used as a starting point for protein expression from these (changing the selection antibiotic if appropriate).
3. Incubate the tube for 30 min on ice.

4. Heat-shock the cells for 30 sec at 42°C in a water bath.
5. Place the cells back on ice for 2 min.
6. Add 900 µl of 2×YT (without antibiotics) and incubate for 1 hr at 37°C on a rotating platform. Meanwhile, warm an LB-agar plate containing carbenicillin and chloramphenicol in the same incubator.
7. Pipette 40 to 200 µl cells onto the plate, and pour about a dozen sterile glass beads onto the plate. The volume of cells to plate depends on the concentration of your plasmid DNA stock and the competency of your cells. This parameter is determined empirically.
8. Shake the plate from side to side to spread out the cells, and then dispose of the glass beads (soak overnight in 10% bleach before disposal).
9. Incubate the plate overnight at 37°C.

2.4.3 Cell growth and expression

1. Pick a single colony from the LB-agar plate with a sterile pipette tip or toothpick and drop into a 250-ml flask containing 50 ml of 2×YT + 100 µg/ml carbenicillin and 33 µg/ml chloramphenicol.
2. Incubate overnight at 37°C in a shaking incubator (200 to 250 rpm).
3. Use this starter culture to inoculate two 2.5-liters flasks each containing 1 liter 2×YT + 100 µg/ml carbenicillin and 33 µg/ml chloramphenicol. Use an inoculum of 5 ml per flask.
4. Incubate the flasks at 37°C in a shaking incubator (200 to 250 rpm) until they reach an optical density at 600 nm (OD600) of 0.6 to 0.7. This usually takes 2 to 3 hr.
5. Set the incubator temperature to 16°C and continue shaking the flasks as the incubator cools. After 25 min, add 250 µl IPTG (1 M) to each flask for a final concentration of 250 µM. The OD600 at this point is usually 0.9 to 1.0.
6. Incubate the flasks overnight (18 to 20 hr) at 16°C with shaking (200-250 rpm). At the end of this period, the OD600 is typically 3.0 to 3.5.

2.4.4 Cell harvesting

1. Harvest the cells by centrifugation in 1-liter bottles for 15 min at 4000 × g, 4°C.
2. Pour off and discard the medium and keep the cell pellet.
3. To each cell pellet from 1 liter media, add 15 ml cold Nickel Buffer A supplemented with 1 µg/ml pepstatin A, 1 µg/ml leupeptin and 0.5 mM PMSF. Resuspend the cells with a 25-ml serological pipette: initially by hand, scraping the pellet until it is dislodged from the bottle, and then by pipetting the cell suspension up and down until it is homogeneous.
4. Freeze the resuspended cells by placing in a −80 °C freezer, or proceed with 2.5 Cas9 Purification. Resuspended cells can be kept frozen at −80 °C for several months without loss of Cas9 activity. Freezing the cells is recommended, as the freeze/thaw process aids cell lysis.

2.5 Cas9 Purification

Purification of Cas effectors is relatively straightforward and comprises just a few column steps. Protein is first passed over a nickel column and the His6-maltose binding protein tag

removed by TEV-protease cleavage, followed intermediate cation exchange column and a final gel filtration step. Gel filtration is strongly encouraged, but not required. We recommend concentrating and freezing the Cas9 protein at a concentration of 40 μM because this allows for a convenient volume to be used in the formation of the CasRNP prior to nucleofection.

2.5.1 Materials

- Cells (from 2.4 Cas9 Protein Bacterial Expression)
- Nickel buffers A and B, Ion-Exchange Buffers A and B, and Size-Exclusion Buffer (see recipes)
- TEV protease (e.g., SelecTEV Protease, Lucigen Corp., cat. no. 30810-1)
- 1 M Dithiothreitol (DTT, in water)
- 0.5 M NaOH Milli-Q water
- Liquid nitrogen
- Sonicator (Sonics VCX 500)
- Centrifuge and rotor for 30- to 40-ml tubes and up to 30000 × g (e.g., Sorval RC 5C plus, with SS34 rotor)
- Chromatography columns: all from GE Life Sciences:
    - 5 ml HisTrap FF Crude (17-5286-01 pack of 5)
    - HiPrep 26/10 Desalting (17-5087-01)
    - 5 ml HiTrap SP HP (17-1152-01 pack of 5)
    - Sephacryl S-300 HR 16/60 (17-1167-01)
- UV/vis spectrometer (e.g., GE Life Sciences NanoVue)
- Centrifugal concentration units, 10 kDa MWCO (e.g., Millipore, cat. no. UFC901024)
- 10-ml and 20-ml sterile syringes and syringe filters (0.2 μm)
- FPLC system with gradient-making capability and fractionation system, with flow rates up to 10 ml/min (e.g., GE Life Sciences AKTA series)
- Tubes or 96-well plates for fractionation
- 1.7-ml microcentrifuge tubes, certified DNase/RNase-free

2.5.2 Cell lysis and nickel affinity

1. Thaw cells (from 2.4 Cas9 Protein Bacterial Expression) by immersion in room temperature water.
2. Pour the thawed cells into a 100-ml glass beaker in an ice bucket, and lyse by sonication. Recommended settings are 20-24 cycles of 10 sec sonication followed by 10 sec cooling, at 40% power. Ideal power setting and sonication duration may vary between sonication units. Complete cell lysis is indicated by a significant decrease in the opacity and viscosity of the suspension. A French Press or similar homogenizer may be used instead of a sonicator
3. Clarify the lysed cells by centrifugation for 30 min at 27000 × g, 4°C.
4. Carefully decant the supernatant. The pellet may be rather soft. Avoid including any of the soft part of the pellet in the supernatant: repeat step 3, if necessary. For steps 5-20, it is assumed that the reader is familiar with basic FPLC use, including but not limited to: column installation and equilibration, setting pressure limits, sample loading (by

superloop, sample pump or injection loop), fractionation, creating gradients, and simple methods. For all chromatography steps, column volumes are stated for purification from 2 liter cells. Default flow-rates and pressure limits are used for all columns (see manufacturer's documentation). All chromatography steps can be performed at room temperature or 4°C.

5. Load the clarified lysate onto a 5 ml HisTrap FF crude column equilibrated in Nickel Buffer A.
6. Wash out unbound material with 25 ml Nickel Buffer A.
7. Elute bound protein with 25 ml Nickel Buffer B, and collect 1-ml fractions.
8. Pool peak fractions (UV absorbance at 280 nm greater than 0.2 for 2 mm path-length cell, or use SDS-PAGE to identify the most concentrated fractions). If necessary, concentrate the pooled fractions to 10 to 12 ml using a centrifugal concentrator.

2.5.3 Desalting and tag removal

1. Load the sample onto a HiPrep 26/10 Desalting column equilibrated in 15% Ion Exchange Buffer B (i.e., a mix of 85% Ion Exchange Buffer A and 15% Ion Exchange Buffer B). Run 50 ml 15% Ion Exchange Buffer B over the column, collecting 1- to 2-ml fractions throughout. Pool all fractions containing protein as judged by A280 (or SDS-PAGE).
2. Quantify protein yield: an A280 of 0.92 corresponds to a concentration of 1 mg/ml. A sample can be taken at this point for SDS-PAGE. Purity is typically about 80% to 90% at this stage as determined by SDS-PAGE
3. Add TEV protease to remove tag: use 0.1 mg TEV protease per 10 mg Cas9 protein.
4. Incubate the Cas9/TEV protease mixture overnight (18 hr) at 4°C.
    a. Alternate Protocol for steps 9 to 12: dialysis can be used instead of desalting to exchange the Cas9 into 15% Ion Exchange Buffer B.
        i. Quantify protein yield as described above.
        ii. Add TEV protease: 0.1 mg enzyme per 10 mg Cas9 protein.
        iii. Load dialysis tubing or cassette (10 kDa MWCO) with Cas9/TEV protease mix: typical volume is 10-12 ml. i
        iv. Dialyze against 2 liters 15% Ion Exchange Buffer B overnight (18 hr) at 4°C with stirring.
        v. Recover the sample from the dialysis tubing or cassette and proceed with step 13 below.
5. There may be some precipitate in the Cas9/TEV protease mix after tag removal. Remove this precipitate by passing the sample through a 0.2-μm syringe filter into a clean 50-ml tube. A sample can be taken at this point for SDS-PAGE if desired to check that tag removal is complete.

2.5.4 Ion exchange

1. Load the filtered Cas9/TEV protease mix onto a 5 ml HiTrap SP HP column equilibrated in 15% Ion Exchange Buffer B.
2. Wash the column with 25 ml of 15% Ion Exchange Buffer B.

3. Elute Cas9 with a gradient from 15% to 50% Ion Exchange Buffer B over 8 column volumes (40 ml), collecting 1-ml fractions throughout. Cas9 elutes as a single peak; the maximum A280 is typically seen at a conductivity of approximately 43 mS/cm, equivalent to about 375 mM KCl.
4. Pool peak fractions: in the unlikely event that multiple peaks are seen, samples from each peak should be run on SDS-PAGE to determine which fractions to pool.

2.5.5 Gel Filtration

1. Concentrate the pooled fractions to 4 to 6 ml using centrifugal concentrators. The Sephacryl S-300 column and FPLC system should be sanitized before beginning the next step. Run 1.5 column volumes of 0.5 M NaOH over the column, and an appropriate volume of 0.5 M NaOH through the FPLC system, including the injection loop and fractionation tubing. Leave the column and system overnight, and then wash thoroughly with Milli-Q water and then Size exclusion buffer (2 column volumes over the column). This will effectively remove any contaminant or precipitated proteins, bacterial contamination or residual endotoxin.
2. Use a sterile syringe and syringe filter (0.2 μm) to remove any precipitate or debris from the sample, and load it onto a Sephacryl S-300 16/60 HR column equilibrated in Size Exclusion Buffer + 1 mM DTT. Always add DTT to the buffer just before use, as it has a limited half-life in solution. Other reducing agents such as Tris-(2-carboxyethyl)phosphine (TCEP) can be used if preferred. If a reducing agent will interfere with downstream use of the purified Cas9 protein, it can be omitted; however, we recommend its use for long-term storage of the purified protein. Columns containing other size-exclusion resins can be used, e.g., Superdex 200. However, for optimal separation between the void-volume peak (aggregated protein and endotoxin) and the Cas9 protein peak, we recommend the use of Sephacryl S-300.
3. Run 120 ml Size Exclusion Buffer + 1 mM DTT over the column, collecting 1-ml fractions. Cas9 elutes at approximately 63 ml (corresponding to about 150 kDa, using globular protein standards), and typically this is the only peak seen in the chromatogram. A small amount of protein may elute in the void volume of the column (40 ml), but this is aggregated material and can be ignored. 2
4. Pool fractions containing Cas9. If unsure which fractions to pool, analyze by SDSPAGE.
5. Quantify the protein yield in the pooled fractions: an A280 of 0.75 corresponds to a concentration of 1 mg/ml. Typical yield is 10 mg (from 2 liters cells), but this can vary depending on exact expression conditions and fractions pooled during purification.
6. Concentrate the protein using centrifugal concentrators to a final concentration of 40 μM (6.4 mg/ml).
7. Filter sterilize the concentrated sample with a syringe and syringe filter, or with centrifugal filter units (e.g., Millipore UFC30GV0S) for small sample volumes (1 ml or less).
8. Transfer the purified protein into 1.7-ml microcentrifuge tubes. Aliquots of 10 to 50 μl are ideal.
9. Flash freeze the tubes with liquid nitrogen and store at −80°C. Cas9 protein will remain fully active in gene editing reactions for up to 6 months when stored in Size Exclusion Buffer +1 mM DTT at −80°C. Longer storage is not recommended. However, some

applications may be more sensitive than others to changes in the Cas9 protein. For this reason, we recommend setting a benchmark for your application using freshly prepared Cas9, so that any changes due to long-term storage can be detected. Purified Cas9 will tolerate several freeze-thaw cycles, but again, certain applications may be more sensitive. We recommend treating each frozen aliquot as single-use, but if this is wasteful for a given experiment, then after thawing a single tube, smaller aliquots can be made and refrozen in liquid nitrogen.

10. Analyze purified protein by SDS-PAGE using standard protocols. Cas9-NLS runs at just under 150 kDa on a 4% to 20% acrylamide gradient gel. Two very low intensity bands are usually seen between 110 to 130 kDa. These most likely represent degradation products of the full-length protein, and they do not affect the activity of the final product.

2.6 gRNA template assembly, amplification, and *in vitro* transcription

Guide RNAs are made in vitro through PCR assembly of a duplex DNA template from short, commercially available oligonucleotides, T7 transcription, and purification of the gRNA. The template is assembled from two oligos: a variable short oligo that contains the protospacer and a shared longer oligo that contains the gRNA constant region. It is not necessary to purify the template after assembly. T7 transcription can be accomplished using homemade T7 RNA polymerase or a commercial kit. Here we describe the use of a commercial kit, which is more accessible to most researchers.

2.6.1 Materials

- T7FwdVar oligo (5 -GGATCCTAATACGACTCACTATAG–protospacer sequence—GTTTTAGAGCTAGAA-3)
- 10 mM dNTPs
- DEPC-treated water
- 5× Phusion HF Buffer
- RNase Away
- T7RevLong oligo (5 -AAAAAAGCACCGACTCGGTGCCACTTTTTCAAGTTGATAACGG ACTAGCCTTATTTTAACTTGCTATTTCTAGCTCTAAAAC-3)
- T7FwdAmp primer (5 -GGATCCTAATACGACTCACTATAG-3)
- T7RevAmp primer (5 -AAAAAAGCACCGACTCGG-3)
- Phusion HF DNA Polymerase
- Agarose
- TAE buffer
- NEB HiScribe T7 High Yield RNA synthesis kit (NEB, cat. no. E2040S) containing: T7 RNA Polymerase Mix
- RNase-free DNase
- Calf intestinal alkaline phosphatase (CIP; NEB, cat. no. M0290)
- Thermal cycler
- Agarose gel rig and power source
- 37°C incubator

2.6.2 Protocol

1. Add the desired protospacer sequence to the T7FwdVar oligo and order the oligo from your favorite oligonucleotide supplier. There are many programs available for protospacer design that attempt to optimize on- and/or off-target activity. Which program is most useful depends upon many factors including type of editing, organism being edited, etc. Choice of protospacer design program is beyond the scope of this protocol. The transcript will start with the bolded G just 5 of the dashes in the T7FwdVar oligo. T7 RNA polymerase requires a 5 G for proper transcript initiation. If your protospacer has a G at the 5 end, you can omit it from the T7FwdVar design to avoid duplication of the G. If your protospacer has a C, T, or A at the 5 end, add the whole protospacer sequence to T7FwdVar. In this case, there will be an extra G added to the 5 end of the protospacer, but literature indicates this will have minimal effect unless your guide is very short.
2. For each T7FwdVar oligo you designed, set up the following PCR (total volume should be 20.0 µl):
    a. 13.4 µl DEPC-treated H2O
    b. 4.0 µl of 5× Phusion HF Buffer
    c. 0.8 µl of 10 mM dNTPs
    d. 0.4 µl T7FwdVar (1 µM)
    e. 0.4 µl T7RevLong (1 µM)
    f. 0.4 µl T7FwdAmp (100 µM)
    g. 0.4 µl T7RevAmp (100 µM)
    h. 0.2 µl Phusion HF DNA polymerase (2 U/µl).
    i. If making multiple gRNA templates, prepare a master mix with all components except T7FwdVar. Include a no template control (omit T7FwdVar).
3. Run the thermal cycler with the following protocol:
    a. 1 cycle: 30 sec 95°C (initial denaturation)
    b. 35 cycles:
        i. 10 sec 95°C (denaturation)
        ii. 10 sec 57°C (annealing)
        iii. 10 sec 72°C (extension)
    c. 1 cycle: 2 min 72°C (final extension)
    d. Final step: indefinite 4°C (hold).
4. Run 2 µl of the assembled DNA product on a 2% TAE-agarose gel to ensure the PCR worked. The expected product size is about 120 bp. It is not necessary to purify the template after assembly PCR before proceeding to transcription.
5. The NEB HiScribe T7 High yield RNA Synthesis kit gives excellent results, but other T7 transcription kits may be used in its place. Since the concentration of the DNA template is unknown at this stage, use the maximum amount of PCR reaction possible. All components below, with the exception of your DNA template, are provided in the NEB HiScribe T7 High Yield RNA Synthesis kit.
    a. 2.0 µl 10× Buffer
    b. 2.0 µl ATP (100 mM)
    c. 2.0 µl GTP (100 mM)
    d. 2.0 µl CTP (100 mM)

e. 2.0 µl UTP (100 mM)
f. 8.0 µl DNA Template
g. 2.0 µl T7 RNA Polymerase Mix.
h. If making multiple gRNAs, prepare a master mix with all components except the DNA template.

6. Incubate the mix 18 hr at 37°C.
7. Add 1 µl of RNase-free DNase and incubate for 20 min at room temp.
8. Remove DNA template by adding 1 µl of RNase-free DNase and incubate for 20 min at room temperature.
9. To remove the 5' RNA triphosphate (leaving a 5' hydroxyl), add 5 U of Calf Intestinal Alkaline Phosphatase (CIP) per 100 µg of gRNA and incubate for 30 min at 37°C. ssRNA containing a 5' phosphate can activate RIG-1 antiviral response.

2.7 gRNA purification with magnetic SPRI beads

After T7 transcription (2.6 gRNA template assembly, amplification, and *in vitro* transcription), the gRNA is purified using columns (lowthroughput) or magnetic SPRI beads (high-throughput). Columns may theoretically yield a cleaner end product, but gRNA purified using homemade SPRI beads gives equal gene editing efficacy and is easily extensible to 96-well plates with a plate magnet. Here we include protocols for both bead and column purification.

2.7.1 Materials

- SPRI-beads (see 2.9 Production of SPRI beads and testing)
- IVT reaction (see 2.6 gRNA template assembly, amplification, and *in vitro* transcription)
- 80% Ethanol
- Agarose
- 10% polyacrylamide TBE-urea gel
- Ethanol
- Pipettes
- Magnetic stand
- Qubit or spectrophotometer
- Polyacrylamide gel rig and power source

2.7.2 Purify sgRNA protocol

1. Add 5× volume of SPRI beads to IVT reaction. 5 × 20 µl IVT gRNA = 100 µl SPRI beads
2. Pipette to mix 10 times.
3. Incubate 5 min at room temperature.
4. Place on a magnetic stand for 5 min.
5. Discard the supernatant.
6. Add 200 µl of 80% ethanol. Incubate on a magnetic stand for 2 min.
7. Remove the ethanol and repeat previous step.
8. Air dry 5 to 10 min.

9. Elute in 20 µl of DEPC-treated H2O or TE. Pipette to mix 10 times.
10. Incubate 2 min at room temperature.
11. Place of a magnetic stand for 5 min.
12. Keep the supernatant. Transfer to a new plate/tubes.

2.7.3 Quality control for sgRNA

1. Measure RNA concentration with Qubit or Nanodrop. Measuring the RNA concentration with a Qubit is more accurate than alternative methods, such as Nanodrop. You should expect an RNA concentration of about 4000 ng/µl (or about 80 µg of RNA total). Multiply the ng/µl concentration by 0.3 to get the concentration in pmol/µl (for subsequent steps.)
2. Run RNA on a 10% polyacrylamide TBE-urea gel to check for purity.

2.8 gRNA purification with RNeasy spin columns

This protocol is a modification of the Qiagen RNeasy kit, with modifications made for small RNAs. This is an alternate protocol to the gRNA purification with magnetic SPRI beads.

2.8.1 Materials

- IVT Reaction (see 2.6 gRNA template assembly, amplification, and *in vitro* transcription)
- Qiagen RNeasy kit containing:
    - RLT Buffer
    - RPE Buffer
    - RNeasy mini spin column
- 100% ethanol
- DEPC-treated water
- 10% polyacrylamide TBE-urea gel
- Benchtop centrifuge
- 1.5-ml microcentrifuge

2.8.2 Protocol

1. To your DNase-treated gRNA synthesis, add 350 µl RLT Buffer to the sample.
2. Add 550 µl of 100% ethanol.
3. Transfer 500 µl into an RNeasy mini spin column. Spin for 15 sec.
4. Transfer the remainder. Spin for 15 sec.
5. Move spin column to a new collection tube.
6. Add 500 µl RPE Buffer. Spin for 15 sec.
7. Repeat this wash step.
8. Move the spin column into a new collection tube. Spin for 1 min.
9. Move the spin column into a 1.5-ml microcentrifuge tube.
10. Add 30 µl DEPC-treated H2O. Spin for 1 min.
11. Repeat the 30 µl elution to collect any remaining RNA.

12. Run RNA on a 10% polyacrylamide TBE-urea gel to check for purity.

2.9 Production of SPRI beads and testing

Magnetic SPRI beads for RNA purification can be made quickly and cost-efficiently with the following protocol. Ensure that all materials are RNase-free before using. (The easiest way to do this is by purchasing solutions.) This protocol is derived from the methods created by Rohland and Reich (2012) and is directly based on Faircloth & Glenn (2014) (Faircloth and Glenn, 2014; Rohland and Reich, 2012). An online protocol including figures for testing SPRI beads, can be found at http://protocols.readthedocs.io/projects/protocols-serapure/en/latest/index.html. https://ethanomics.files.wordpress.com/2012/08/serapure_v2-2.pdf

2.9.1 Materials

- 0.5 M EDTA, pH 8.0 (Amresco, cat. no. E177)
    - M Tris, pH 8.0 (Amresco, cat. no. E199)
- Sera-mag SpeedBeads (Fisher, cat. no. 09-981-123)
- PEG-8000 (Amresco, cat. no. 0159)
- 5 M NaCl (Amresco, cat. no. E529)
- Tween 20 (Amresco, cat. no. 0777)
- Nuclease-free water (Amresco, cat. no. E476)
- Fermentas ladder(s) (Ultra-low range: Fisher, cat. no. FERSM1211, 50 bp: cat. no.
- FERSM0371)
- Ethanol (EtOH)
- Loading dye (Thermo Fisher, cat. no. R0611)
- Agarose
- TAE
- 50-ml conical tubes
- 1.5-ml microtube
- Rare-earth magnet stand (e.g., Ambion, cat. no. AM10055 or NEB, cat. no.
- S1506S)
- 200-µl or 1000-µl pipettors
- Aluminum foil
- Agarose gel rig and power source

2.9.2 Protocol for production of SPRI beads

1. In a 50-ml conical tube using sterile stock solutions, prepare TE (10 mM Tris·Cl, 1 mM EDTA = 500 µl 1 M Tris, pH 8 + 100 µl of 0.5 M EDTA, fill conical tube to 50 ml mark with dH2O).
2. Mix Sera-mag SpeedBeads and transfer 1 ml into a 1.5-ml microtube.
3. Place the SpeedBeads on a magnet stand until the beads are drawn to the magnet.
4. Remove the supernatant with a 200-µl or 1000-µl pipettor.
5. Add 1 ml TE to the beads, remove from the magnet, mix by pipetting three times, and return to the magnet.

6. Remove the supernatant with a 200-µl or 1000-µl pipettor.
7. Add 1 ml TE to the beads, remove from the magnet, mix by pipetting three times, and return to the magnet.
8. Remove the supernatant with a 200-µl or 1000-µl pipettor.
9. Add 1 ml TE to the beads and remove from the magnet. Fully resuspend and set the microtube in the rack (i.e., not on the magnet stand).
10. Add 9 g PEG-8000 to a new 50-ml, sterile conical tube.
11. Add 10 ml 5 M NaCl (or 2.92 g) to the conical tube.
12. Add 500 µl 1 M Tris·Cl to the conical tube.
13. Add 100 µl of 0.5 M EDTA to the conical tube.
14. Fill the conical tube to 49 ml using sterile dH2O. You can do this by eye, just go slowly.
15. Mix by vortexing the conical tube for about 3 to 5 min until PEG goes into solution (solution, upon sitting, should be clear).
16. Add 27.5 µl Tween 20 to the conical tube and mix gently.
17. Mix 1 ml SpeedBead + TE solution and transfer into a 50-ml conical tube.
18. Fill the conical tube to the 50 ml mark with dH2O (if not already there) and gently mix by hand the 50-ml conical tube until brown.
19. Test against AMPure XP using aliquots of ladder (Fermentas GeneRuler). I recommend the 50-bp ladder in place of the ultra-low range ladder. The protocol for testing SPRI beads is provided below (see 2.9.3).
20. Wrap in aluminum foil (or place in dark container) and store at 4°C.
21. Test monthly using the protocol 2.9.3 Testing SPRI beads.

2.9.3 Testing SPRI beads

It is recommended to test the Serapure mixture to ensure that it is working as expected. The original protocol authors indicated the protocol works best with Fermentas GeneRuler, and other ladders did not work well (Faircloth and Glenn, 2014; Rohland and Reich, 2012).

1. Prep fresh aliquots of 80% EtOH.
2. Mix 2 µl GeneRuler with 18 µl dH2O.
3. Add 20 µl GeneRuler mixture to a volume of Serapure and/or AMPure (the specific volume depends on whether you are trying exclude small fragments or not; see the figure at https://ethanomics.files.wordpress.com/2012/08/serapure_v2-2.pdf
4. Incubate the mixture for 5 min at room temperature.
5. Place on the magnet stand.
6. Remove the supernatant.
7. Add 500 µl of 80% EtOH.
8. Incubate on the stand for 1 min.
9. Remove the supernatant.
10. Add 500 µl of 80% EtOH.
11. Incubate on the stand for 1 min.
12. Remove the supernatant.
13. Allow the beads to sit until dry (or use toothpicks to remove residual EtOH).
14. Rehydrate with 20 µl dH2O.
15. Place on the magnet stand.

16. Transfer the supernatant into a new 1.5-ml tube.
17. Mix the supernatant with 1 µl loading dye.
18. Electrophorese in 1.5 % TAE- agarose for 60 min at 100 V. Run the comparison of the homemade SPRI beads next to the AMPure beads to ensure the homemade SPRI beads are working properly. Your homemade SPRI beads should have size selecting capabilities equivalent to AMPure beads. For reference on gel images, refer to the protocol in Faircloth and Glenn (2014), or the figure found at https://ethanomics.files.wordpress.com/2012/08/serapure_v2-2.pdf

2.10 CasRNP complex formation and electroporation

With Cas effector protein and gRNA in hand, the next step is to combine them to form a CasRNP complex, prepare cells, and nucleofect. This protocol is written for nucleofection of HEK293T cells using the Lonza 4D. However, one may use other cells and other electroporators. For example, the appropriate nucleofection solution and program code for other cell types can be found on the Lonza website, and the ThermoFisher Neon and BioRad electroporator have been successfully used for electroporation. If using a different cell line, use the medium appropriate for your cell line of interest throughout the protocol. This protocol is based on the CasRNP protocol originally published by (Lin et al., 2014).

2.10.1 Materials

- Purified Cas9 protein (see 2.5 Cas9 Purification)
- Cas9 buffer (see recipe)
- Purified gRNA (2.6 gRNA template assembly, amplification, and *in vitro* transcription)
- Single-stranded DNA (Richardson et al., 2016a, 2016b)
- HEK293Ts or cell line of your choice
- Trypsin
- Cell culture medium appropriate for HEK293Ts:
    - DMEM (Thermo Fisher, cat. no. 10566016)
    - 10% Fetal bovine serum (FBS; Seradigm, cat. no. 1500-500)
- Nucleofector solution
- Pipettes and pipette tips
- Hemacytometer
- 15-ml conical tubes
- Centrifuge
- 12-well tissue culture plates
- Lonza nucleofection cuvetter and solution for your cell type
- 4D Lonza Nucleofector
- 200-µl pipette

2.10.2 Prepare CasRNP complex

1. Bring 100 pmol of Cas9 protein to a final volume of 5 µl using Cas9 buffer (Lin et al., 2014).We recommend using a cas9 stock of 40 µM, using 2.5 µl of cas9 protein and 2.5 µl of cas9 buffer.
2. Bring 120 pmol gRNA to a final volume of 5 µl using Cas9 buffer. This means you will need a minimum gRNA concentration of 24uM.
3. Add Cas9 to gRNA slowly while swirling with a pipette tip, should take 30 sec to 1 min.
4. If you wish to add a short, single-stranded DNA template for HDR or potential increased editing efficiency, add 100 pmol of single-stranded DNA (Richardson et al., 2016a, 2016b)
5. Allow CasRNP to form for 10 to 20 min.

2.10.3 Prepare cells

1. Trypsinize HEK293T cells, resuspend in 5 ml medium, and count the cells using a hemacytometer. We recommend using cells that are 60% to 90% confluent, so the cells are most healthy.
2. For each nucleofection, pipette 200,000 cells into a 15-ml conical tube.
3. Centrifuge for 10 min at 100 × g, 4°C, to pellet the cells softly.
4. Prepare a 12-well plate with 1-ml medium per well, and pre-warm at 37°C in the incubator.

2.10.4 Nucleofection

1. Prepare and label wells on 20 µl nucleofection strips.
2. Configure Lonza 4D using program DS150.
3. Pipette off medium from cells, gently but completely, using a 200 µl pipette. The pellet is very soft so be careful.
4. Resuspend cells in 20 µl of nucleofector solution for HEK293T (SF solution) using a 200-µl pipette.
5. Add the entire 10 µl CasRNP mix to the 20 µl resuspension and mix by pipetting.
6. Add nucleofection mixes to the multi-well cuvette, and cap. Pay attention to the orientation of the cap and cuvette in the nucleofector, which is noted in the manufacturer's instructions. Add carefully to one short side of the well, at an angle. Do not produce any bubbles. Solution need not be completely filling the well as long as there are no bubbles.
7. Insert the cuvette into nucleofector and nucleofect the cells.
8. Allow the cells to sit in nucleofection strips for 10 min post-nucleofection. This is supposed to increase efficiency.
9. Add 80 µl of pre-warmed medium to each well. Pipette the mixture out with a 200-µl into your pre-warmed 12-well plate.
10. Allow the cells 24 to 72 hr to settle and recover before attempted downstream analysis. Analysis of the efficacy of genome editing (e.g., by T7E1 assay) is not included here, but detailed protocols can be found online at https://www.protocols.io/groups/igi.

2.11 Reagents and solutions

Use deionized, distilled water in all recipes (unless otherwise noted). Filter (0.2 μm) all buffers before use. All buffers can be stored for several months at 4°C, or for 1 month at room temperature.

Cas9 buffer

- 20 mM HEPES-KOH, pH 7.5
- 150 mM KCl
- 1 mM MgCl2
- 10% glycerol
- 1 mM TCEP

Ion-exchange buffer A

- 20 mM HEPES [4-(2-Hydroxyethyl)piperazine-1-ethanesulfonic acid]
- 150 mM KCl
- 5% (v/v) glycerol
- Adjust to pH 7.5 with 1 M KOH

Ion-exchange buffer B

- 20 mM HEPES
- 1 M KCl
- 5% (v/v) glycerol
- Adjust to pH 7.5 with 1 M KOH

Nickel buffer A

- 20 mM Tris [2-Amino-2-(hydroxymethyl)-1,3-propanediol]
- 500 mM NaCl
- 5% (v/v) glycerol
- 25 mM imidazole
- Adjust to pH 8.0 with 1 M HCl

Nickel buffer B

- 20 mM Tris
- 500 mM NaCl
- 5% (v/v) glycerol
- 250 mM imidazole
- Adjust to pH 8.0 with concentrated HCl

Size-exclusion buffer

- 20 mM HEPES
- 150 mM KCl
- 10% (v/v) glycerol
- Adjust to pH 7.5 with 1 M KOH

TE buffer

- 10 mM Tris·Cl

- 1 mM EDTA

2.12 Background Information

The discovery of CRISPR-Cas9 as an easy to-use genome-editing tool is leading a revolution in functional genetics for fundamental discovery and disease therapy research. The modularity and efficacy of CRISPR-Cas9 allows researchers to address many questions that were previously out of reach. The delivery of CasRNP directly to cells (versus plasmid transfection) further simplifies genome editing. Bacterial and archaeal CRISPR loci and Cas genes are heterogeneous mechanisms to provide adaptive immunity against viruses (Barrangou et al., 2007; Makarova et al., 2006). There are many multicomponent Cas nucleases, and the CRISPR-Cas system's DNA targeting ability initially was demonstrated in Staphylococcus epidermis (Marraffini and Sontheimer, 2008). Further research revealed that Cas9 is the only Cas protein required for the Type II system, and it is directed by a tracrRNA and crRNA combination that can be simplified to a single guide RNA (Deltcheva et al., 2011; Jinek et al., 2012). The simple two-component CRISPR-Cas9 system was quickly demonstrated to function effectively in genome editing mammalian cells (Cong et al., 2013; Jinek et al., 2012; Mali et al., 2013). Shortly thereafter, CRISPRCas9 was demonstrated to be functional as a ribonucleoprotein complex in C. elegans and mammalian cells (Cho et al., 2013; Kim et al., 2014; Lin et al., 2014). CasRNPs have rapidly gained popularity because, in comparison to plasmid transfections, they are highly efficacious and reduce off-target effects (possibly because Cas9 is cleared from cells within 24 hr). Furthermore, CasRNP delivery is particularly useful in hard-to-transfect cell lines, such as fibroblasts and pluripotent stem cells. CasRNP editing is now routinely applied to many model and non-model organisms (Chen et al., 2016; Sung et al., 2014). Strikingly, CasRNP electroporation has even allowed groups to skip microinjection procedures in favor of bulk electroporation, greatly reducing CasRNP editing has led to its rapid adoption in many contexts, though barriers still remain with regards to in vivo delivery to somatic tissues.

2.13 Critical Parameters: gRNA synthesis

It is important that the concentration of gRNA be determined accurately in order for the nucleofection to be successful. Measuring the RNA concentration with a Qubit is far more accurate than alternative methods, such as a Nanodrop.

2.14 Troubleshooting

Table 1: Troubleshooting guide for production of purified CasRNPs

Problem	Probable cause	Solution
Low Cas9 Yield	Low expression in bacteria	Use only freshly transformed cells for expression.
	Cells not lysing properly	Check efficiency of cell lysis by microscopy or SDS-PAGE and optimize lysis conditions if necessary.
	Elution of protein failing	Use more TEV protease for tag removal: check for efficiency of tag removal by SDS-PAGE.
Low gRNA Yield	RNA degraded	Ensure only RNase-free reagents are used in the preparation of gRNAs.
	In vitro transcription failed	Use free T7 Polymerase, as it is prone to losing function if not stored properly.
No editing in cells	gRNAs are not effective	Include a validated positive control gRNA from the literature in your given cell type.
	Nucleofection not optimized for the cell type	Try optimizing the nucleofection code. The codes provided by Lonza work well for those cell types, but your given cell line may be variable. Details on optimizing Lonza codes can be found online.

2.15 Anticipated results

Expect a gRNA concentration of about 4000 ng/µl (or about 80 µg of RNA total) and a yield of 10 mg of cas9 protein. gRNA activity is currently determined empirically, and the efficiency of editing can even vary by cell type. We recommend testing two to four gRNAs for each locus you wish to edit. In most cases, you will be able to find a successful gRNA.

2.16 Time considerations

This entire protocol can be completed within a week. The Cas9 protein preparation takes about five days. The gRNA template PCR, in vitro synthesis, and purification can be completed in parallel and takes two days. The nucleofection protocol takes about two hours, and we recommend waiting two to three days before collecting the cells for analysis.
If you wish to make clones with your nucleofected cell lines, plate the cells in 96-well plates, averaging 0.7 cells/well. (This ensures that very few wells end up with two cells.) Depending on

your cell type, the clones may take anywhere from one to three weeks to grow into colonies. The colonies can then be split for genotype and continued growth.

3 A genome-wide screen for ER autophagy highlights key roles of mitochondrial metabolism and ER-resident UFMylation

A version of the material in this chapter was previously reported as

Liang, J. R., Lingeman, E., Luong, T., Ahmed, S., Nguyen, T., Olzmann, J. and Corn, J. E. (2019). A genome-wide screen for ER autophagy highlights key roles of mitochondrial metabolism and ER- resident UFMylation. *BioRxiv*. 2019 Feb 25.

The work has been adapted here with permission from all co-authors.

3.1 Connection to overall dissertation

In the previous chapter, I described a protocol for using genome-editing techniques to make a specific edit. In our work, we were most interested in not just developing scientific tools, but using those tools to uncover new biology. In this chapter, we used a variety of genome-editing technologies to discover new regulators of ER autophagy (ER-phagy). In particular, the protocol described in chapter 2 was used to make specific cell lines used within this chapter. Genome editing allowed us to make these cell lines and more conclusively answer a specific biological question. Overall, this portion of my dissertation moves from tool-development to applying those tools to uncover new biology.

3.2 Summary

Selective degradation of organelles via autophagy is critical for cellular differentiation, homeostasis, and organismal health. Autophagy of the ER (ER-phagy) is implicated in human neuropathy but is poorly understood beyond a few specialized autophagosomal receptors and remodelers. Using an ER-phagy reporter and genome-wide CRISPRi screening, we identified 200 high-confidence factors involved in human ER-phagy. We mechanistically investigated two pathways unexpectedly required for ER-phagy. First, reduced mitochondrial metabolism represses ER-phagy, which reverses the logic of general autophagy. Mitochondrial crosstalk with ER-phagy bypasses the energy sensor AMPK, instead directly impacting ULK1. Second, ER-localized UFMylation is required for ER-phagy that represses the unfolded protein response. The UFL1 ligase is brought to the ER surface by DDRGK1, analogous to PINK1-Parkin regulation during mitophagy. Our data provide insight into the unique cellular logic of ER-phagy, reveal parallels between organelle autophagies, and provide an entry point to the relatively unexplored process of degrading the ER network.

3.3 Introduction

Macroautophagy (herein referred to as autophagy) mediates the delivery of cellular cargo to the lysosome for degradation. Once thought to be a non-specific process, it has become clear that autophagy is complexly regulated and induced by various stresses to remove damaged or excessive cellular components. Targeted removal of entire organelles by autophagy is necessary for cellular homeostasis, and during selective autophagy of mitochondria (mitophagy), the surface proteins of damaged mitochondria are marked by phosphorylation and ubiquitylation to recruit autophagic machinery (Nguyen et al., 2016; Youle and Narendra, 2011). Dysregulation of selective organelle autophagy negatively impacts cellular fitness and is linked to degenerative diseases, particularly in non-regenerative cell types such as neurons. Mutations of key mitophagy genes, such as PINK1 and Parkin, are strongly associated with disorders such as Parkinson's disease (Deas et al., 2011; Dodson and Guo, 2007; Geisler et al., 2010; Pickrell and Youle, 2015; Pilsl and Winklhofer, 2012).

The endoplasmic reticulum (ER) plays a critical role in numerous cellular functions, such as the folding, modification, and transport of secretory proteins; the storage of calcium; and the biosynthesis of lipids (Schwarz and Blower, 2016). The ER is tightly regulated by multiple quality control mechanisms, such as ER-associated degradation (ERAD) and ER to Lysosome Associated Degradation (ERLAD) (Fregno et al., 2018; Ruggiano et al., 2014). The ER-autophagy (ER-phagy) pathway intersects with the selective autophagy machinery to send portions of the ER for wholesale lysosomal degradation. While ER-phagy has long been observed in yeast (Hamasaki et al., 2005), it has only recently been described in mammalian cells (Khaminets et al., 2015).

During ER-phagy at least two ER surface proteins, FAM134B and RTN3L, act as specific receptors through LC3-interacting regions (LIR) that recruit autophagy machinery (Grumati et al., 2017; Khaminets et al., 2015). ER expansion can also be reversed via ER-phagy that is mediated by the SEC62 and CCPG1 LIR-containing ER-phagy receptors (Fumagalli et al., 2016; Smith et al., 2018). The reticular ER network is remodeled for delivery to the lysosome by Atlastin GTPases that are also involved in normal ER morphology (Liang et al., 2018; Rismanchi et al., 2008; Wang et al., 2016; Zhao et al., 2016). Failure to execute ER-phagy through mutations in known ER-phagy proteins causes neuropathy in mice, and cross-referencing with ClinVar reveals that mutations in human ER-phagy proteins are linked to hereditary neuropathies and paraplegia (Guelly et al., 2011; Khaminets et al., 2015; Kurth et al., 2009; Liang et al., 2018). But beyond the few receptors and remodelers most proximal to autophagosomal function, relatively little is known about the signals that regulate ER-phagy.

We performed a genome-wide CRISPR interference (CRISPRi) reporter-based screen to identify new players in ER-phagy, identifying both activators and inhibitors in a variety of cellular compartments. We mechanistically interrogated two pathways that positively regulate ER-phagy in unexpected ways: (1) mitochondrial oxidative phosphorylation (OXPHOS) and (2) ER-resident UFMylation. While inhibition of OXPHOS reduces cellular energy levels and stimulates general autophagy, genetic or chemical inhibition of OXPHOS instead represses ER-phagy. Mitochondrial regulation of ER-phagy bypasses the canonical energy-sensing AMP-dependent protein kinase (AMPK), and instead directly modulates ULK1 levels during starvation. We furthermore found that UFMylation, a post-translational modification similar to ubiquitination, is required for ER-phagy. The protein DDRGK1 recruits the UFMylation machinery to the ER surface in a striking parallel to the mitophagic recruitment of Parkin by

PINK1. Interfering with DDRGK1-dependent UFMylation inhibits ER-phagy, leading to the accumulation of misfolded proteins and inducing the unfolded protein response (UPR) via IRE1α signaling. Overall, our data provide a detailed map of ER-phagy regulators and highlight how organelle crosstalk and ER-resident factors mediate this emerging process of quality control.

3.4 Results

3.4.1 A genome-wide flow cytometry CRISPRi screen for ER-phagy

To develop a genome-wide screen for ER-phagy, we employed the previously-developed ER-Autophagy Tandem Reporter (EATR) system (Figure 3A) (Liang et al., 2018). In HCT116 colon cancer cells that stably express the EATR construct, we found that inducing general autophagy via inactivation of the mTOR complex did not induce ER-phagy (Figure 10A-B). Similarly, ER stress-inducing drugs that induce the unfolded protein response (UPR) did not cause ER-phagy. Only prolonged starvation (16 hours) using Earl's Buffered Saline Solution (EBSS) robustly induced ER-phagy.

Using EBSS as an ER-phagy stimulus, we coupled EATR-based FACS screening with genome-wide CRISPR transcriptional inhibition (CRISPRi) to identify novel pathways involved in ER-phagy (Figure 3A-B) (Gilbert et al., 2014; Horlbeck et al., 2016; Liang et al., 2018). Since autophagy is influenced by the availability of cellular energy, we reasoned that complete knockout of ER-phagy regulators via CRISPR cutting could be detrimental to cells and mask interesting players. The variability in sgRNA efficiencies of CRISPRi leads to different knockdown efficiencies, allowing for allelic series and residual function of essential genes involved in cellular energy regulation (Horlbeck et al., 2016).

As a proof-of-concept, we first assessed the suitability of EATR for CRISPRi screening by conducting a pilot screen with a custom CRISPRi library targeting known autophagy genes (Table 2). We used EATR-based FACS to isolate the top 25% of cells with the most ER-phagy ('enhanced' sort gate), and the bottom 25% of cells with the least ER-phagy ('inhibited' sort gate) (Figure 10C). This pilot screen successfully identified gRNAs targeting core autophagy genes as required for ER-phagy, and correctly assigned their role in promoting ER-phagy such that knockdown of autophagy components was enriched in the 'inhibited' gate (Figure 10D) and depleted in the 'enhanced' sort gate (Figure 10E).

We scaled up to perform an unbiased, genome-wide CRISPRi-v2 screen (Gilbert et al., 2014; Horlbeck et al., 2016) for ER-phagy regulators using EATR-FACS. From the gene-level statistics, we defined a high-confidence list of ER-phagy genes by first performing a cutoff at $p < 0.01$, and then requiring that true hits have opposite phenotypes in the "enhanced" and "inhibited" sort gates relative to the unsorted background. For example, gRNAs that knockdown a *bona fide* gene required for ER-phagy should be depleted in a population undergoing more ER-phagy but enriched in one undergoing less ER-phagy. We quantified involvement in ER-phagy by ratiometrically comparing gRNA distributions in the enhanced gate to those in the inhibited gate (Figure 3B), so that a positive $\log_2$-fold-change indicates a gene whose knockdown increases ER-phagy and a negative $\log_2$-fold-change indicates a gene whose knockdown inhibits ER-phagy. The resulting high-confidence hit list includes 200 genes involved in ER-phagy, with gene-level $\log_2$-fold-change phenotypes ranging from 3.62 to -5.38 (Table 3).

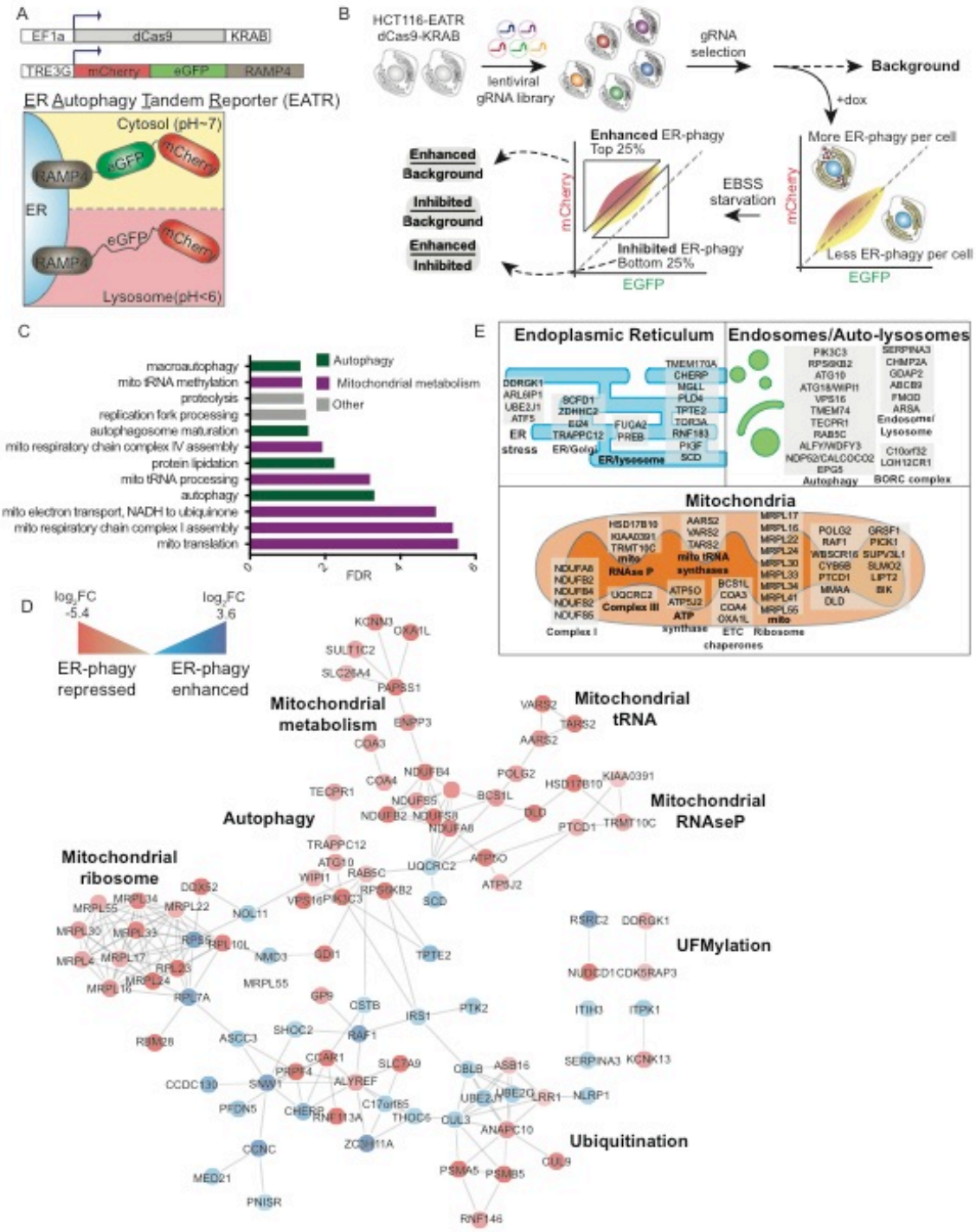

Figure 3: Unbiased identification of human ER-phagy regulators by genome-wide CRISPRi screening

(A) Schematic of the ER Autophagy Tandem Reporter (EATR) and CRISPR inhibition (CRISPRi) system used for screening. HCT116 cells stably express a doxycycline-inducible EATR construct that consists of mCherry and eGFP fused to ER localized RAMP4. Cells also stably express dCas9-KRAB for gRNA-targeted transcriptional repression of targeted genes.

(B) FACS screening strategy for identifying human genes whose knockdown enhances or inhibits ER-phagy. HCT116 cells stably expressing dCas9-KRAB and dox-inducible EATR were transduced with a genome-wide lentiviral CRISPRi gRNA library. After selection for gRNA expression and removal of essential genes, doxycycline was added for 24 hr to express EATR. Cells were then treated with EBSS starvation media for 16 hr to induce ER-phagy. The top and bottom quartiles of cells correspond enhanced or inhibited ER-phagy in response to CRISPRi knockdown. Cells were sorted and processed for next generation sequencing to identify gRNA representation in each sort bin. (C) Gene ontology analysis identifies autophagy and mitochondrial metabolism as major signatures of ER-phagy. High-confidence ER-phagy genes were defined as having opposite phenotypes in the enhanced and inhibited sort gates and gene-level $p < 0.01$. Ontologies with Benjamini-Hochberg FDR < 0.05 are shown. (D) Genes involved in ER-phagy form a physical interaction network. For clarity, only interactions between two or more high-confidence hits are shown. Red circles represent genes whose knockdown represses ER-phagy and blue circles represent genes whose knockdown enhances ER-phagy. The shades of red/blue correspond to the log2-fold-change associated with each gene. (E) Subcellular classification of high-confidence ER-phagy genes highlights roles in the ER, auto-lysosomes, and mitochondria.

As expected, multiple stages of general autophagy and membrane trafficking were prominent hits from the genome-wide library (Figure 10F). Individual stable knockdown of these autophagy-related factors and testing using EATR, an mCherry-Cleaved ER-phagy Reporter (CCER) western blot assay, and other measures of autophagy verified their requirement for ER-phagy (Figure 10G-I). These data indicate that the EATR assay and hence the genome-wide screen reports on ER-phagy pathways rather than ERAD or ERLAD, since the latter do not depend on autophagic components (Fregno et al., 2018; Ruggiano et al., 2014). We noticed that some of the established ER-phagy receptors such as FAM134B were not gene-level hits, and examining the performance of individual gRNAs by qRT-PCR, we found that none of the CRISPRi gRNAs in the genome-wide library successfully knocks down FAM134B (Figure 10J). This highlights a tradeoff in current CRISPRi screening technology, where allelic series enable interrogation of otherwise essential genes but may introduce false negatives. Failure to observe a gene in the ER-phagy screen dataset therefore does not imply that it plays no role in ER-phagy, but positive membership in the high-confidence set of 200 genes does indicate a role in ER-phagy.

We used unbiased GO term analysis of the high-confidence gene-level hit list to determine the cellular functions and pathways involved in ER autophagy (Figure 3C) (Huang et al., 2009). As expected for ER-phagy, GO terms related to autophagy were significantly enriched. However, we were surprised to find that multiple aspects of mitochondrial metabolism were even more prominent. We cross-referenced the high-confidence genetic hits against physical interaction databases to create a putative physical network of ER-phagy (Chatr-Aryamontri et al., 2017; Szklarczyk et al., 2015) (Figure 3D). This network falls into several major classes: autophagic execution, such as ATG10, (Phillips et al., 2008; Wartosch et al., 2015; Yuan et al., 2013); ubiquitination, such as the ER-localized UBE2J1 ubiquitin-conjugating enzyme involved in recovery from ER stress (Elangovan et al., 2017); mitochondrial metabolism, including nuclear-encoded OXPHOS genes, OXPHOS chaperones, and components of the mitochondrial ribosome required for translation of mitochondrially-encoded OXPHOS

genes; and post-translational modification by the ubiquitin-like protein UFM1, including CDK5RAP3 and DDRGK1 (Cai et al., 2015; Wei and Xu, 2016; Wu et al., 2010). Finally, we manually annotated all 200 high-confidence hits based on their subcellular localization (Binder et al., 2014). The localization analysis subdivided factors involved in ER-phagy into those associated with the lysosome/endosome, ER-associated factors, and nuclear-encoded mitochondrial proteins (Figure 3E).

3.4.2 Mitochondrial oxidative phosphorylation promotes ER-phagy by regulating levels of ULK1

We were surprised to find that the largest set of genes required for ER-phagy are involved in OXPHOS (Figure 4A), since cross-talk between ER-phagy and mitochondrial processes has not yet been described. While interference with mitochondrial energy metabolism induces general cytoplasmic autophagy, loss of mitochondrial factors instead repressed ER-phagy. Mitochondrial factors required for ER-phagy are directly associated with multiple aspects of the electron transport chain (ETC) and OXPHOS: Complex I (NDUFA8, NDUFB2, NDUFB4, NDUFS2, NDUFS5), Complex III (UQCRC2), and the ATP synthase/Complex V (ATP5O and ATP5J) (Figure 11A). We also found a large number of factors indirectly required for OXPHOS either through ETC maturation or the synthesis of mitochondrially-encoded ETC components (Taanman, 1999): mitochondrial chaperones (BCS1L, COA3, COA4, and OXA1L), mitochondrial ribosome subunits (MRPL17, MRPL16, MRPL22, MRPL24, MRPL30, MRPL33, MRPL34, MRPL41, MRPL55), mitochondrial tRNAs (AARS2, VARS2, TARS2), mitochondrial tRNA maturation (PTCD1 and mitochondrial RNAse P KIAA0391, TRMT10C, and HSD17B10). To further interrogate the link between mitochondrial metabolism and ER-phagy, we focused on mechanistic characterization of three factors that are involved in different parts of OXPHOS: NDUFB2, NDUFB4, and ATP5O.

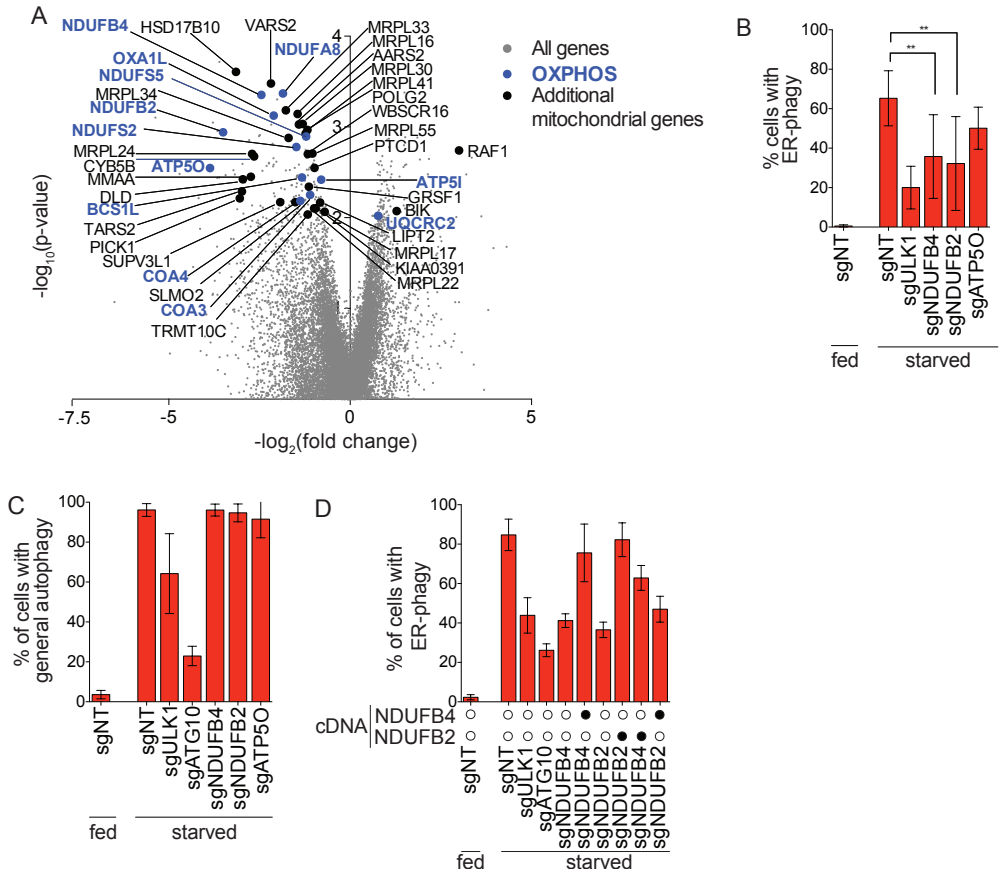

Figure 4: Intact OXPHOS promotes ER-phagy
(A) Genes that are components of the OXPHOS pathway were top hits in screen (highlighted in blue). Additional mitochondria-related genes are indicated in black and all other targeting sgRNAs are indicated in grey. (B) Knockdown of NDUFB4 and NDUFB2 significantly inhibit ER-phagy. HCT116 CRISPRi EATR cells were transduced with sgRNAs targeting ULK1, NDUFB4, NDUFB2, or ATP5O and starved for 16hr before FACS measurement for ER-phagy. Data presented as mean ± SD of eight biological replicates. P value indicates two-tailed paired t-test (**, $P < 0.01$). (C) General autophagy proceeds in cells where NDUFB2, NDUFB4, or ATP4O are knocked down. HCT116 CRISPRi cells expressing eGFP-mCherry-LC3B were transduced with sgRNAs targeting either ULK1, ATG10, NDUFB4, NDUFB2, or ATP5O. Cells were starved for 16hr before FACS measurement for general autophagy. Data represents mean ± SD of two biological replicates. (D) Re-expression of NDUFB4 and NDUFB2 rescues ER-phagy. HCT116 CRISPRi EATR cells were transduced with NDUFB4 or NDUFB2 cDNA constructs, and then transduced with sgRNAs targeting ULK1, ATG10, NDUFB4, NDUFB2. Cells were starved for 16hr before FACS measurement for ER-phagy. Data presented as mean ± SD of three biological replicates.

Individual, stable knockdown of OXPHOS components quantitatively inhibited starvation-induced ER-phagy in multiple assays in a manner that paralleled knockdown efficiency (Figure 4B, Figure 11B). However knockdown of NDUFB2, NDUFB4, or ATP5O did not inhibit starvation-induced general autophagy (Figure 4C, Figure 11C). Re-expressing the appropriate OXPHOS cDNA rescued ER-phagy, while cross-expressing a non-cognate

OXPHOS cDNA had no effect, indicating that each knockdown was specific and on target (Figure 4, Figure 11D-F). We further explored the necessity of functional OXPHOS for normal ER-phagy using chemical genetics (Figure 5A). Rotenone is a known inhibitor of both general autophagy and Complex I (Mader et al., 2012), and reduced both general autophagy and ER-phagy by multiple assays (Figure 5B – E, Figure 11G). By contrast, inhibiting Complex III with antimycin A or ATP synthase with oligomycin A increased general autophagy but reduced ER-phagy (Figure 5B – E, Figure 11G - H). Using Cell-Titer Glo to measure ATP levels (Figure 11I) and Seahorse to measure oxygen consumption (Figure 11J), we confirmed that knockdown of NDUFB2, NDUFB4, or ATP5O reduced cellular energy levels.

Depolarized mitochondria can be degraded via mitophagy, and dysregulation of OXPHOS might lead to mitochondrial depolarization by reducing the proton gradient across the mitochondrial inner membrane. Using Mitotracker, we found that OXPHOS conditions that repressed ER-phagy did not grossly alter mitochondrial abundance or membrane potential (Figure 12A). Consistent with prior reports, starvation actually increased the amount of Mitotracker accumulation (Johnson et al., 2014; Xiao et al., 2016). We furthermore found no evidence of increased mitophagy during knockdown of OXPHOS components to repress ER-phagy, either with or without stable over-expression of Parkin (Figure 12B - F). We therefore disfavor a model in which OXPHOS depletion inhibits ER-phagy through potent upregulation of mitophagy.

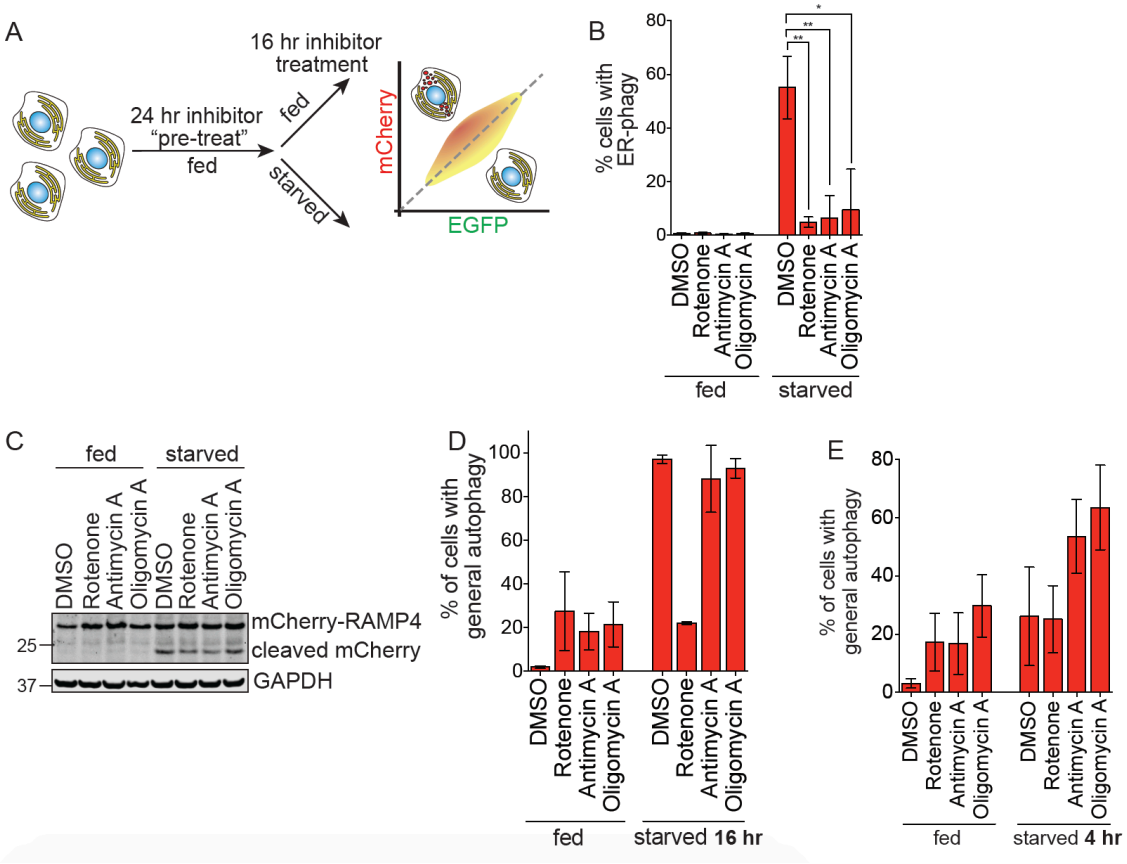

Figure 5: Electron transport chain inhibitors impair ER-phagy
(A) Schematic of experimental setup for chemical genetic inhibition of electron transport chain function in ER-phagy. HCT116 CRISPRi cells were treated with each inhibitor for 24 hours in complete media, then maintained in inhibitor for another 16 hours in fed or EBSS starvation media. Cells were then harvested for FACS to measure autophagy. (B) OXPHOS inhibitors disrupt ER-phagy as measured by flow cytometry. HCT116 EATR cells were treated with small molecule inhibitors of rotenone, antimycin A, or oligomycin A, and starved for 16 hours before FACS measurement of ER-phagy. Data presented as mean ± SD of three biological replicates. P value indicates two-tailed unpaired t-test (*, $P < 0.05$, **, $P < 0.01$). (C) OXPHOS inhibitors disrupt ER-phagy as measured by Western blot. HCT116 CRISPRi CCER cells were treated with rotenone, antimycin A, and oligomycin A and starved for 16hr. Cells were lysed for Western blotting to measure mCherry-RAMP4 cleavage. (D) Rotenone, a known autophagy inhibitor, inhibits general autophagy, while antimycin A and oligomycin A have no effect at time points where ER-phagy is disrupted. HCT116 CRISPRi cells expressing eGFP-mCherry-LC3B were treated with rotenone, antimycin A, or oligomycin A and starved for 16hr before FACS measurement for general autophagy. Data represents mean ± SD of three biological replicates. (E) Antimycin A and oligomycin A promote general autophagy at short time points. HCT116 CRISPRi cells expressing eGFP-mCherry-LC3B were treated with rotenone, antimycin A, or oligomycin A and starved for 4hr before FACS measurement for general autophagy. Data represents mean ± SD of three biological replicates.

The inhibition of ER-phagy by interfering with OXPHOS is counter-intuitive, since a reduction in energy levels is generally accepted to induce bulk cytoplasmic autophagy via 5' AMP-activated Protein Kinase (AMPK) signaling. Reductions in cellular ATP levels activate AMPK, which has also recently been implicated in the regulation of mitophagy (Egan et al., 2011; Kim et al., 2011; Toyama et al., 2016). We therefore asked whether the reduced energy levels caused by repression of OXPHOS leads to AMPK activity that somehow stimulates general autophagy while simultaneously repressing ER-phagy. However, we were surprised to find that AMPKα CRISPR-Cas9 knockout cells still mount a robust ER-phagy response, and this response is unaffected by stable re-expression of constitutively active or kinase dead AMPKα (Figure 6A-B, Figure 12G).

Unexpectedly, we instead found that interfering with OXPHOS reduces levels of the autophagic kinase ULK1 under conditions that promote ER-phagy. Knockdown of NDUFB2, NDUFB4, and ATP5O did not affect ULK1 under basal conditions, but during starvation the knockdown of OXPHOS components reduced levels of ULK1 almost as much as knockdown of ULK1 itself (Figure 6C), with ULK1 transcript levels moderately affected (Figure 12H). Cognate cDNA re-expression in the appropriate stable knockdown background rescued levels of ULK1, and these same conditions also rescued ER-phagy (Figure 6C, Figure 4D-E). Expressing a non-cognate OXPHOS cDNA in a mismatched knockdown background did not rescue levels of ULK1 nor the ability to perform ER-phagy (Figure 6C, Figure 4D). General autophagy proceeds normally when OXPHOS components are knocked down (Figure 4C, Figure 11C), and so the amount of ULK1 remaining is apparently sufficient to support general autophagy but not ER-phagy. These data reveal an unanticipated mode of regulation for ULK1 and imply a prioritization of general autophagy over ER-phagy during severe energy stress (Figure 12I).

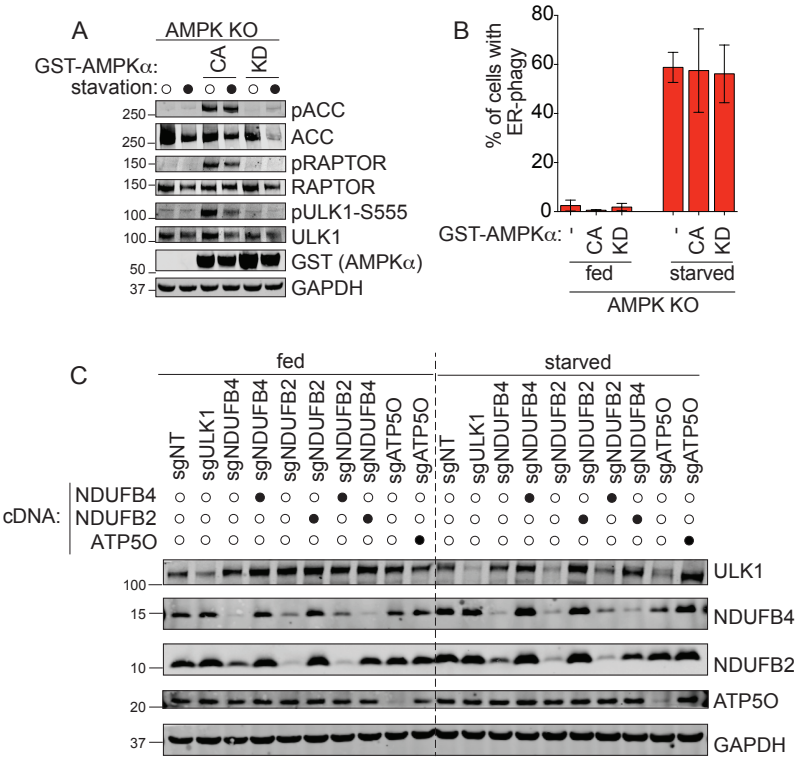

Figure 6: The OXPHOS pathway regulates ER-phagy via ULK1
(A) AMPK CRISPR-Cas9 knockout and re-expression. Phosphorylation status of downstream AMPKα targets were analyzed to verify the catalytically active (CA) and kinase dead (KD) AMPKα constructs. AMPKα knockout HCT116 EATR clone from Figure 12G were starved for 16 hours and samples were lysed for Western blotting and immunoprobed for the indicated proteins. (B) Catalytically active (CA) AMPKα does not inhibit ER-phagy. AMPKα knockout HCT116 EATR cells stably expressing catalytically active (CA) AMPKα, or kinase dead (KD) AMPKα were starved for 16hr before FACS measurement of ER-phagy. Data presented as mean ± SD of three biological replicates. (C) ULK1 protein levels are reduced during starvation in NDUFB4, NDUFB2, and ATP5O knockdown cell lines. HCT116 CRISPRi EATR cells were transduced with NDUFB4, NDUFB2, or ATP5O cDNA constructs, and then transduced with sgRNAs targeting ULK1, NDUFB4, NDUFB2, or ATP5O. Cells were lysed for Western blotting and immunoprobed for the indicated proteins.

3.4.3 DDRGK1-mediated UFMylation regulates ER-specific autophagy

The genome-wide screen for ER-phagy regulators yielded several hits that are localized to the ER and/or involved in ER-related processes ER (Figure 3E, Figure 7A). We focused on one of these factors, DDRGK1/C20orf116/UFBP1, which has emerging roles in ER homeostasis (Leto et al., 2019; Liu et al., 2017; Walczak et al., 2019).

Individual, stable knockdown of DDRGK1 resulted in inhibition of starvation-induced ER-phagy (Figure 7B-C, Figure 13A), but had no effect on general autophagy (Figure 7C-D). Immunofluorescence confirmed that an mCherry-tagged DDRGK1 construct co-localized with

the ER (Figure 7E). DDRGK1 is reported to be post-translationally modified by UFMylation, and which is in turn required for further UFMylation of other factors (Cai et al., 2015; Liu et al., 2017; Wei and Xu, 2016; Wu et al., 2010). UFMylation involves the sequential activation, conjugation and ligation of UFM1 to a target substrate via an E1 (UBA5), E2 (UFC1), and E3 (UFL1) cascade that mirrors ubiquitin conjugation (Figure 13B) (Daniel and Liebau, 2014; Komatsu et al., 2004). We found that stable knockdown of UFL1 led to decreased DDRGK1 protein levels in a proteasome-dependent manner and also inhibited ER-phagy (Figure 8A-B, Figure 13), as did knockdown of the UFM1 modifier (Figure 8C). Double knockdown of both UFL1 and DDRGK1 did not result in greater inhibition of ER-phagy as compared to individual depletion of either factor, suggesting that UFL1 and DDRGK1 act in the same pathway to regulate ER-phagy (Figure 13D - E). Stable re-expression of UFL1 in UFL1-depleted cells rescued levels of DDRGK1 and restored ER-phagy (Figure 8D-E), but over-expression of DDRGK1 in UFL1-depleted cells led to high levels of DDRGK1 without ER-phagy (Figure 8D-E). Hence, DDRGK1-dependent UFMylation is a key mediator of ER-phagy.

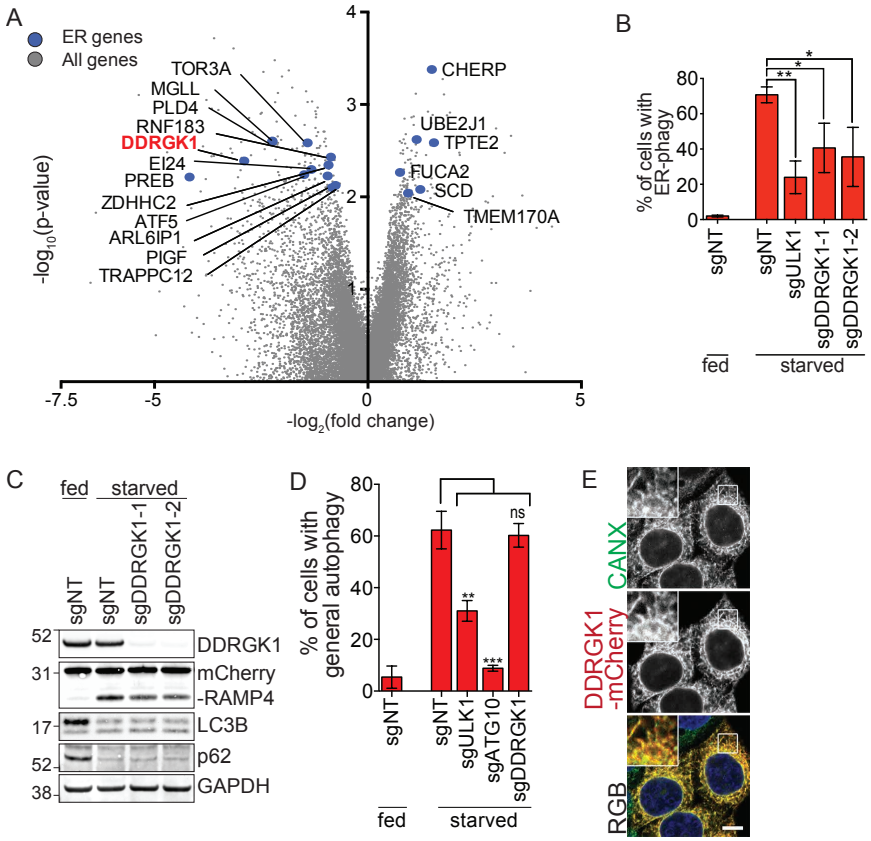

Figure 7: DDRGK1 is specifically required for ER-phagy
(A) ER-phagy CRISPRi screen identifies genes that are functionally or physically associated with the ER. DDRGK1 is highlighted in bold and red. (B) DDRGK1 depletion results in inhibition of ER-phagy based on EATR assay. HCT116 CRISPRi EATR cells were transduced with sgRNAs targeting ULK1 or DDRGK1 and starved for 16hr before FACS measurement for ER-phagy. Data presented as mean ± SD of three biological replicates. P value indicates two-tailed unpaired t-test (*, P < 0.05, **, P < 0.01). (C) CCER assay shows ER-phagy inhibition

upon DDRGK1 knockdown. HCT116 CRISPRi CCER cells were transduced with sgRNAs targeting DDRGK1 and starved for 16hr. Cells were lysed for Western blotting of the indicated proteins. (D) DDRGK1 knockdown does not affect general autophagy. HCT116 CRISPRi cells stably expressing eGFP-mCherry-LC3B constructs were transduced with sgRNAs targeting either ULK1, ATG10 or DDRGK1. Cells were starved for 16hr before FACS measurement for general autophagy. Data represents mean ± SD of three biological replicates. P value indicates two-tailed unpaired t-test (**, $P < 0.01$, ***, $P<0.001$). (E) DDRGK1 localizes to the ER. HeLa cells were stably transduced with DDRGK1-mCherry construct and immunostained for calnexin (CANX) as an ER marker. Insets represent three-fold enlargement of boxed areas. Scale bar represents 10μm.

DDRGK1 is reported to be UFMylated by UFL1 on one or more lysines and thereby stabilized (Figure 8F) (Wu et al., 2010). Using immunoprecipitation of DDRGK1 point mutants, we indeed found higher molecular weight species consistent with lysine post-translational modification of DDRGK1 (Figure 8G, Figure 13F). However, this modification was unaffected by CRISPR-Cas9 knockout of UFL1 or knockdown of UFM1 (Figure 8G and Figure 13F). Furthermore, knockdown of UFM1 had no effect on the abundance of DDRGK1 (Figure 13G), and DDRGK1 still stably interacted with UFL1 even when all twelve conserved lysines were mutated (Figure 8G). Taken together, these data indicate that the stability of endogenous DDRGK1 is maintained not by UFMylation, but by its interaction with UFL1. Along these lines, we found that DDRGK1's ability to promote ER-phagy was independent of its major reported site of UFMylation on Lys267 (Figure 8H, Figure 13H). Eleven other lysine mutants could also substantially support ER-phagy (Figure 13I-J), as could a DDRGK1 mutant with all twelve conserved lysines mutated (Figure 8H & Figure 13H).

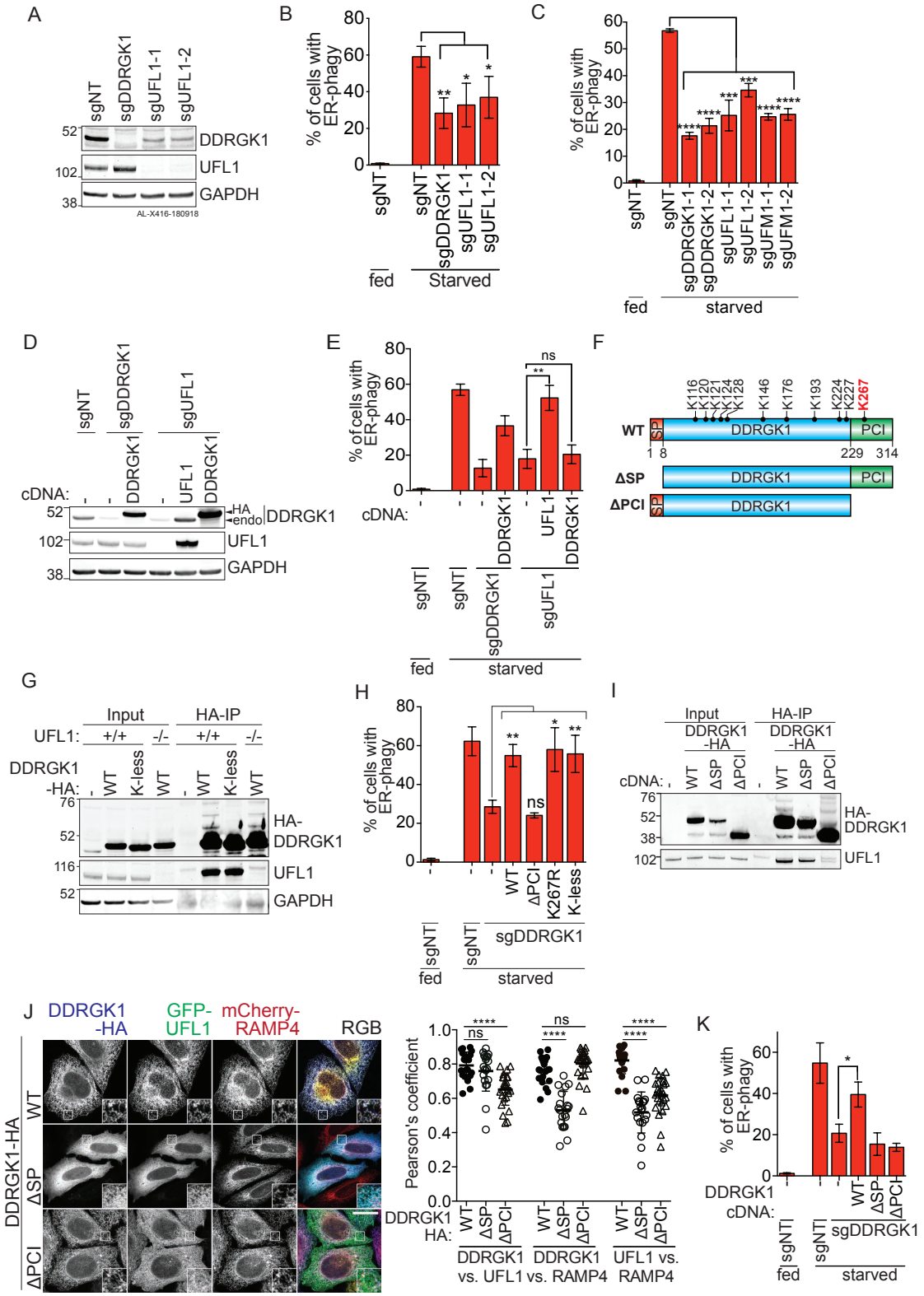

Figure 8: ER-phagy is mediated by DDRGK1-dependent UFMylation and ER localization

(A) UFL1 knockdown results in decreased DDRGK1 protein levels. HCT116 CRISPRi EATR cells were transduced with sgRNAs targeting either DDRGK1 or UFL1. Cells were harvested for Western blotting to assess the effect of UFL1 knockdown of DDRGK1 protein levels. (B) UFL1 knockdown phenocopies DDRGK1 knockdown and results in ER-phagy inhibition. The cells generated in (A) were starved for 16hr before FACS measurement for ER-phagy. P value indicates two-tailed unpaired t-test (*, $P < 0.05$, **, $P<0.01$). (C) UFMylation components, including UFL1, DDRGK1 and UFM1 are required for ER-phagy. HCT116 CRISPRi EATR cells expressing the indicated sgRNAs were starved for 16hr before FACS measurement for ER-phagy. P value indicates two-tailed unpaired t-test (***, $P < 0.001$, ****, $P<0.0001$). (D) Re-expression of UFL1 restores DDRGK1 protein levels. HCT116 CRISPRi EATR cells were transduced with sgRNAs targeting either DDRGK1 or UFL1. Cells were then further transduced with either DDRGK1-HA or HA-UFL1. Cells were harvested for Western blot analysis of DDRGK1 and UFL1 protein levels. (E) Re-expression of DDRGK1 in UFL1 knockdown cells does not rescue ER-phagy. The cell lines generated in (E) were starved for 16hr and then subjected to FACS measurement for ER-phagy. Data represents mean ± SD of three biological replicates. P value indicates two-tailed unpaired t-test (**, $P<0.01$). (F) Schematic of DDRGK1 domains and conserved Lysine residues. There are twelve conserved Lysine residues on DDRGK1. The reported Lysine residue that is a major site for UFMylation (K267) is labelled in red. Also shown are the two truncated forms of DDRGK1 that either lacks the N-terminal signaling peptide (ΔSP) or the C-terminal proteasome component (ΔPCI). (G) Post-translational modification of DDRGK1 occurs on lysine residues. Parental or UFL1 knock-out HCT116 cells were transfected with either wildtype (WT) DDRGK1-HA or the Lysine-less (K-less) DDRGK1-HA constructs. Cells were then harvested for immunoprecipitation of the HA-epitope and the higher molecular weight species of DDRGK1 is resolved by Western blotting. (H) DDRGK1's role during ER-phagy does not require post-translational modification on any lysine residue. HCT116 CRISPRi EATR cells were transduced with DDRGK1 sgRNA and then rescued using the indicated DDRGK1-HA mutant constructs. Cells were then starved for 16hr and ER-phagy was measured by FACS analysis. Data represents mean ± SD of three biological replicates. P value indicates two-tailed unpaired t-test (*, $P< 0.05$, **$P<0.01$). (I) DDRGK1 interacts with UFL1 via DDRGK1's PCI domain. Parental HCT116 cells were stably transfected with the indicated DDRGK1-HA mutant constructs. Cells were then harvested for HA-immunoprecipitation to determine the DDRGK1 domains that are required for UFL1 interaction. (J) DDRGK1 recruits UFL1 to the ER. DDRGK1 knock-out HeLa cells were stably transduced with mCherry-RAMP4 (ER marker) and the indicated DDRGK1-HA mutant constructs. Cells were then transiently transfected with GFP-UFL1 for 24hr. Cells were then fixed and immunostained for HA epitope. Representative images are shown. Insets represent three-fold enlargement of boxed areas. Scale bar represents 10μm. Pearson's Correlation coefficient was measured between DDRGK1 vs. UFL1, DDRGK1 vs. RAMP4, and UFL1 vs. RAMP4. Data was generated from one biological replicate and 20-26 cells were analysed from each condition. P-value indicates two-tailed unpaired t-test (****, $P<0.0001$). (K) DDRGK1's role during ER-phagy requires both the SP and PCI domains. HCT116 CRISPRi EATR cells with DDRGK1 knockdown were rescued using the indicated DDRGK1-HA mutant constructs. Cells were then starved for 16hr and ER-phagy was measured by FACS analysis. Data represents mean ± SD of three biological replicates. P value indicates two-tailed unpaired t-test (*, $P< 0.05$).

Using immunoprecipitation and immunofluorescence, we found that UFL1 interacts strongly with DDRGK1 and is localized to the ER (Figure 8I - J, Figure 14C). Deleting DDRGK1's N-terminal ER-targeting signal peptide (SP) still supported the DDRGK1-UFL1 interaction, but led to cytoplasmic localization of both DDRGK1 and UFL1 and did not support ER-phagy (Figure 8I-K, Figure 14A-C). Removing DDRGK1's C-terminal PCI protein-interaction domain led to normal ER localization of DDRGK1 (Figure 8J, Figure 14B), but abolished its interaction with UFL1 (Figure 8I, S5C). This led to cytoplasmic localization of UFL1 and abolished the cell's ability to perform ER-phagy (Figure 8J - K, Figure 14C).

Overall, we found that DDRGK1-dependent ER-phagy is not mediated by UFMylation of DDRGK1, as has been reported for DDRGK1's involvement in UPR and other signaling pathways (Lemaire et al., 2011; Yoo et al., 2014). Instead, ER-phagy is mediated by a functional interaction between DDRGK1 and UFL1 that recruits UFL1 to the ER. This suggested that UFMylation of some downstream ER-resident target(s) mediates ER-phagy. UFMylation is reported to stabilize the proteins it modifies (Cai et al., 2015; Egunsola et al., 2017; Liu et al., 2017; Wu et al., 2010; Yoo et al., 2014), and we knocked down previously reported substrates of UFL1, but found that none of them affected ER-phagy (Figure 14D-E).

We likewise found no evidence for DDRGK1-mediated UFMylation and stabilization of IRE1α (Figure 15A), which was previously reported to promote the UPR (Liu et al., 2017). However, we conversely found that depletion of DDRGK1, UFL1, or UFM1 in multiple cell types resulted in elevated levels of IRE1α (Figure 9A, Figure 15B-D). These results suggested that an inability to perform UFMylation-dependent ER-phagy could lead to upregulation of an ER stress response through IRE1α, which senses misfolded proteins in the ER lumen. Indeed, knockdown of UFMylation ER-phagy factors led to elevated levels of several other UPR proteins including PERK, BiP and CANX (Figure 9A, Figure 15B). We also observed an increase in levels of CLIMP63 (ER sheet marker) and REEP5 (ER tubule marker), suggesting ER expansion (Figure 9A, Figure 15B) (Schuck et al., 2009). Consistent with this idea, immunofluorescence of DDRGK1 CRISPR-Cas9 knockout HeLa cells showed increased CANX staining (Figure 14D-E). Knockdown of DDRGK1, UFL1, or both DDRGK1 and UFL1 led to modest but consistent transcriptional upregulation of the UPR transcripts PERK and BiP, increased differential splicing of XBP1, and transcriptional upregulation of CLIMP63 and REEP5 (Figure 9B). IRE1α showed higher protein levels upon DDRGK1 knockdown but no change in transcript abundance (Figure 9A-B), indicating that IRE1α protein levels could be post-translationally regulated in response to UFM1 signaling. The transcriptional upregulation of multiple UPR transcripts, differential splicing of XBP1, post-translational upregulation of IRE1α, and ER expansion are all consistent with increased ER stress and consequent UPR under conditions where UFMylation-dependent ER-phagy cannot be executed.

IRE1α senses unfolded proteins in the ER lumen and so is a good candidate to mediate stress signals caused by defective ER-phagy. We did not observe direct UFMylation of IRE1α under either fed or starved conditions (Figure 15A). But knockdown of IRE1α in DDRGK1 depleted cells reversed the high levels of ER stress markers caused by an inability to execute ER-phagy (Figure 15F). Knockdown of IRE1α had only a modest reciprocal effect upon ER-phagy, and only somewhat reversed the ER-phagy defect induced by loss of DDRGK1 (Figure 9C). Hence, UFMylation-induced ER-phagy is upstream of IREα signaling, further indicating that the loss of ER-phagy induces ER stress through the accumulation of unfolded proteins that are sensed by IRE1α.

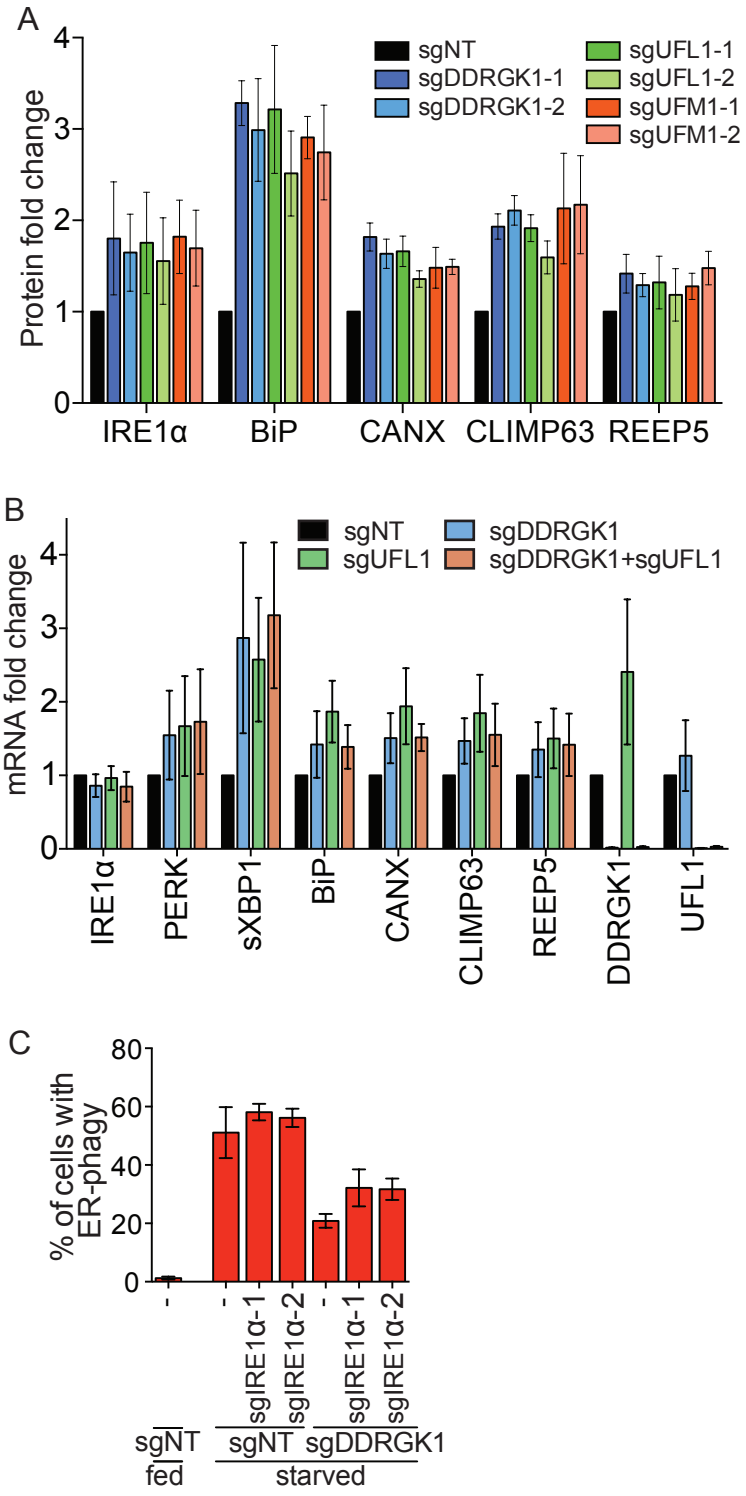

Figure 9: UFMylation-mediated ER-phagy represses IRE1α UPR
(A) Knockdown of DDRGK1, UFL1 or UFM1 results in upregulation of UPR and general ER protein levels. HCT116 cells were transduced with sgRNAs targeting DDRGK1, UFL1 and UFM1 (two sgRNAs per gene). Cells were harvested for Western blot analysis of the depicted

proteins. Graph represents densitometry measurement of the indicated proteins upon protein knockdown. Data represents mean ± SD of three biological replicates. A representative blot is shown in Figure 15B. (Note that Figure 15B is an expansion of Figure 13G). (B) Knockdown of UFL1 and/or DDRGK1 causes transcriptional upregulation of UPR and ER markers, except IRE1α. HCT116 CRISPRi cells were transduced with sgRNA targeting DDRGK1, UFL1 or both. Cells were then harvested for qRT-PCR measurement of the indicated ER or UPR genes. Data represents mean ± SD of three biological replicates. (C) Knockdown of IRE1α partially restores ER-phagy in DDRGK1 depleted cells. HCT116 CRISPRi EATR cells transduced with the indicated sgRNAs and then starved for 16hr before FACS measurement for ER-phagy. Data represents mean ± SD of three biological replicates.

Overall, our data indicate that DDRGK1-mediated, ER-resident UFMylation through UFL1 is critical for ER-phagy. DDRGK1 recruits UFL1 to the ER surface, analogous to the role of PINK1 substrates in recruiting Parkin to the mitochondria during mitophagy (Genschik et al., 2013; Léon and Haguenauer-Tsapis, 2009). We propose that the inability to UFMylate downstream ER substrates leads to an inability to execute ER-phagy, resulting in the consequent build-up of ER stress, and eventual activation of the unfolded protein response via IRE1α (Figure 15G).

3.5 Discussion

ER-phagy is a new and relatively unexplored branch of ER quality control that sends entire portions of the ER for destruction in the lysosome. Beyond a handful of ER-phagy receptors and ER remodeling proteins, knowledge of the logic and factors that regulate ER-phagy is still in its infancy. Our genome-wide ER-phagy screen provides a rich set of genes and pathways that are involved in ER-phagy. Among these, we identified several aspects of the core autophagy machinery, consistent with studies showing that ER-phagy shares effectors with general autophagy (Grumati et al., 2017; Khaminets et al., 2015; Smith et al., 2018). In particular, autophagosomal membrane activation and expansion separates ER-phagy from ERLAD, as the latter overrides the need for autophagosomal engulfment and instead forms ER-derived vesicles that directly fuse with lysosomes (Fregno et al., 2018). Moreover, ER-phagy and ERLAD pathways are activated by different upstream signals of starvation and proteasome-resistant protein aggregation, respectively.

So far, nutrient starvation is the only stress known to induce ER-phagy. We found that ER stress-inducing compounds do not lead to ER-phagy, but repression of ER-phagy by knockdown of DDRGK1 UFMylation induces ER stress and the UPR. UFMylation has previously been linked to ER stress through unclear mechanisms, which we now connect to inhibition of ER-phagy (DeJesus et al., 2016; Leto et al., 2019; Walczak et al., 2019). How is it that ER stress does not induce ER-phagy, but an inability to perform ER-phagy induces ER stress? Under nutrient depletion, protein misfolding may increase in the ER, but these signals are repressed as cells catabolize the protein- and lipid-rich organelle. Blocking ER-phagy could then result in the toxic accumulation of excessive ER and misfolded ER-resident proteins that cannot be sufficiently kept in check by ERAD, thus activating the UPR. Under this model, blocking ER-phagy leads to UPR as a byproduct of ER stress that is no longer relieved by eating portions of the ER. This hypothesis and ordered prioritization of ER stress-relief pathways will require a

great deal of investigation but could lead to a molecular rationale for why cells go to the extreme of ER-phagy.

We found extensive interplay between the mitochondria and ER-phagy. The ER and mitochondria exhibit crosstalk at membrane contact sites, including transfer and expansion of the lipid bilayer, Ca^{2+} homeostasis, and mitochondria division (Friedman et al., 2011; Lombardi and Elrod, 2017). The interactions previously described between the two organelles all indicate a regulatory role of ER processes towards mitochondrial homeostasis. We found that impairment of mitochondrial OXPHOS represses ER-phagy, demonstrating that mitochondrial metabolism can also inform decisions in the ER. It remains to be seen whether this ULK1-mediated communication is directly orchestrated via mitochondria-ER contacts or indirectly as a result of metabolic products. Alternatively, inhibition of OXPHOS could initiate an UPR that takes over to repress last-resort ER-phagy. Consistent with this idea, a recent screen for regulators of IRE1α found that knockdown of mitochondrial metabolism genes stimulates the UPR, though the mechanism remains to be determined (Adamson et al., 2016). Cellular energy levels are regulated by multiple energy sensing mechanisms that have complex roles during general autophagy (Egan et al., 2011; Herzig and Shaw, 2018; Kim et al., 2011). The interplay between mitochondrial metabolism and ER homeostasis will no doubt involve a similarly rich set of pathways.

We found that DDRGK1-mediated UFMylation at the ER surface is a key regulator of ER-phagy. Post-translational modifications of an organelle's surface are widely involved in organelle autophagy. For example, ubiquitination of PEX5 serves as a signal for peroxisomal autophagy (Nordgren et al., 2015; Zhang et al., 2015), and ubiquitination of multiple mitochondrial substrates promotes mitophagy (Chan et al., 2011; Karbowski and Youle, 2011). Since DDRGK1 recruits UFL1 to the ER surface and their combined ER-resident activity with UFM1 are all required for ER-phagy, we speculate that UFMylation of ER surface protein(s) serves as an effector of ER-phagy. This would be strikingly similar to PINK1's recruitment of the ubiquitin ligase Parkin to modify multiple mitochondrial surface proteins and initiate mitophagy (Chan et al., 2011; Glauser et al., 2011; Karbowski and Youle, 2011; Wang et al., 2011). UFMylation may play multiple cellular roles, and we have ruled out several previously reported UFMylation targets in the regulation of ER-phagy, though more substrates are still being uncovered (Walczak et al., 2019). In the case of mitophagy, a single causative ubiquitination substrate has remained elusive, and it remains to be seen if this will be the case for UFMylation-dependent ER-phagy.

While defects in ER-phagy have not been explicitly linked to human disease, we note that human mutations in ER-phagy genes such as FAM134B and Atlastins are associated with hereditary neuropathies in OMIM and ClinVar (Abel et al., 2004; Amberger et al., 2015; Kurth et al., 2009). This is similar to the mouse phenotype of FAM134B knockout (Khaminets et al., 2015). Several of the ER-phagy genes we identified by genome-wide screening are also associated with human neurodegenerative phenotypes with previously unclear mechanistic bases, such as Leigh Syndrome (mitochondrial OXPHOS, including ETC chaperones) (Lake et al., 2016), spastic paraplegia (ARL6IP1) (Novarino et al., 2014), encephalopathy (TRAPPC12) (Milev et al., 2017), spinocerebellar ataxia and encephalopathy (UBA5) (Daida et al., 2018; Mignon-Ravix et al., 2018), and severe early-onset encephalopathy and progressive microcephaly (UFC1, UFM1) (Nahorski et al., 2018). It is premature to broadly link deficits in ER-phagy to human disease, but the similar phenotypes stemming from mutations in different ER-phagy factors is provocative. Our work lays the foundation for future understanding of ER-

phagy and its interplay with the ER stress response, as well as the consequences of ineffective ER-phagy. Further mechanistic dissection of the 200 high-confidence ER-phagy regulators and executors identified here will hopefully shed light on this dramatic process.

3.6 Methods

Design, Production and titering of sgRNA library lentivirus

The genome-wide CRISPRi-V2 library was a gift from the Weismann lab (Addgene catalog #1000000093) and contains 5 sgRNAs per gene. For the pilot autophagy screen, we designed a comprehensive sgRNA library that targets all the reported TSS (10 gRNAs per TSS) of 31 genes that are involved in general autophagy. Overall, a total of 3301 gRNAs were designed (Table 2). The protospacer oligos were annealed and ligated to pCRISPRia vector (Addgene 84832) according to the protocol established by the Weissman lab (https://weissmanlab.ucsf.edu/CRISPR/Pooled_CRISPR_Library_Cloning.pdf) (Horlbeck et al., 2016). In addition, we added in 10% of a custom-built non-targeting sgRNA library prior to virus production.

The following paragraph describes the transfection protocol for one 15 cm plate of HEK293T cells. On Day 0, 7.5 x 10^6 HEK293T cells were seeded in a 15 cm plate in 20 mL of DMEM medium with 10% FBS. The following day HEK293T cells were transfected. In a 15 mL tube, 2.8 mL of Opti-MEM was mixed with 90 µL of Mirus LT1 transfection reagent and incubated at room temperature for 5 minutes. In an eppendorf tube, 12 µg of delta VPR, 3 µg of VSVG, and 15 µg of library plasmid were combined. The plasmids were then added to the Opti-MEM and Mirus mixture and incubated at room temperature for 20 minutes. The media was changed the following day. On Day 3, the virus was harvested using a 0.45 µm syringe filter, aliquoted into 1 mL tubes, and snap frozen. If more than one 15 cm plate of virus was produced for one library, the virus across those plates were pooled and mixed prior to aliquoting into eppendorf tubes. Virus was harvest on Day 4 as well.

Next, the virus was titered to determine the infectivity of the virus in the HCT116 cells. HCT116 were plated in a series of 6 well plates such that each well had cells and there was one 6 well plate per sub-library per time point (i.e. 48 or 72 hour virus harvest). One well on each plate was not transduced with any virus. The virus was titered such that is diluted 2-fold, 4-fold, 8-fold, 16-fold, and 32-fold. Polybrene was used at a concentration of 8 µg/mL. Fresh media were replaced 24hr post transduction. The cells were harvested 48 hours post viral transduction for flow cytometry and the percentage of BFP positive cells was recorded. The optimal virus dilution is defined as dilution-fold that results in less than 20% of BFP positive cells.

CRISPRi screen: cell generation, virus transduction, puro selection, and sort

HCT116 cells expressing a dcas9-KRAB and EATR reporter was constructed as described previously (Liang et al., 2018). The library contained seven unique sub-libraries and each sub-library was transduced separately, such that each sgRNA had an average of 500x coverage after transduction (Day 1). Puromycin selection for positively-transduced cells was performed 48 hours post transduction (Day 3). On Day 7, the sub-libraries were pooled proportionally based on the number of sgRNAs and cells were maintained at 500x coverage. On Day 10, cells were treated with doxycycline (4 µg/ml) for 16 hours to induce EATR expression and on Day 11, cells were treated with EBSS for 16 hours. Cells were then collected for sorting - cells were gated into the 25% of cells with most ER-phagy and 25% of cells with the least ER-phagy. A background population of cells was collected for downstream NGS analysis of relative enrichment. The entire CRISPRi screen was performed in two biological replicates.

NGS Sample Preparation and screen analysis

Genomic DNA was harvested using the Macherey-Nagel gDNA extraction protocol. The background samples required the XL kit whereas the midi kit was sufficient for sorted cells. After elution, the genomic DNA was treated with SbfI-HI restriction enzyme and incubated overnight at 37 °C to liberate the DNA fragment encoding the sgRNA sequences.

Samples were run an agarose gel and the gel piece around the 500 bp size (region containing the sgRNA sequence) was excised. The gel was melted in 55□ water bath and 1/100 by volume of 3 M NaAc (pH 5.2) was added to each tube and then solution was passed through an MN column. Each column was washed twice with NT3 buffer. The column was incubated for 5 minutes in 20 μL of heated elution buffer (98 °C) and then spun. The elution step was repeated so that the final elution volume was 40 μL.

A standard PCR protocol was used with Phusion High Fidelity Enzyme and 3% DMSO final concentration.The forward primer contained a TruSeq Index that would be subsequently used during NGS analysis. Before proceeding with a full scale PCR of the samples, a test PCR for each sample was run to determine the proper number of cycles (21, 23, or 25 cycles). The cycle number was identified individually for each sample that allowed a visible band on a TBE gel after staining with ethidium bromide, but not an oversaturated PCR product that could compromise the representation of gRNAs within the sample.

After the optimal cycle number was determine, a total of twelve 100 μL PCRs were done with 3 μL of template per reaction (from the abovementioned elution). The forward primer contained a TruSeq Index that would be subsequently used during NGS analysis. After completion of the PCR, the twelve reactions were pooled together and mixed. 300 μL of the pooled PCR was taken for subsequent PCR clean-up.

195 μL of SPRI beads was added to the pooled PCR and incubated at room temperature for 10 minutes. The samples were attached to a DynaMag for 5 minutes. The supernatant (which has the sample) was transferred to a new tube. 300 μL of SPRI beads were added and incubated for another 10 minutes. The samples were attached to a DynaMag for 5 minutes and the supernatant was discarded (samples attached to the beads). The beads were washed twice with 80% ethanol. After removal of the last supernatant, the beads were spun down, and excess ethanol was removed. The samples were air dried for 10 minutes and resuspended in 35 μL of water. DNA concentration was quantified using Qubit Fluorometric Quantitation (Thermo Fisher Scientific) and the samples were pooled proportionally to cell number and sequenced on a HiSeq 2500 such that each sgRNA sequence was covered at least 30 times.

Screening data was analyzed using standard protocols in MaGECK and ScreenProcessing (Horlbeck et al., 2016; Li et al., 2014, 2015). MaGECK was used for the pilot autophagy library, while ScreenProcessing was used for the genome-wide library. Briefly, gRNAs were quantified in each pool of cells based by matching reads back to the appropriate library reference, each pool was normalized by total number of reads, and gRNA distributions were compared to the background. Non-targeting gRNAs were explicitly used in each software package. MaGECK and ScreenProcessing integrate multiple gRNAs into gene-level phenotypes (e.g. $\log_2$-fold-change) and p-values using different approaches (Horlbeck et al., 2016; Li et al., 2014, 2015).

sgRNA plasmid cloning procedures for individual plasmids

The sgRNA sequences for genome-wide screening were based on the Weissman CRISPRi-v2 library and contained 5 sgRNAs per gene. The sgRNA sequences for autophagy-related genes used for the pilot test run were custom-designed to target all reported transcription start site (TSS) of each gene and contained 10 sgRNAs per TSS. sgRNA plasmids were cloned

by annealing and ligating sgRNA-containing short oligos to the CRISPRi-v2 vector (addgene 84832) via the previously described protocol (Horlbeck et al., 2016). Knockdown efficiency of each guide was measured either by western blot or qRT-PCR. All sgRNA constructs used in this study are detailed in Table 4.

shRNA plasmid cloning for DDRGK1

Short hairpin RNA (shRNA) was used to knockdown DDRGK1 in cell lines that do not express dCas9-KRAB constructs. Briefly, non-targeting (5'-CCTAAGGTTAAGTCGCCCTCG-3') and DDRGK1-targeting (5'-GGCTCTGCTAGTCGGCTTTAT-3') shRNAs were cloned into pLKO.1 puro construct (Addgene #8453) according to protocol described in Addgene (https://www.addgene.org/tools/protocols/plko/?gclid=Cj0KCQiAm5viBRD4ARIsADGUT25ZCGNPeQSFvLqSwvg2tHDkCc9zOZsLdaUffZzNTRYzI_YOlKFVQdUaAqbfEALw_wcB)

cDNA plasmid cloning procedures

The open reading frame (ORF) of the constitutively active-AMPK construct (CA-AMPK) was sub-cloned from addgene #27632 (Egan et al., 2011). The AMPK kinase dead (AMPK-KD) plasmid was a Lys-to-Arg mutation at position K47R (AAG to CGG) generated by extension PCR followed by Gibson Assembly (Gibson et al., 2009). The pBMN-YFP-Parkin construct was from Addgene (Addgene #59416). Unless stated otherwise, all remaining ORFs described in this article were obtained from PCR amplification of pooled HCT116 cDNA. The ORFs were cloned into pLenti-XI destination vector with neomycin resistance. Briefly, an original pLenti-X1-Neo-eGFP-LC3B vector was first digested with restriction enzymes BamHI and XbaI to remove the insert. Then, Gibson Assembly was used to insert the gene-of-interest and the desired epitope or fluorescent tag into the pLenti-X1 vector. All overexpression constructs used in this study are detailed in Table 5.

Cell culture

Cells were cultured at 37 °C with 5% CO_2 in a humidified atmosphere. All cells were cultured in DMEM-GlutaMAX medium supplemented with 10% FBS, 0.1 mM non-essential amino acids (Gibco), 1 mM sodium pyruvate (Gibco), 100 U/mL penicillin (Gibco), and 100 g/mL streptomycin (Gibco). Cell lines were obtained from the Berkeley Cell Culture Facility and were verified mycoplasma free with MycoAlert Mycoplasma Detection Kit (Lonza).

Lentiviral packaging and transduction

Lentiviral packaging was performed in HEK293T cells using either TransIT-LT1 Transfection Reagent (Mirus) or Lipofectamine 3000 (ThermoFisher Scientific) according to the manufacturer's protocol. For more details, refer to previously described methods (Liang et al., 2018).

Knockout Cell Line Generation

AMPK knockout cell lines were generated using Cas9 RNPs and nucleofection as detailed previously (Lingeman et al., 2017). The sgRNA protospacer sequences were validated and used previously by the Shaw lab (Toyama et al., 2016). The protospacer sequences are as follow: AMPKα1-sgRNA1- GGCTGTCGCCATCTTTCTCC; AMPKα1-sgRNA2- GAAGATCGGCCACTACATTC; AMPKα2-sgRNA1- TCAGCCATCTTCGGCGCGCG; AMPKα2-sgRNA2- GAAGATCGGACACTACGTGC. After nucleofection, HCT116 cells were

serial diluted into 96 well plates such that there was on average of 0.7 cells/well. AMPK KO clones were screened by Western blotting. DDRGK1 and UFL1 knockout cell lines were generated by transient transfection of two pSpCas9(BB)-2A-GFP (PX458) (Addgene #48138) plasmids carrying sgRNAs that each target the downstream and upstream regions of the transcription start site. The protospacer sequences are as follow: DDRGK1-sgRNA1- ATGAGATCCCGGCCTCAGGG; DDRGK1-sgRNA2- TAGGAGATGCCGCTGCACCA; UFL1-sgRNA1- CTGACTCGCAGTAGACGCGG; UFL1-sgRNA2- GCCTAATT TGGGCTCCACAA. GFP-positive cells were single-cell sorted 48hrs post transfection and DDRGK1/UFL1 KO clones were screened by Western blotting.

Flow Cytometry Analysis of EATR cells

Flow cytometry of EATR assay was performed using an Attune NxT Flow Cytometer and subsequent analysis was performed using FlowJo 10.1 (Liang et al., 2018). All EATR experiments were performed using live cells to prevent reversal of eGFP quenching post-fixation. The intensities for both eGFP and mCherry of the EATR cells at fed condition were used as references to define the gate for zero ER-phagy events. Following stimulation, ER-phagy detection is based on the shift of cell population into the ER-phagy gate. On average, 5 to 10,000 cells were analyzed per condition and all statistical analyses were performed using data from at least three biological replicates.

Cell Treatments

ER-phagy was induced with media starvation using EBSS with calcium, magnesium, and phenol red (Invitrogen 10043). For EATR and CCER assays, cells were plated 48 hours prior to EBSS treatment. EATR expression is induced using 4 μg/ml doxycycline 24 hrs prior to starvation. Unless otherwise stated, starvation treatment was carried out for 16 hours. Cells in fed conditions indicate incubation in complete DMEM described above.

For all experiments except the Seahorse assay, rotenone was used at a final concentration of 3 μM, antimycin A was used at a concentration of 0.5 μM, and oligomycin A was used at a concentration of 3 μM. Cells were treated with these drugs in two phases for a total of 40 hours. First, cells were treated for 24 hours with complete DMEM, then immediately treated again for 16 hours in EBSS media or complete DMEM. Epoxomicin and folimycin treatments were co-administered with EBSS starvation at 100 nM final concentration.

Quantitative real-time PCR (qRT-PCR)

RNA extraction was performed using Directzol RNA miniprep kit (Zymo Research) according to manufacturer's instruction. 1μg of RNA per sample were used for reverse transcription using SuperScript™ III First-Strand Synthesis System (Invitrogen) according to manufacturer's instruction. qRT-PCR reaction was set up using Fast SYBR Green Mastermix (Applied Biosystems) and run in triplicates using StepOne Plus Real-Time PCR system (Applied Biosystems) (Liang et al., 2018). A complete list of all primers used are compiled in Table 6.

Western blotting

To prepare samples for western blot, cells were lysed in RIPA buffer (Millipore), supplemented with Halt Protease Inhibitor Cocktail and Phosphatase Inhibitor Cocktail (both ThermoFisher). Cells were lysed on ice for 30 minutes and spun at 14000 rpm for 10 minutes to remove insoluble debris. Protein concentrations were quantified by Bradford assay. Lysates were

normalized based on protein concentration and NuPage LDS Sample Buffer (4x) was added (Invitrogen). Samples were boiled at 98°C for 5 minutes.

Between 40-50µg of samples were run on NuPAGE Bis-Tris 4–12% gels in NuPage MES SDS Buffer (Invitrogen) for 40 minutes at 200 V and transferred to 0.4-µm nitrocellulose membranes using a semi-dry transfer system (Bio-Rad Catalog #1704150) at 1.3 A and 25 V for 15 minutes. After transfer, membranes were blocked with 5% (w/v) milk in TBS-T for 30 minutes, and subsequently washed with TBS-T three times. Primary antibodies were diluted at the appropriate concentration in 5% BSA (w/v) in TBS-T. The membrane was incubated in primary antibody for either 1-2 hours at room temperature or overnight at 4°C. The membrane was washed with TBST three times for five minutes each. The blots were incubated for 30 minutes in the milk solution with a 1:10,000 dilution of Li-Cor near-infrared fluorescence secondary antibodies. The blots were scanned using Li-Cor's Near-InfraRed fluorescence Odyssey CLx Imaging System, and quantifications were done using LiCor's ImageStudio software complementary of Odyssey.

Immunofluorescence

Immunofluorescence was conducted as previously described (Liang et al., 2018). Briefly, cells were fixed in 4% (wt/vol) paraformaldehyde for 15 min followed by permeabilization using 0.1% Triton-X100 in PBS for 10 min. Cells were then blocked in 1% BSA in PBS for 20 min. Primary antibodies were incubated for 1hr at room temperature, followed by three PBS washes for 5min each. Secondary antibodies were incubated for 30 min at room temperature, followed by three PBS washes for 5min each. Coverslips were mounted onto glass slides using ProLong Gold Antifade reagent with or without DAPI addition for nucleus visualization. Images were taken using either Zeiss LSM 710 Axio Observer (in Berkeley) or Leica TCS SP8 confocal microscope (in ETH Zurich) with 63x objective lens and post-processed in Adobe Photoshop for specific inset enlargement and RGB channel separation. Colocalization analysis in Figure 6J was determined by Pearson's Correlation coefficient using ImageJ with colocalization plugin from McMaster Biophotonics Facility (MBF). The frequency scatterplot in Figure 14C was generated using the same plugin.

Primary and secondary antibodies for Western blotting and immunofluorescence

All primary and secondary antibodies used were detailed in Table 7.

MitoTracker

The MitoTracker assay was performed according the manufacturer's protocol (ThermoFisher Catalog #M7512). Cells were plated 48 hours before starvation. Cell starvation and drug concentrations was performed according to protocols described above. The MitoTracker Red CMXRos was dissolved in DMSO for a stock concentration of 1 mM. MitoTracker was added to samples such that the concentration in each well was 50 nM. The cells were incubated for 30 minutes, washed with media, and then fixed in 4% formaldehyde. The cells were stained with calnexin according to the immunofluorescence protocol.

ATP Assay

The assay was performed according to the manufacturer's protocol for the CellTiter-Glo 2.0 reagent (Promega). Briefly, the cells treated with starvation were starved for 25 hours. The cells treated with rotenone or antimycin A were used as positive controls and cells were treated

for 1 hour. Cells were harvested, washed with PBS, and counted and normalized. The cells were spun down again and resuspended such that there were 25,000 cells per 50 μL of PBS. 50 μL of PBS was added to each well in an opaque-walled 96-well plate. Each sample was done in technical triplicate. Wells with PBS, but no cells, were used as a blank control. 50 μL of CellTiter-Glo 2.0 reagent was added to each well. The plate was placed on an orbital shake for 2 minutes, followed by a 10 minute bench-top incubation to stabilize the signal. Sample luminescence was determined by the SpectraMax M2 Microplate Reader (Molecular Devices).

Mitochondrial Respiration Measurements

Mitochondrial activity was determined using the Seahorse Flux Analyzer XF24 according to the manufacturer's protocol. Briefly, 4 X 10^4 HCT116 cells were seeded on XF24-well cell culture microplates. After 24hr, growth medium was exchanged with XF assay base medium supplemented with 1 mM sodium pyruvate, 2mM L-glutamine, and 10mM D-glucose (pH 7.4). The microplates were incubated at 37°C without CO_2 for 1 hr prior to the assay. Samples were mixed for 3 min, time delayed for 2 min, and measured for 3 min. Oligomycin (1 μM), FCCP (1 μM), and rotenone / antimycin (0.5 μM) were sequentially injected at the indicated time points. OCR data were normalized by protein concentration and the average values were taken for each experiment. Seven replicates were performed for each cell line. The mean +/- SEM was determined and statistical significance was evaluated using the Student's *t* test with a P value <0.05.

Statistical analysis

All analysis was performed using data from three independent analysis, unless otherwise stated. Statistical analyses were performed in PRISM6 software using either paired Student's *t*-test or ANOVA and are indicated in the figure legend.

3.7 Supplemental Figures

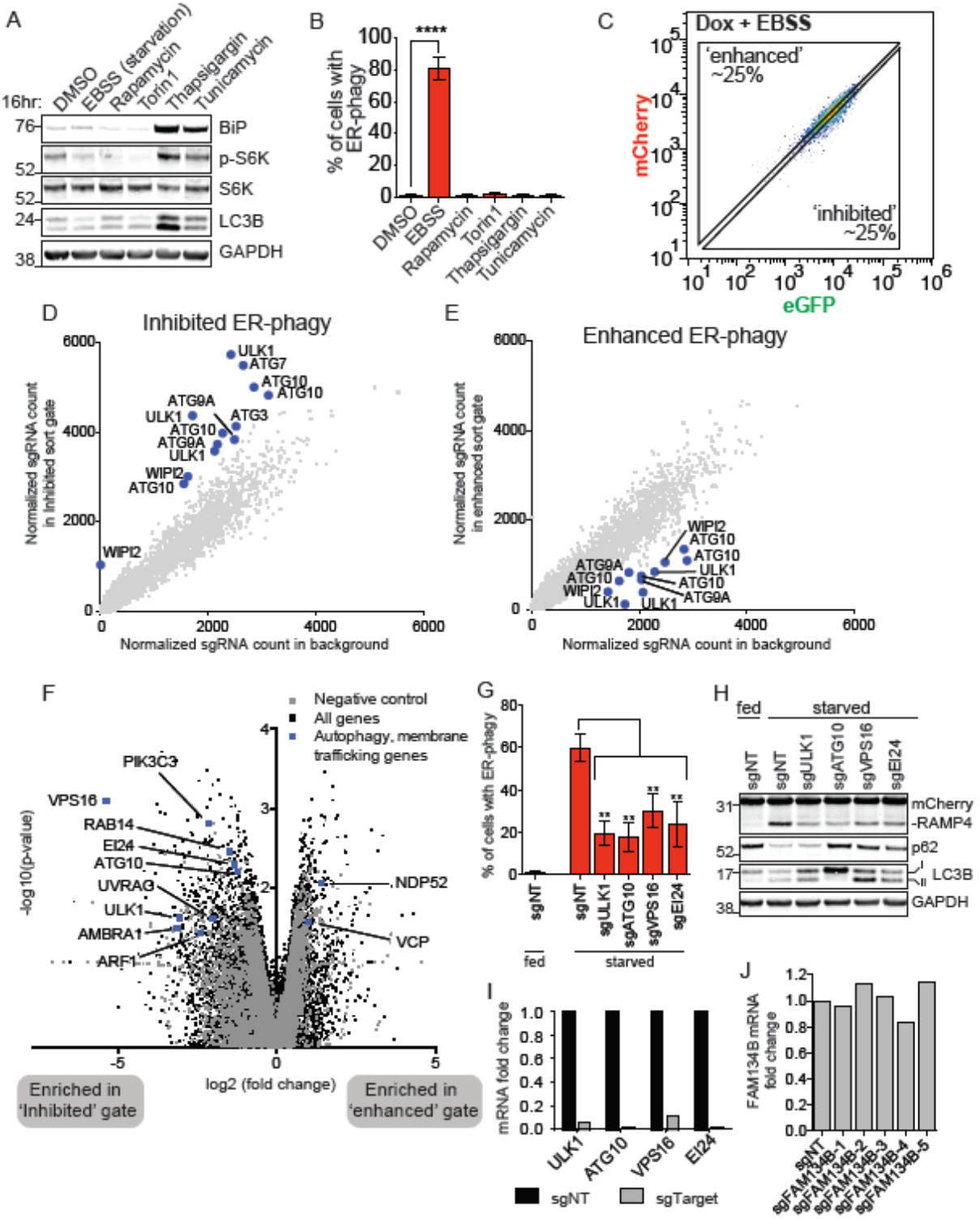

Figure 10: Related to ER-phagy screen

(A) EBSS (amino acid starvation), rapamycin, and Torin1 show a decrease in p-S6K while thapsigargin inhibits LC3B turnover. HCT116 EATR cells were treated with the indicated media or drugs (Rapamycin: 1μM, Torin1: 10μM, Thapsigargin: 1μM, Tunicamycin: 0.5μg/ml) for 16hr. Cells were then harvested for Western blotting to check for UPR and autophagy response. (B) Only starvation (using EBSS) inhibits ER-phagy. The same cells and treatment conditions in Figure 10A were also subjected to FACS measurement of ER-phagy. Data represents mean ± SD of three biological replicates. P value indicates two-tailed unpaired t-test (****, P< 0.0001). (C) Gating strategy for ER-phagy screen. HCT116 CRISPRi EATR cells transduced with the CRISPRi library of sgRNAs were starved for 16hr and subjected for FACS measurement for ER-phagy. Based on the EATR assay, the top and bottom 25% of cells correspond to sgRNA knockdown that results in 'enhanced' and 'inhibited' ER-phagy, respectively and were processed for next generation sequencing of sgRNA barcode. (D) Multiple autophagy genes (highlighted in blue) were enriched in the 'inhibited' ER-phagy sort gate. The normalized sgRNA count from the 'Inhibited' ER-phagy sort gate was plotted against the normalized sgRNA count of the background sample. The labelled genes are enriched in the 'Inhibited' ER-phagy gate upon knockdown and indicate active transcription start sites (TSS) that are being used in HCT116 cells. (E) Autophagy genes (highlighted in blue) that are depleted in the 'enhanced' ER-phagy sort gate corresponds to the genes that are enriched in the 'inhibited' sort gate of (D). (F) Autophagy and membrane trafficking genes are hits in the ER-phagy screen. Those genes that are significantly enriched in either the 'inhibited' or 'enriched' gate are indicated in blue. Volcano plot describes data from the genome-wide CRISPRi screen. All negative control sgRNAs are indicated in grey and targeted sgRNAs are indicated in black. Data were generated from two biological replicates. log2 fold change and Mann-Whitney P-value were calculated as described (Horlbeck et al. 2016). (G) Knockdown of genes involved in general autophagy also inhibit ER-phagy. HCT116 CRISPRi EATR cells were transduced with sgRNAs targeting the indicated candidate genes reported from the CRISPRi genome wide screen. Cells were starved for 16hr and subjected to FACS measurement for ER-phagy. Data represents mean ± SD of three biological replicates. P value indicates two-tailed unpaired t-test (**, P< 0.01). (H) CCER assay complements the EATR data in Figure 10G. HCT116 CRISPRi CCER cells were also transduced with the same sgRNAs as Figure 10G. Cells were then starved for 16hr and harvested for Western blot analysis and immunoprobed for two general autophagy markers, p62 and LC3B. (I) The same cell lines in Figure 10H were harvested for qRT-PCR analysis to measure the knockdown efficiency of individual sgRNAs. (J) The FAM134B sgRNAs used in this CRISPRi screen do not effectively knock down FAM134B. HCT116-CRISPRi EATR cells stably expressing FAM134B sgRNAs were harvested for qRT-PCR to determine the knockdown efficiency.

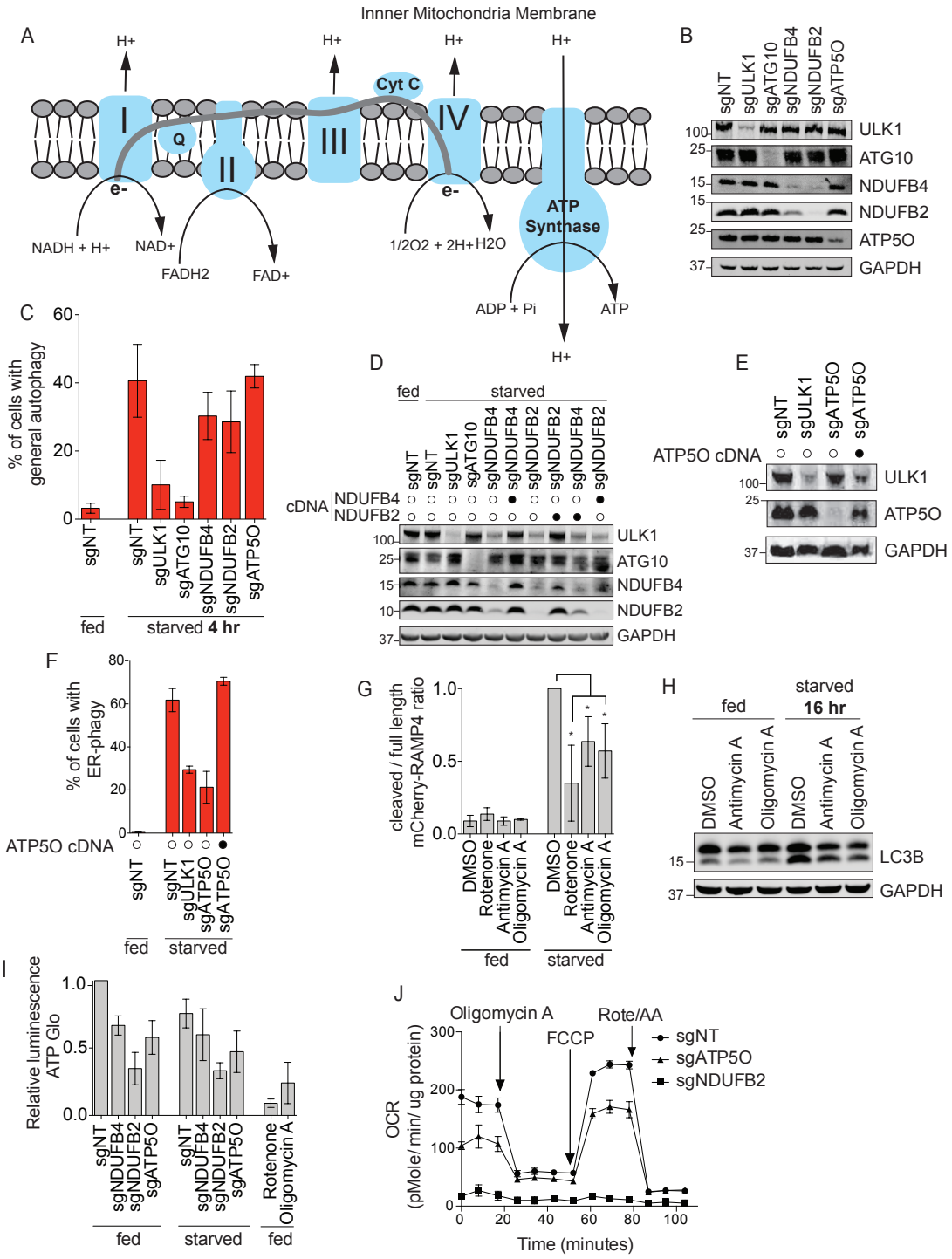

Figure 11: Related to OXPHOS regulation of ER-phagy

(A) Schematic of the oxidative phosphorylation (OXPHOS) pathway. (B) Cells from Figure 4B were harvested to assess the knockdown efficiency of each sgRNA by Western blotting. (C) Knockdown of ULK1 and ATG10 inhibits general autophagy after 4 hours of starvation while NDUFB4, NDUFB2, and ATP5O does not. HCT116 CRISPRi cells expressing eGFP-mCherry-LC3B were transduced with sgRNAs targeting either ULK1, ATG10, NDUFB4, NDUFB2, or

ATP5O. Cells were starved for 4hr before FACS measurement for general autophagy. Data represents mean ± SD of four biological replicates. (D) Cells from the same experiment as Figure 4D were harvested for Western blot analysis to verify the protein levels of ULK1, ATG10, NDUFB4 and NDUFB2. (E) Cells from the same experiment as Figure 11F were harvested for Western blot analysis to verify the protein levels of ULK1 and ATP5O. (F) Knockdown of ATP5O inhibits ER-phagy, but ATP5O cDNA rescues ER-phagy. HCT116 CRISPRi EATR cells were transduced with ATP5O cDNA constructs, and then transduced with sgRNAs targeting ULK1 or ATP5O. Cells were starved for 16hr before FACS measurement for ER-phagy. Data presented as mean ± SD of three biological replicates. (G) Rotenone, antimycin A, and oligomycin A significantly inhibit ER-phagy during starvation. Densitometry measurement of the ratio between the cleaved and full length mCherry-RAMP4 in Figure 5C. Data represents mean ± SD of three biological replicates. P value indicates two-tailed unpaired t-test (*, $P < 0.05$). (H) General autophagy is unaffected by antimycin A and oligomycin A treatment in starvation conditions. HCT116 cells were treated with the indicated small molecule inhibitors of antimycin A, or oligomycin A for 24hr and then were subsequently starved for 16hr with treatment of small molecule inhibitors. Cells were lysed for Western blotting and immunoprobed for the indicated proteins. (I) NDUFB2, NDUFB4 and ATP5O depletions affect cellular ATP levels. HCT116 CRISPRi cells were transduced with sgRNAs targeting either NDUFB4, NDUFB2, or ATP5O and starved for 16hr or treated with rotenone or oligomycin A. Cells were collected for ATP Glo luminescence assay. Data represents mean ± SD of three biological replicates. (J) Oxygen consumption is reduced in NDUFB4, NDUFB2, and ATP5O knockdown cells. HCT116 CRISPRi cells were transduced with sgRNAs targeting either NDUFB2 or ATP5O and the Seahorse Flux Analyzer was conducted to determine the oxygen consumption rate.

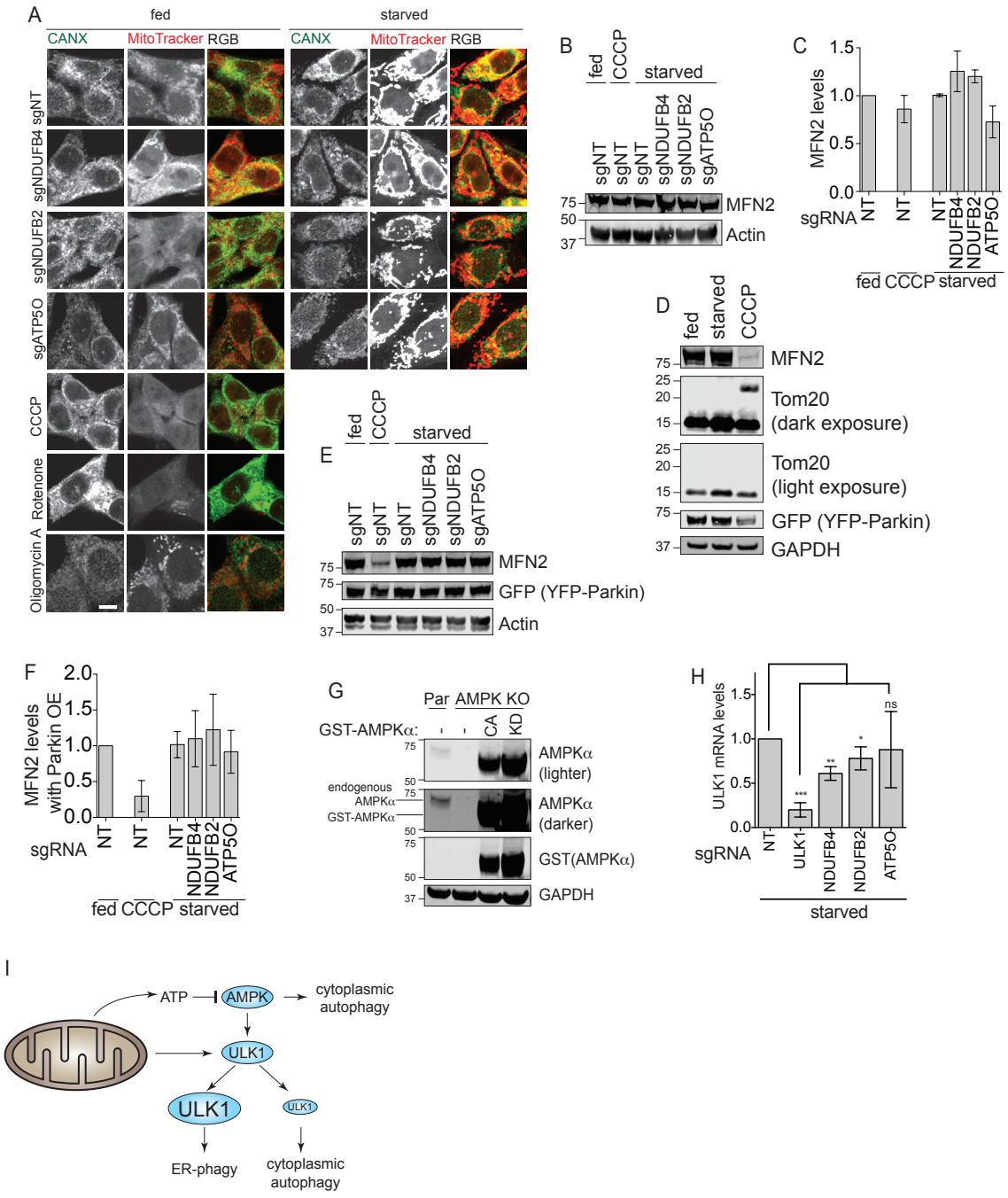

Figure 12: Mitophagy and mitochondrial health
(A) sgNDUFB4, sgNDUFB2, and sgATP5O showed no major differences in MitoTracker staining compared to sgNT. HCT116 CRISPRi cells were transduced with sgRNAs targeting either NDUFB4, NDUFB2, or ATP5O or treated with indicated small molecule inhibitors. Cells were subsequently treated with MitoTracker, then fixed and immunostained for calnexin. Representative images are shown. Scale bar represents 10μm. (B) Disruption of the OXPHOS pathway does not induce mitophagy based on the protein levels of MFN2. HCT116 CRISPRi cells were transduced with sgRNAs targeting either NDUFB4, NDUFB2, or ATP5O and starved

for 16hr or treated with CCCP. Cells were harvested for western blot analysis and immunoprobed for the indicated proteins. A representative western blot is shown. (C) Densitometry measurement of the ratio between MFN2/actin from Figure 12B. Data represents mean ± SD of two biological replicates. (D) HCT116 CRISPRi were transduced with YFP-Parkin construct and treated with starvation or CCCP (10 uM) for 16hr. Cells were harvested for Western blot analysis and immunoprobed for the indicated proteins to verify mitophagy in CCCP-treated cells. (E) MFN2 is not degraded in Parkin overexpression cell lines. HCT116 CRISPRi-YFP-Parkin cells were transduced with sgRNAs targeting either NDUFB4, NDUFB2, or ATP5O and starved for 16hr or treated with CCCP. Cells were harvested for Western blot analysis and immunoprobed for the indicated proteins. A representative western blot is shown. (F) MFN2 is not degraded in Parkin overexpression cell lines during OXPHOS disruption. Densitometry measurement of the ratio between MFN2/actin from Figure 12E. Data represents mean ± SD of three biological replicates. (G) AMPKα knockout cell lines stably expressing either catalytically active (CA) or kinase dead (KD) AMPKα were generated to test the role of AMPK in ER-phagy. "Par" represents HCT116 CRISPRi EATR cells. AMPKα KO (knockout) cells were generated using CRISPR/Cas9 (sgRNA sequences and methods are described in the methods section). GST-AMPKα-CA (catalytically active) was re-expressed in the AMPKα KO background. Note that the catalytically active AMPKα is a truncation form of AMPKα, resulting in the smaller size. GST-AMPKα-KD (kinase dead) is derived from GST-AMPKα-CA with a K47R point mutation. (H) ULK1 mRNA levels are significantly reduced during starvation when NDUFB4 and NDUFB2 are knocked down. HCT116 CRISPRi EATR cells were transduced with sgRNAs targeting ULK1, NDUFB4, NDUFB2, or ATP5O and starved for 16hr. RNA was extracted and cDNA was synthesized for qRT-PCR. Data presented as mean ± SD of three biological replicates. P value indicates two-tailed paired t-test (*, $P < 0.05$, **, $P < 0.01$, ***, $P < 0.001$). (I) Schematic representation of the interplay between mitochondrial metabolism, ULK1, and ER-phagy. Disruption of the mitochondrial OXPHOS pathway results in decreased ATP levels and leads to activation of cytoplasmic autophagy. In parallel, impairment of the mitochondrial OXPHOS also transcriptionally lowers ULK1 levels to an extent that inhibits ER-phagy while still permits cytoplasmic autophagy to take place.

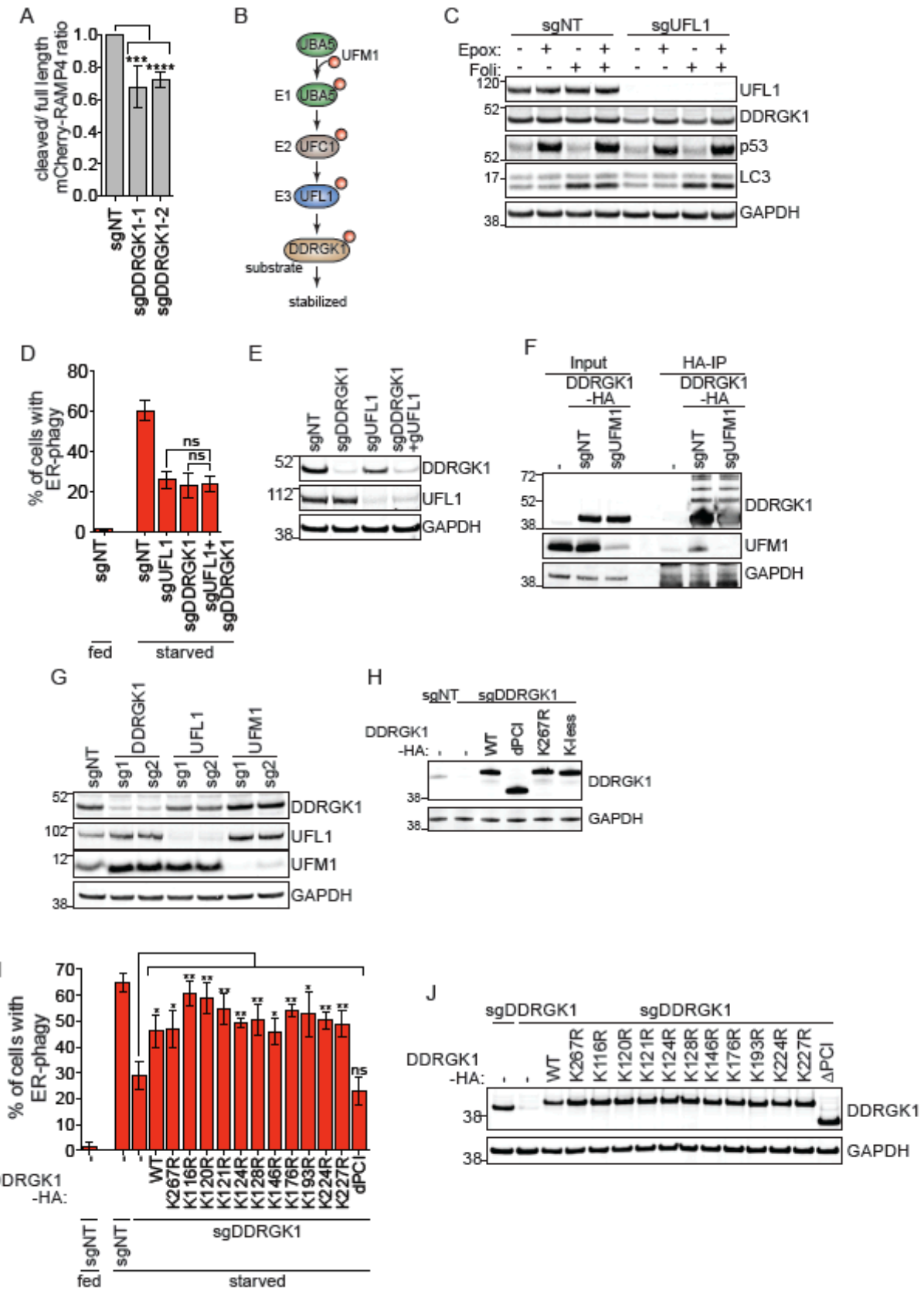
A
cleaved/ full length mCherry-RAMP4 ratio
1.0
0.8
0.6
0.4
0.2
0.0
***
****
sgNT
sgDDRGK1-1
sgDDRGK1-2
B
UBA5
UFM1
E1
UBA5
E2
UFC1
E3
UFL1
DDRGK1
substrate
stabilized
C
sgNT
sgUFL1
Epox:
Foli:
120
52
52
17
38
UFL1
DDRGK1
p53
LC3
GAPDH
D
% of cells with ER-phagy
80
60
40
20
0
ns
ns
sgNT
sgNT
sgUFL1
sgDDRGK1
sgUFL1+ sgDDRGK1
fed
starved
E
sgNT
sgDDRGK1
sgUFL1
sgDDRGK1 +gUFL1
52
112
38
DDRGK1
UFL1
GAPDH
F
Input
HA-IP
DDRGK1 -HA
DDRGK1 -HA
sgNT
sgUFM1
sgNT
sgUFM1
72
52
38
38
DDRGK1
UFM1
GAPDH
G
sgNT
DDRGK1
sg1
sg2
UFL1
sg1
sg2
UFM1
sg1
sg2
52
102
12
38
DDRGK1
UFL1
UFM1
GAPDH
H
sgNT
sgDDRGK1
DDRGK1 -HA:
WT
dPCI
K267R
K-less
38
38
DDRGK1
GAPDH
I
% of cells with ER-phagy
70
60
50
40
30
20
10
0
DDRGK1 -HA:
WT
K267R
K116R
K120R
K121R
K124R
K128R
K146R
K176R
K193R
K224R
K227R
dPCI
ns
sgNT
sgNT
sgDDRGK1
fed
starved
J
sgDDRGK1
sgDDRGK1
DDRGK1 -HA:
WT
K267R
K116R
K120R
K121R
K124R
K128R
K146R
K176R
K193R
K224R
K227R
ΔPCI
38
38
DDRGK1
GAPDH

Figure 13: DDRGK1 knockdown inhibits ER-phagy
(A) Densitometry measurement of the ratio between the cleaved and full length mCherry-RAMP4 in Figure 7C. Data represents mean ± SD of five biological replicates. P value indicates two-tailed unpaired t-test (***, $P < 0.001$, ****, $P<0.0001$). (B) Schematic illustration of the three-step enzymatic reaction of the UFMylation cascade. UBA5 acts as an E1 enzyme to activate UFM1 and UFC1 acts as an E2 conjugating enzyme that interacts with the E3 ligase, UFL1. UFL1 recognizes and transfer UFM1 from UFC1 to its target substrate. In this case, DDRGK1 is reported as a substrate of UFMylation. (C) UFL1 protein expression prevents DDRGK1 degradation via the proteasomal degradation pathway. HCT116 CRISPRi cells were transduced with sgRNA targeting UFL1. Cells were treated with Epoxomicin (100nM) or Folimycin (100nM) for 6hr and then harvested for Western blot analysis. p53 and LC3B were used as positive controls for proteasomal and lysosomal inhibitions, respectively. (D) UFL1 and DDRGK1 act in series during ER-phagy. HCT116 CRISPRi EATR cells were transduced with the indicated sgRNAs and then starved for 16hr before FACS analysis for ER-phagy. Data represents mean ± SD of three biological replicates. Statistical significance was determined based on two-tailed unpaired t-test. (E) The same cell lines in Figure 13B were harvested for Western blotting to verify knockdown of targeted genes. (F) Knockdown of UFM1 does not prevent the appearance of higher molecular weight species of DDRGK1. HCT116 CRISPRi cells stably expressing DDRGK1-HA construct were transduced with sgRNA targeting UFM1. Cells were then harvested for HA-immunoprecipitation and Western blotted for the indicated proteins. (G) Knockdown of UFL1 but not UFM1 reduces DDRGK1 protein levels. HCT116 CRISPRi EATR cells used in Figure 8C were harvested for Western blotting to assess the protein levels of DDRGK1 upon knockdown of the targeted genes. (H) The cDNA of DDRGK1-HA mutant variants in Figure 8F were stably expressed in HCT116 cells to verify their respective protein sizes in DDRGK1 knockdown cells. (I) All individual Lysine mutant constructs of DDRGK1 are able to rescue ER-phagy in DDRGK1 knockdown cells. HCT116 CRISPRi EATR cells with sgDDRGK1 were transduced with the indicated DDRGK1-HA mutant constructs. Cells were then starved for 16hr before FACS measurement of ER-phagy. Data represents mean ± SD of three biological replicates. P value indicates two-tailed unpaired t-test. (*, $P<0.05$, **, $P< 0.01$). (J) The cell lines generated for Figure 13I were harvested for Western blotting to verify the expression of the indicated DDRGK1-HA mutant constructs.

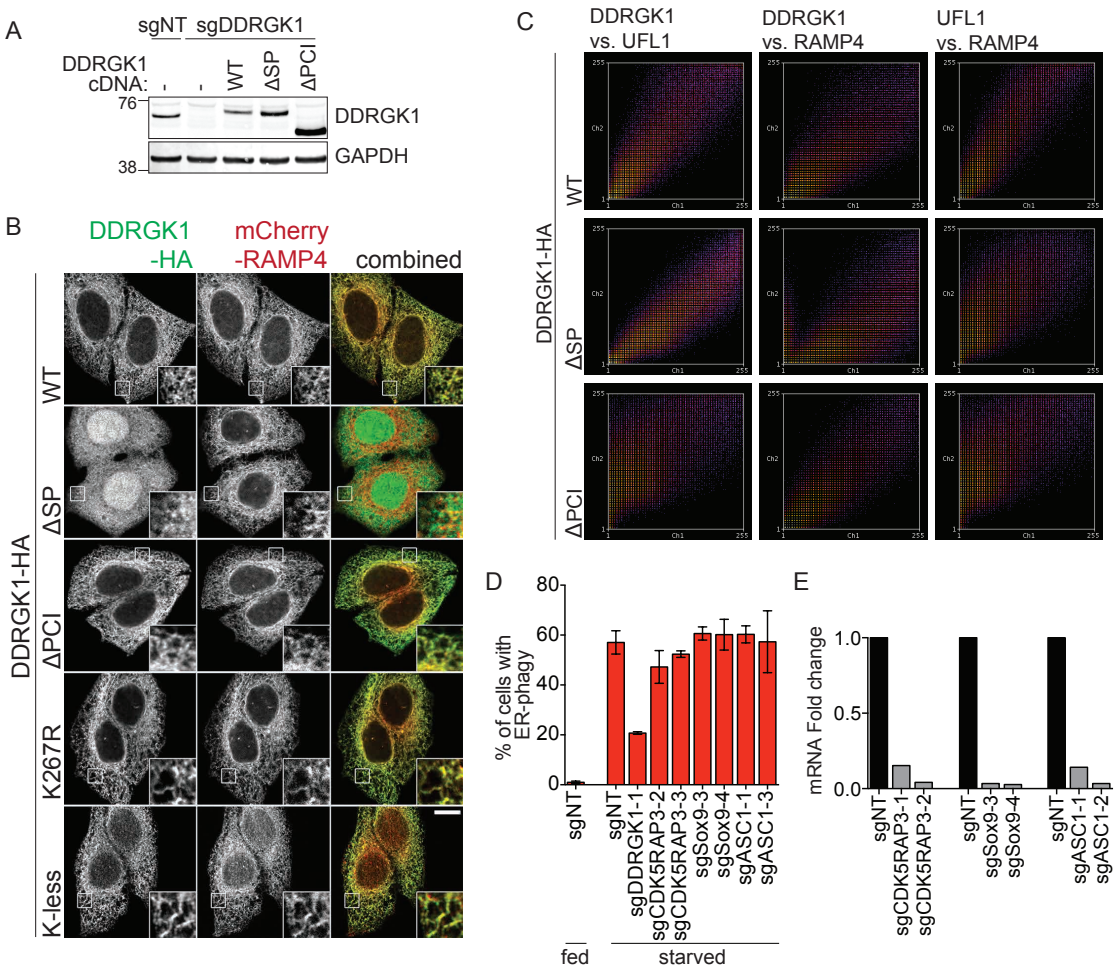

Figure 14: DDRGK1 localization
(A) The cell lines generated for Figure 8K were harvested for Western blotting to verify the expression of the indicated DDRGK1-HA mutant constructs. (B) The ER signaling peptide (SP) of DDRGK1 is required for its localization to the ER. HeLa cells stably expressing mCherry-RAMP4 were transduced with the indicated DDRGK1-HA constructs. Cells were then fixed and stained for HA-epitope. Insets represent three-fold enlargement of the boxed areas. Scale bar represents 10µm. (C) Additional colocalization data analysis of Figure 8J for DDRGK1, UFL1 and the ER marker, RAMP4 based on frequency of colocalization. Conditions with good or near perfect colocalization have good correlation between the X- and Y-axes. Representative frequency scatterplot from each condition is presented. (D) None of the previously reported targets of UFMylation are involved in ER-phagy regulation. HCT116 CRISPRi EATR cells were transduced with sgRNAs targeting CDK5RAP3, Sox9 or ASC1 and starved for 16hr before FACS measurement of ER-phagy. Data represents mean ± SD of three biological replicates. (E) The same cell lines used in Figure 14D were harvested for qRT-PCR to assess the knockdown efficiency of each sgRNA.

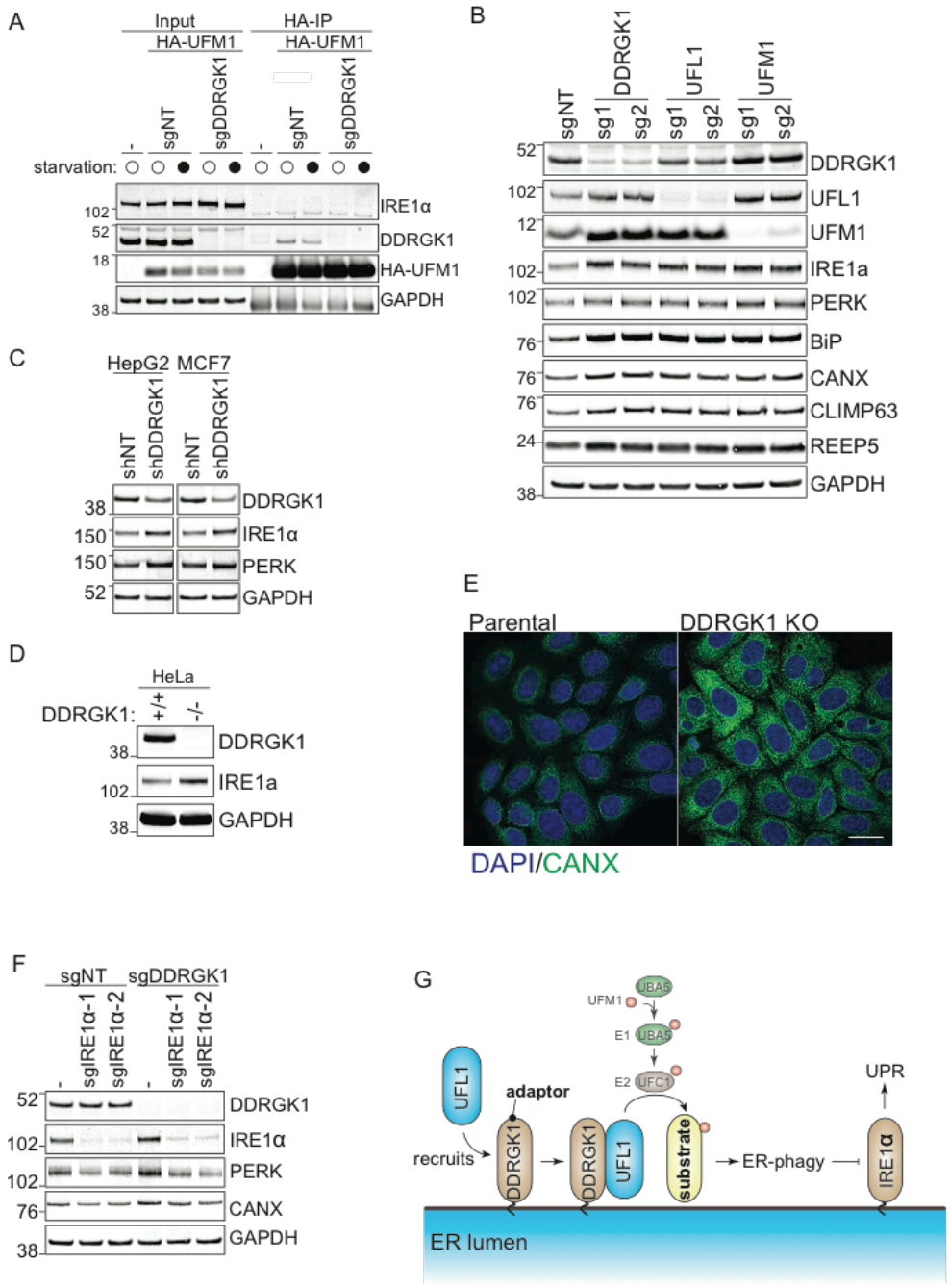

Figure 15: DDRGK1 mechanism

(A) IRE1α is not a target of DDRGK1-mediated UFMylation. HCT116 CRISPRi cells stably expressing HA-UFM1 were transduced with sgRNA targeting DDRGK1. Cells were then starved for 16hr before being harvested for HA-immunoprecipitation of UFM1 and Western blot analysis of its interaction with IRE1α and DDRGK1. (B) The same experiment shown in Figure 13G were further probed for the indicated ER or UPR markers. The densitometry measurements for IRE1α, BiP, CANX, CLIMP63 and REEP5 are shown in biological triplicates in Figure 9A. (C) DDRGK1 depletion results in the upregulation of UPR markers in various cell lines. HepG2 and MCF7 cells were transduced with shRNAs targeting DDRGK1. Cells were then harvested for

Western blot analysis of DDRGK1 knockdown efficiency and UPR response. (D) HeLa cells were transduced with shRNAs targeting DDRGK1. Cells were then harvested for Western blot analysis of DDRGK1 knockdown efficiency and UPR response. (E) The same HeLa cell lines generated in S6D were fixed and stained for an ER marker (CANX). Scale bar represents 20μm. (F) IRE1α depletion prevents UPR response in DDRGK1 knockdown cells. The same cell lines in Figure 9C were harvested for Western blotting to measure the protein levels of the indicated UPR genes. (G) Proposed model for UFMylation regulation on ER-phagy. DDRGK1 acts as an adaptor/anchor for UFL1 to recruit the latter to the ER surface. ER-localized DDRGK1-UFL1 then UFMylates a yet-to-be-identified substrate(s) that regulates ER-phagy. Loss of UFMylation factors results in ER-phagy inhibition and accumulation of ER stress. This in turn triggers UPR via the IRE1α pathway.

3.8 Supplemental Tables

Table 2: General ATG targets

Gene Name	Ensembl No.
ULK1	ENSG00000177169
ULK2	ENSG00000083290
ATG13	ENSG00000175224
FIP200	ENSG00000023287
ATG101	ENSG00000123395
ATG9A	ENSG00000198925
ATG9B	ENSG00000181652
WIPI1	ENSG00000070540
WIPI2	ENSG00000157954
PIK3R4	ENSG00000196455
VPS34	ENSG00000078142
BECN	ENSG00000126581
ATG14	ENSG00000126775
UVRAG	ENSG00000198382
ATG3	ENSG00000144848
ATG4A	ENSG00000101844
ATG4B	ENSG00000168397
ATG4C	ENSG00000125703
ATG4D	ENSG00000130734
ATG5	ENSG00000057663
ATG7	ENSG00000197548
LC3A	ENSG00000101460
LC3B	ENSG00000140941
LC3B2	ENSG00000258102
GABARAP	ENSG00000170296
GABARAPL1	ENSG00000139112
GABARAPL2	ENSG00000034713
ATG10	ENSG00000152348
ATG12	ENSG00000145782
ATG16L1	ENSG00000085978
ATG16L2	ENSG00000168010

Table 3: High confidence hits with enhanced/inhibition P < 0.01

gene	Localization	Enhanced(P-value)	Enhanced(log 2 Fold change)	Enh/Inh (P-value)	Enh/Inh (Fold change)	Inhibit (P-value)	Inhibit (log2 Fold change)
RPL23	cyto	0.756285351	-2.475453159	0.00019178	-3.601661823	0.327921303	3.792143706
GCA	cyto	0.216189227	0.483814537	0.001194771	1.409670926	0.01729053	-1.217225931
MAP4	cyto	0.001428437	-1.838371532	0.001226223	-2.489291163	0.452292888	0.647155016
SULT1C2	cyto	0.01872663	-0.803818781	0.001379418	-1.216517506	0.135563554	0.695583255
UBE2J1	ER	0.57269201	0.139195267	0.002394439	1.143545872	0.017758576	-1.085900392
NUDCD1	cyto	0.021323916	-0.913357857	0.002419018	-2.030882966	0.276427599	0.588897405
RACGAP1	cyto	0.008758219	-1.759501856	0.00260249	-2.109561238	0.749560144	1.215735686
PSMA5	cyto	0.262930811	-1.152300148	0.003294868	-4.701179439	0.041956294	2.596936072
PSMB5	cyto	0.003268205	-2.789645988	0.003329076	-3.176218175	0.140008818	0.381441483
RPL7A	cyto	0.428227235	0.927034367	0.003521865	2.15245058	0.003634874	-2.292541151
CAPN3	cyto	0.022112233	-1.076032933	0.003579957	-1.473523267	0.024146275	0.60454337
E2F8	cyto	0.475891634	0.256319848	0.003598896	1.116862537	0.004598461	-0.866497924
CUL3	cyto	0.012748529	1.046867534	0.00392484	0.99312011	0.887645603	-0.058106148
NLRP1	cyto	0.117818383	0.411196515	0.003976499	0.944883613	0.021218215	-0.620723102
CDK5RAP3	cyto	0.042836414	-0.76402663	0.003997336	-0.784510215	0.308022425	0.208226853
ATF5	cyto	0.183455532	-0.805798066	0.00409233	-2.895057996	0.392043093	2.431940946
MAGEA11	cyto	0.00537836	-2.550109987	0.004288492	-1.34240558	0.054797744	0.999615347
ITPK1	cyto	0.598703458	0.022360726	0.004767502	1.026017963	0.008390655	-0.947515284
PTK2	cyto	0.010252614	0.93980224	0.00504403	1.067654253	0.436153662	-0.188396952
DOCK2	cyto	0.552167023	0.175576363	0.005108866	0.77105917	0.02907199	-0.787158686
CORO2A	cyto	0.237882159	-1.363035963	0.006412166	-3.796143716	0.019399854	1.567152607
RPL10L	cyto	0.264839315	-1.687755006	0.006412166	-1.843893364	0.507930646	0.28539202
RNF146	cyto	0.013492996	-1.151807438	0.006456692	-1.244596005	0.38952564	0.180654639
IRS1	cyto	0.460261167	0.228970523	0.006557704	0.92643424	0.162837984	-1.055798076
GDI1	cyto	0.070957408	-1.422375762	0.006606873	-1.920298208	0.116669065	0.201681289
CUL9	cyto	0.030798782	-2.429872364	0.007294504	-1.675119229	0.199760473	0.668372125
PAPSS1	cyto	0.065726239	-2.277449454	0.008066137	-3.11448735	0.242121738	0.895113549
CSTB	cyto	0.420332406	0.264569115	0.00824491	0.794819849	0.073079292	-0.775686648
PRUNE2	cyto	0.403928962	-0.391894517	0.008717987	-0.957016211	0.079477039	0.931335778
KRTAP2-3	cyto	0.056109934	0.739720425	0.008739095	0.998149345	0.244111523	-0.278120086
ASB16	cyto	0.319750123	-0.102866728	0.008866705	-0.820806008	0.10333993	0.738972794
WDR64	cyto	0.029694917	0.822416124	0.008866705	0.766527998	0.811717162	-0.118734068
LACTBL1	cyto	0.104898265	0.650847474	0.009439125	1.056718246	0.263237419	-0.500483843
DCLK2	cyto	0.360945598	-0.277845298	0.009552911	-0.781952059	0.174525636	0.57952767
RPS5	cyto	0.270707596	1.631876657	0.009666172	3.618838654	0.033516749	-1.593896616
S100A6	cyto	0.062072551	0.664308159	0.009667918	0.90336401	0.215152793	-0.39159638
PIK3C3	cyto/lyso	0.114760283	-1.249839435	0.001532625	-2.135341559	0.046018286	1.093880349

RPS6KB2	cyto/nuc	0.098900277	-2.247505979	0.001395272	-2.780083218	0.230742034	1.759285832
SHOC2	cyto/nuc	0.141492591	0.498410981	0.001419369	0.855782158	0.037465673	-0.686606953
ASCC3	cyto/nuc	0.038020011	0.814939826	0.0016635	1.072536629	0.121334779	-0.624595537
PNISR	cyto/nuc	0.007046346	0.64482256	0.002492693	0.747734333	0.535686107	-0.254950538
DFFA	cyto/nuc	0.058478932	-2.106252659	0.002718846	-2.122318228	0.220675086	0.215424171
ALYREF	cyto/nuc	0.030888003	-1.352667199	0.002793271	-1.118145767	0.798366942	0.190802757
CBLB	cyto/nuc	0.589595312	0.181796524	0.002954256	0.923660743	0.006566318	-1.475024772
GNAS	cyto/nuc	0.036964947	-1.752183849	0.005375807	-2.101531855	0.178734382	0.295892897
ANAPC10	cyto/nuc	0.229221332	-0.550642517	0.00565528	-1.407840195	0.706105033	0.501377029
SGOL1	cyto/nuc	0.028389988	-2.50883884	0.00738234	-2.473619558	0.597970519	0.969138265
INTS7	cyto/nuc	0.211347673	0.391098069	0.007928814	1.512940961	0.021558708	-1.201425559
TRAPPC12	cyto/nuc	0.115709157	-0.532510585	0.007929499	-0.838037627	0.044430016	0.44929545
WDFY3	cyto/nuc	0.117818383	-0.649882885	0.00824491	-0.902425657	0.430368186	0.456250573
CALCOCO2	cyto/nuc	0.175374631	0.70726716	0.008654936	1.398157178	0.030054888	-1.05719667
WIPI1	endosom e	0.011807242	-0.993279913	0.002340923	-0.990519842	0.651427352	0.24220704
LY96	endosom e	0.073169656	0.749672284	0.004730876	1.213989981	0.073079292	-0.822490642
CHMP2A	endosom e	0.255122309	-0.075802153	0.009368418	-1.273790409	0.482502888	1.184988858
CHERP	ER	0.061842718	0.908835287	0.00041786	1.496657651	0.036867853	-1.199124533
MGLL	ER	0.031727836	-2.244027647	0.002479147	-2.235467918	0.252185383	0.197177299
PLD4	ER	0.124932735	-2.143643771	0.002526856	-2.238206485	0.073474665	0.600655854
TPTE2	ER	0.195283135	0.546390782	0.002582407	1.545074782	0.151228343	-0.701218693
TOR3A	ER	0.005270289	-1.318908222	0.002596468	-1.41346999	0.64198669	0.057018935
RNF183	ER	0.031337818	-0.634551255	0.003704702	-0.866108625	0.129433767	0.445341856
ARL6IP1	ER	0.217720013	-0.601273125	0.005741641	-1.492693014	0.001586627	0.668968724
DDRGK1	ER	0.014171266	-0.794353202	0.00591794	-0.944465656	0.578142271	0.165803515
PIGF	ER	0.181476702	-0.254479557	0.007513459	-0.757908529	0.133212583	0.460985905
SCD	ER	0.351089847	0.333581918	0.008285116	1.227948292	0.091093429	-1.164380133
TMEM170A	ER	0.110107434	0.665106389	0.009083091	0.940635488	0.179531858	-0.40334322
ZDHHC2	ER/golgi	0.715652897	-0.239373155	0.004516418	-0.924334746	0.003023674	0.776659956
EI24	ER/golgi	0.504325183	-0.567456942	0.005056938	-1.322180457	0.001825261	0.764689731
FUCA2	ER/lyso!	0.100226053	0.485179161	0.005430683	0.754002033	0.064455928	-0.424889556
PREB	ER/lyso!	0.045157163	-1.512628083	0.006083818	-4.176983221	0.02293547	2.901727435
CNTF	extracell	0.004371114	-0.881330726	0.002526856	-1.022833863	0.479416517	0.165054375
SCG5	extracell	0.229928084	0.229179544	0.002711504	1.12160078	0.002629432	-0.721964304
ITIH3	extracell	0.145543565	0.619438299	0.003126613	0.824220628	0.055842562	-0.599466876
LYVE1	extracell	0.226120987	0.399239727	0.005056938	0.840903377	0.008249549	-0.519542994
FGFBP3	extracell	0.096378232	-1.817912962	0.005814515	-2.078460838	0.047286428	0.466461042
TRABD2B	extracell	0.051315911	0.797264095	0.006428192	0.872667563	0.864337743	-0.449262813
DMXL2	extracell	0.79435002	0.027791	0.007794938	0.848366144	0.010431642	-0.903877867

ABHD8	extracell	0.01815505	-2.20418117	0.007871577	-2.128922558	0.988203281	0.056294622
SERINC2	extracell	0.315767069	-1.539895127	0.008995977	-2.943823907	0.064897892	0.552868765
PRSS33	extracell	0.014564725	0.780282624	0.009925289	0.87592161	0.714101945	-0.124331305
MMP24	golgi/extra	0.032990469	-3.140160332	0.003395489	-3.433078869	0.096073689	0.358117931
COG7	golgi/nuc	0.699143777	0.04590016	0.006380222	0.857999258	0.055527388	-1.041210735
VPS16	lyso	0.076614266	-4.578192657	0.000788667	-5.367899836	0.002399697	1.337900738
SERPINA3	lyso	0.030824198	0.676658282	0.002091194	0.888981434	0.277153198	-0.442817558
TMEM74	lyso	0.025203144	-0.56607196	0.004779768	-0.904585327	0.53491169	0.181606913
GDAP2	lyso	0.079863476	-1.519324185	0.006606873	-1.635083014	0.338176745	0.477150062
C10orf32	lyso	0.462261721	0.376796503	0.006807235	0.81826992	0.04487757	-0.704830109
ABCB9	lyso	0.275555826	0.222051804	0.007385249	1.633229581	0.193508757	-0.286943792
FMOD	lyso	0.329447291	-0.293279372	0.008468221	-1.870381103	0.118983997	1.755892699
TECPR1	lyso	0.060470422	-0.794619605	0.008547493	-1.187434615	0.454331367	0.507410971
RAB5C	lyso	0.072644115	-0.572504958	0.008866705	-0.795839749	0.100416661	0.263368197
LOH12CR1	lyso	0.013787215	0.813384484	0.009393951	0.725977061	0.893488596	-0.013967387
ATG10	lyso/cyto	0.142609071	-0.541198405	0.006316762	-1.239604983	0.023083878	0.876358692
ARSA	lyso/ER	0.00684045	-1.155910709	0.003404503	-1.453922557	0.196610108	0.292056613
HSD17B10	mito	0.000402688	-2.929592657	0.00024702	-3.149567971	0.039465873	0.491537152
VARS2	mito	0.001581811	-1.74044248	0.000332338	-2.183759375	0.002943908	0.659835997
NDUFA8	mito	0.002559968	-1.696173848	0.000428389	-1.852511557	0.313906381	0.421526225
NDUFB4	mito	0.002391684	-2.232977549	0.000443273	-2.449104046	0.056690317	0.379299948
MRPL33	mito	0.000759137	-1.515981101	0.000655836	-1.771217015	0.418459224	0.262042455
MRPL16	mito	0.004758796	-0.999959506	0.000719967	-1.445710824	0.007800746	0.551988418
OXA1L	mito	0.007511657	-1.531102035	0.000750799	-2.106949439	0.007762773	0.771957184
MRPL30	mito	0.004930389	-0.976447167	0.000927577	-1.306784019	0.090011889	0.511704315
AARS2	mito	0.002601936	-1.297619089	0.000937902	-1.410470231	0.376335866	0.143722704
MRPL41	mito	0.052706676	-1.291425144	0.001079409	-1.175449538	0.247789226	0.337276282
NDUFB2	mito	0.451813067	-2.580176779	0.001144002	-3.504003428	0.002636548	1.050916432
POLG2	mito	0.099886671	-0.877002037	0.001184454	-1.229085233	0.008616757	0.675400424
NDUFS8	mito	0.025364359	-2.024771306	0.001262066	-2.514497463	0.119373296	0.940304778
NDUFS5	mito	0.020136594	-1.035518049	0.001273006	-1.21422212	0.048210131	0.458098858
MRPL34	mito	0.012456511	-1.231559734	0.001321432	-1.697888412	0.013113061	0.521227473
NDUFS2	mito	0.068425289	-1.181285666	0.0016635	-1.484873458	0.023889551	0.576657952
RAF1	mito	0.010623156	1.290087675	0.001814711	3.004871091	0.059243768	-1.414331673
MRPL55	mito	0.088114164	-0.615727987	0.001967502	-1.039128661	0.007037298	0.570828795
MRPL24	mito	0.00923118	-2.653423504	0.001978463	-2.700925798	0.350328221	0.205772388
WBSCR16	mito	0.004820177	-0.783860021	0.001995009	-1.165301252	0.271742786	0.370629712
CYB5B	mito	0.016605312	-2.443878934	0.002114436	-2.646824107	0.128192831	0.196624558
PTCD1	mito	0.009846895	-0.834876319	0.002819722	-0.980350082	0.412362625	0.184272596

ATP5O	mito	0.156059102	-3.427560752	0.002838815	-3.861781522	0.006814981	0.637364797
MMAA	mito	0.003888577	-2.45017936	0.00354235	-2.735580964	0.29043601	0.290875751
BCS1L	mito	0.200726664	-0.613240876	0.0036084	-1.327380308	0.504252812	0.84929956
DLD	mito	0.044067561	-0.800033993	0.003783419	-2.955745987	0.045750301	1.446295373
GRSF1	mito	0.012456511	-1.033261244	0.004551538	-1.137815931	0.522781561	0.184320302
TARS2	mito	0.03500048	-2.572694286	0.00513501	-2.982551764	0.025737404	0.705726286
COA4	mito	0.082298985	-1.004723912	0.005598359	-1.100023106	0.184372332	0.334039476
PICK1	mito	0.030163317	-2.722022753	0.006128586	-3.040967998	0.143495414	0.313201981
COA3	mito	0.02145125	-0.82734181	0.006541388	-1.373729348	0.204115619	0.540432303
SUPV3L1	mito	0.120153638	-0.848210094	0.006739614	-1.929377244	0.042635741	0.937365341
SLMO2	mito	0.05936073	-1.359449292	0.006756374	-1.513069198	0.287447875	0.147664671
LIPT2	mito	0.052106823	-0.848192831	0.006806879	-0.829069324	0.473313411	0.106283446
ATP5J2	mito	0.027600652	-0.771161331	0.007385249	-0.949346276	0.275703297	0.184272596
MRPL22	mito	0.149450465	-0.378190099	0.007871577	-0.95003224	0.023685879	0.641413283
MRPL17	mito	0.064528737	-1.030101804	0.007871577	-0.991091469	0.920827321	0.15198664
BIK	mito	0.052007405	1.191503343	0.008447698	1.284951115	0.382571585	-0.247824755
KIAA0391	mito	0.029880622	-0.609288274	0.008592292	-0.700137392	0.362320075	0.210180423
TRMT10C	mito	0.19556691	-0.639694724	0.009237354	-1.168323678	0.041473914	0.715862517
UQCRC2	mito	0.015732307	0.779118067	0.009507251	0.770019979	0.926698935	-0.008430699
KLK6	mito/nuc	0.119371226	-1.015456506	0.006007906	-0.867864011	0.922131763	0.318051176
C21orf91	MTs	0.158715175	0.417645262	0.007205495	0.928074076	0.183829779	-0.655559405
JUNB	nuc	0.00425942	0.76361431	0.000778197	1.782656806	0.055213698	-1.155084057
LRRC34	nuc	0.473483753	-0.739665609	0.000892052	-3.783214929	0.079477039	2.325088432
MED21	nuc	0.611330251	0.160098008	0.001344351	1.073717124	0.001655014	-1.057672157
NOL11	nuc	0.360513511	0.447799956	0.00137548	1.023967435	0.062234687	-0.921060827
ETV1	nuc	0.027083179	-1.217294825	0.001962043	-1.018201784	0.784444019	0.210337275
RSRC2	nuc	0.017095728	0.661113961	0.002179577	3.354986228	0.019485289	-2.794231015
CCNC	nuc	0.005530225	1.945232038	0.002252734	2.171504461	0.576176436	-0.171712241
MMS22L	nuc	0.180404303	0.307487866	0.002283874	1.922810767	0.015419932	-1.752760149
DR1	nuc	0.018561737	-2.756980117	0.002554493	-2.967470852	0.134277264	0.374306782
CHAF1A	nuc	0.098706046	-1.101333504	0.0029636	-1.194501435	0.170391328	0.731104848
HLTF	nuc	0.142161671	-1.838252962	0.003011671	-1.772626886	0.533524257	0.396063426
CCAR1	nuc	0.070957408	-2.976401226	0.003035064	-2.417988367	0.230103444	0.047017536
SNW1	nuc	0.016892201	3.081419839	0.003329053	3.204144891	0.208707526	-0.26940826
C17orf82	nuc	0.231207191	0.423584948	0.003523681	1.362331357	0.117052411	-1.25991456
RNF113A	nuc	0.017971036	-3.572132589	0.003613592	-3.606642995	0.181264821	1.241958682
PRPF4	nuc	0.018353548	-3.304906756	0.003638281	-3.662245144	0.086225969	1.500607061
ZNF333	nuc	0.066575343	-0.82163584	0.003894137	-1.248524084	0.041803096	0.63495791
LOC441155	nuc	0.058808323	-1.866207706	0.003976499	-2.163469107	0.984271487	0.168672388

C16orf45	nuc	0.017133973	-0.899516013	0.004288492	-0.979366926	0.610556344	0.197058785
NR2C1	nuc	0.03025503	-1.907308195	0.004730876	-1.903224158	0.800905429	0.028300223
LEO1	nuc	0.101936775	-1.725665602	0.004853963	-1.800573645	0.183558946	0.413712549
EPG5	nuc	0.188010608	-0.367972817	0.00496721	-0.913836531	0.065651039	0.708090318
NMD3	nuc	0.025364359	1.210872081	0.005031153	1.068705418	0.840505025	-0.05132253
PFDN5	nuc	0.002233585	0.949605747	0.00565528	1.191641463	0.791397162	-0.279484619
UBE2O	nuc	0.016792452	0.818119737	0.00605335	0.978535172	0.379891417	-0.264219934
TWIST2	nuc	0.024410307	0.775911399	0.006129778	1.187400059	0.247789226	-0.509423337
ZPBP2	nuc	0.319750123	0.092156537	0.006269541	0.842062838	0.010407003	-0.669287179
CCDC130	nuc	0.012057641	0.935492323	0.006285246	1.493502216	0.188203432	-0.733901012
FOXK2	nuc	0.008484592	0.658017612	0.006790007	0.832106055	0.709816474	-0.180043678
ZNF414	nuc	0.029880622	-0.744576579	0.007170019	-1.16302278	0.211226876	0.331158666
CDR2	nuc	0.498567708	0.451237257	0.007495022	1.114177723	0.006664787	-0.620004947
TC2N	nuc	0.0743635	0.491270458	0.007495022	0.878922112	0.128192831	-0.535564263
DDX52	nuc	0.126967242	-1.969065834	0.007756869	-2.407918612	0.214545407	0.228289006
ZNF711	nuc	0.009164964	-1.307546115	0.007968326	-1.443179419	0.948913977	0.216334506
NUCKS1	nuc	0.249647209	0.442225806	0.008066137	1.708774579	0.143033032	-1.325003999
C17orf85	nuc	0.337250017	0.416057913	0.008530055	1.018385324	0.062119556	-0.856117558
POLE2	nuc	0.135579314	-0.715477168	0.008592292	-0.928937728	0.117436746	0.388046242
C1orf194	nuc	0.023842715	0.88368769	0.008823984	0.750994115	0.845646456	-0.169602218
RBM28	nuc	0.011240829	-1.583459227	0.008866705	-2.024844238	0.210029387	0.359554407
LRR1	nuc	0.281758119	-0.198618593	0.009061242	-0.593910379	0.128812137	0.523428215
THOC6	nuc	0.974416762	0.188189443	0.009371436	0.86676652	0.012463041	-0.898295841
GPR133	PM	0.039492762	0.651462742	0.000764384	1.121099494	0.031974944	-0.742721717
FAP	PM	0.012689645	1.166233483	0.001306354	1.854649941	0.812354288	-1.037877286
KCNK13	PM	0.012085751	-0.702451344	0.002191616	-1.201409359	0.047469969	0.563083075
ADAM18	PM	0.069977409	-2.342846138	0.002213331	-2.112587252	0.968549086	0.044798473
OR5A2	PM	0.02472481	0.469504439	0.002386193	0.835206313	0.047378124	-0.371657109
TMTC4	PM	0.015070072	0.62452021	0.002646236	0.871142463	0.335284674	-0.476982008
ENPP3	PM	0.013914198	-1.139382371	0.002831178	-1.526753382	0.089067686	0.520681703
GP9	PM	0.835198128	-0.388178806	0.002947733	-1.142266341	0.010680909	1.07302071
FZD6	PM	0.195850988	-0.558512165	0.005873414	-0.808340936	0.202074696	0.469339585
RIMBP2	PM	0.705242189	-0.817275088	0.005903064	-1.550536681	0.003080678	0.835690746
SEMA4G	PM	0.071861601	0.647739264	0.006541388	1.051701001	0.032637905	-0.482541462
MTNR1A	PM	0.1459991	-1.005663031	0.006773172	-1.961747146	0.057010974	1.024113039
OR56A1	PM	0.011945777	0.685308548	0.007330905	1.476255599	0.304914346	-0.734024372
CEACAM5	PM	0.084349615	-0.827039273	0.007495022	-0.67913992	0.358437811	0.015205297
SLC26A4	PM	0.003960311	-0.823012654	0.007700079	-0.949332156	0.881160555	0.008619798
OR7E24	PM	0.497003575	0.238589921	0.007871577	0.919164375	0.128399008	-0.881441907

KCNN3	PM	0.297484909	-1.475778247	0.008509399	-1.727670997	0.095093125	0.464084078
MS4A3	PM	0.456072454	-1.308729772	0.009268318	-1.540630379	0.441145475	0.495953881
TMC4	PM	0.167647167	0.505553568	0.009507251	0.649305165	0.184372332	-0.485188204
LILRB4	PM	0.059694237	0.80995302	0.009530057	0.616095009	0.140361489	-0.358314685
SCUBE1	PM	0.038634324	0.636564269	0.009530057	0.620470029	0.692767391	-0.112321051
SLC7A9	PM	0.019399084	-2.104482597	0.009901642	-2.404382153	0.224726131	0.389860958
CRYGS	cyto/nuc	0.054026176	0.444491133	0.004255217	0.870700577	0.157944541	-0.646297216

Table 4: sgRNA constructs

Construct	Protospacer	Addgene Number
pLG1-puro NT sgRNA	GCGCCAAACGTGCCCTGACGG	Addgene #109002
pLG1-puro ULK1 sgRNA	GGCGGCGGCACAGAGACCGT	Addgene #109004
pLG1-puro ATG10 sgRNA	GAGGCCGCGGACCTGACTGA	
pLG1-puro VPS16 sgRNA	GAAAGGCAGAGTCCCCGAGT	
pLG1-puro EI24 sgRNA	GACGGGGCCGCTGGGAAGTC	
pLG1-puro NDUFB4 sgRNA	GGGCCTCCCAGGCGGGAATA	
pLG1-puro NDUFB2 sgRNA	GGGGGAAGCGAAGTAGGCAG	
pLG1-puro ATP5O sgRNA	GGTCCCCCGGGATGCCTACG	
pLG1-puro DDRGK1 sgRNA-1	GCCGCTACCAAGTACCACAC	
pLG1-puro DDRGK1 sgRNA-2	GGCGGCGCGACGGTCCACAA	
pLG1-puro UFL1 sgRNA-1	GGCCTGACTCGCAGTAGACG	
pLG1-puro UFL1 sgRNA-2	GCGCCTGGGAAGAGATTAGG	
pLG1-puro UFM1 sgRNA-1	GAAGAGATGAAGACTGCGTG	
pLG1-puro UFM1 sgRNA-2	GGGAAGTCGTGCTACCCCCG	
pLG1-puro IRE1a sgRNA-1	GGGCGGTGACCGAGCCTCAG	
pLG1-puro IRE1a sgRNA-2	GAGCGGACGCAGAACTGACT	
pLG1-puro FAM134B sgRNA-1	GGGACTGGAGAGAGAATGCG	
pLG1-puro FAM134B sgRNA-2	GAGGTGAAGTCATCCAATGA	
pLG1-puro FAM134B sgRNA-3	GTCCTAGCTTCATTCAAGGG	
pLG1-puro FAM134B sgRNA-4	GCTCCCAGTACTGTGACAGG	
pLG1-puro FAM134B sgRNA-5	GGCACGAACTCACTCAAGAG	
pLG1-puro CDK5RAP3 sgRNA-1	GGAGTCGAGATGCTGACCAC	

pLG1-puro CDK5RAP3 sgRNA-2	GGGAGGGAGACCGGAGACAC	
pLG1-puro Sox9 sgRNA-3	GGGAGTTGGAGAGCCGAAAG	
pLG1-puro Sox9 sgRNA-4	GGTCCGAGCCGGAGCCCGAC	
pLG1-puro ASC1 sgRNA-1	GTAGTCCGGTGCAGGACGTG	
pLG1-puro ASC1 sgRNA-2	GTGGTTCCGGCTGGGGAAGA	

Table 5: Overexpression constructs

Plasmids	**ORF source**
pLenti-X1-Neo-NDUFB4	HCT116 cDNA
pLenti-X1-Neo-NDUFB2	HCT116 cDNA
pLenti-X1-Neo-ATP5O	HCT116 cDNA
pLentiXI-Neo-GST-Constitutively Active AMPK	Addgene 27632
pLentiXI-Neo-GST-Constitutively Active AMPK- Kinase Dead (K to R)	Addgene 27632
pBMN-YFP-Parkin	Addgene 59416
pLenti-X1-Neo-HA-hULK1	Addgene 31963
pLenti-X1-Neo-DDRGK1-WT-HA	HCT116 cDNA; NM_023935.2
pLenti-X1-Neo-DDRGK1-dSP-HA	subcloned from pLenti-X1-Neo-DDRGK1-WT-HA
pLenti-X1-Neo-DDRGK1-dPCI-HA	subcloned from pLenti-X1-Neo-DDRGK1-WT-HA
pLenti-X1-Neo-DDRGK1-K267R-HA	subcloned from pLenti-X1-Neo-DDRGK1-WT-HA
pLenti-X1-Neo-DDRGK1-K-less-HA	subcloned from pLenti-X1-Neo-DDRGK1-WT-HA
pLenti-X1-Neo-DDRGK1-K116R-HA	subcloned from pLenti-X1-Neo-DDRGK1-WT-HA
pLenti-X1-Neo-DDRGK1-K120R-HA	subcloned from pLenti-X1-Neo-DDRGK1-WT-HA
pLenti-X1-Neo-DDRGK1-K121R-HA	subcloned from pLenti-X1-Neo-DDRGK1-WT-HA
pLenti-X1-Neo-DDRGK1-K124R-HA	subcloned from pLenti-X1-Neo-DDRGK1-WT-HA
pLenti-X1-Neo-DDRGK1-K128R-HA	subcloned from pLenti-X1-Neo-DDRGK1-WT-HA
pLenti-X1-Neo-DDRGK1-K146R-HA	subcloned from pLenti-X1-Neo-DDRGK1-WT-HA
pLenti-X1-Neo-DDRGK1-K176R-HA	subcloned from pLenti-X1-Neo-DDRGK1-WT-HA
pLenti-X1-Neo-DDRGK1-K193R-HA	subcloned from pLenti-X1-Neo-DDRGK1-WT-HA
pLenti-X1-Neo-DDRGK1-K224R-HA	subcloned from pLenti-X1-Neo-DDRGK1-WT-HA
pLenti-X1-Neo-DDRGK1-K227R-HA	subcloned from pLenti-X1-Neo-DDRGK1-WT-HA
pLenti-X1-Neo-HA-UFL1	HCT116 cDNA; NM_015323.4
pLenti-X1-Neo-IRE1A-no-tag	HCT116 cDNA; NM_001433.4
pLenti-X1-Neo-IRE1A-K121Y-no-tag	subcloned from pLenti-X1-Neo-IRE1A-HA with a Lys to Tyr mutation at a.a. 121.
pLenti-X1-Neo-HA-UFM1	HCT116 cDNA; NM_016617.4
pLKO.1-puro-shNon-targeting	Addgene 109012
pLKO.1-puro-shDDRGK1	sequence obtained from

Table 6: qRT-PCR primers

Target	Primer 1	Primer 2
EI24	AGTGTTGTGCTTGGAATGGTGG	GCCACGACCAAACATCTCCATG
VPS16	ACTCGGGGACTCTGCCTTTTAC	GGCAATCCCTGAGTTCCTCCTT
ULK1	GTCGCCGTCAAGTGCATTAACA	CGTACAGGGCCACGATGTTTTC
ATG10	GTGATAGTTGGGAATGGAGACC	GGTAGATGCTCCTAGATGTGAC
sXBP1	TGCTGAGTCCGCAGCAGGTG	GCTGGCAGGCTCTGGGGAAG
ACTB	GGGTCAGAAGGATTCCTATG	GGTCTCAAACATGATCTGGG
IRE1A	ACTTTGTCATCGGCCTTTGCAG	AGTGAGGCCGCATAGTCAAAGT
PERK	TGGTGTCATCCAGCCTTAGCAA	CATGCTTTCACGGTCTTGGTCC
DDRGK1	AAGGAGGAGGAGGAGAGGAAGG	CTCTGTCAGGAAGCTCTGGGAC
UFL1	TCGGTTGGCAGAAGAGGTCAAT	AAGTCGCTGAGTTAGTGCCTGT
FAM134B	CCAGATGAAAGACCCAGGCTCA	TGCACACACTACAGACCAGGAG
CDK5RAP3	TGCTGGAGGATCTGATTGGCAA	ACTCGGTCCACATACCTTGGTG
SOX9	GGCAAGCTCTGGAGACTTCTGA	GGCTGGTACTTGTAATCCGGGT
ASC1	CCCACAGAGGACGACTTTGGAT	CCCAGAAGACAACCTGACGGAT

Table 7: Antibody List

Target	Company	Cat. No.	Species	WB Dilution	IF Dilution
ACC (Acetyl-CoA Carboxylase)	Cell Signaling	3676	Rabbit	1 in 1000	
Actin	Cell Signaling	3700	mouse	1 in 1000	
AMPKa	Cell Signaling	5831	rabbit	1 in 1000	
ATG10	MBL International	M151-3	mouse	1 in 500	
ATP5O	Abcam	ab110276	mouse	1 in 1000	
BiP	Cell Signaling	3177	Rabbit	1 in 1000	
Calnexin (CANX)	Cell Signaling	2679	rabbit	1 in 1000	1 in 50
Calnexin (CANX)	Santa Cruz	SC-46669	mouse	1 in 1000	
CKAP4/ CLIMP63	bethyl	A302-257A	rabbit		1 in 250
CLIMP63	Bethyl	A302-257A	rabbit	1 in 1000	
DDRGK1	Protein Tech	21445-1-AP	rabbit	1 in 1000	
GAPDH	Cell Signaling	#97166	mouse	1 in 2000	
GFP	Abcam	ab6556	rabbit	1 in 2000	
GFP	Santa Cruz	sc-9996	mouse	1 in 2000	
GST	Cell Signaling	2625	Rabbit	1 in 1000	
Ha epitope tag	Cell Signaling	3724	rabbit	1 in 2000	1 in 250
IRE1a	Cell Signaling	3294	rabbit	1 in 1000	
LC3B	Nanotools	0231-100	mouse	1 in 200	1 in 200
LC3B	Novus Biologicals	NB100-2220	rabbit	1 in 1000	1 in 250
mCherry	Abcam	ab183628	rabbit	1 in 2000	
MFN1	Cell Signaling	14739	Rabbit	1 in 1000	
MFN2	Cell Signaling	11925	Rabbit	1 in 1000	
NDUFB2	Abcam	ab186748	rabbit	1 in 1000	
NDUFB4	Abcam	ab110243	mouse	1 in 1000	
p62	Santa Cruz	sc-28359	mouse	1 in 1000	
pACC S79	Cell Signaling	11818	Rabbit	1 in 1000	
PERK	Cell Signaling	3192	rabbit	1 in 1000	
pRaptor S792	Cell Signaling	2083	Rabbit	1 in 1000	
pS6K T389	Cell Signaling	9206	mouse	1 in 1000	
pULK1 S555	Cell Signaling	5869	Rabbit	1 in 1000	
Raptor	Cell Signaling	2280	Rabbit	1 in 1000	
REEP5	Protein Tech	14643-1-AP	rabbit	1 in 1000	
S6K (p70 S6 Kinase)	Cell Signaling	9202	Rabbit	1 in 1000	
Tom20	Sigma	HPA011562	mouse	1 in 1000	
UFL1	Novus Biologicals	NBP1-90691	rabbit	1 in 1000	
UFM1	Abcam	ab109305	rabbit	1 in 1000	
ULK1	Cell Signaling	#8054	rabbit	1 in 1000	

Conclusion

This dissertation aims to utilize genome-editing tools to understand ER autophagy. I articulated a step-by-step protocol for using CasRNPs to efficaciously genome edit a cell line. In the forthcoming appendices, we also created numerous genome-editing tools that we hope serve as great resources in the autophagy and ubiquitin cell biology fields.

We used CRISPR-Cas9 technologies to make a significant impact in the field of ER autophagy. Thus far, researchers in the field have primarily described individual ER-localized autophagy adaptors. The genome-wide screen revealed 200 high-confidence hits that may be key regulators of ER autophagy. In our follow-up mechanistic work, we chose to characterize two pathways that our screen identified: mitochondrial oxidative phosphorylation and UFMylation. These pathways have been described in the literature, but never in relation to ER-phagy. We hope that the understanding of these pathways and their connection to ER-phagy grows further. In addition, our hope is that the 200 high-confidence hits serve as fodder for many future dissertations.

Even with all these high-confidence hits, the ER-phagy field has a long way to go. The largest questions – when and why ER-phagy occurs in humans – remains unclear. We can induce this process in tissue culture cells, but everything about that process (the starvation and the cell lines) are very artificial compared to what is happening within a human body. ER-phagy impairment has been linked to neurodegeneration, but the evidence making that connection is weak.

A strong biological phenotype will be necessary for related cell biology fields to take ER-phagy seriously. For example, many labs study mitophagy due to its link with Parkinson's disease. That link makes it compelling for researchers to study the process and makes funding agencies interested in supporting that work. It will be impossible for ER-phagy to mature as a field (both with funding and in the number of researchers) without any human disease phenotype from impairment of ER-phagy.

However, when that strong connection is made, the field of ER-phagy will explode. The hundreds of autophagy labs already have the tools to study ER-phagy, and they may all suddenly become more interested in it. I hypothesize that multiple pathways of ER-phagy regulators will be identified. Those pathways may be used redundantly within a given cell or used in different contexts or cell types.

Altogether, this dissertation takes a large step forward in the ER-phagy field and is the foundation for many future discoveries. It is our sincerest hope that the ER-phagy field will continue to grow in its importance and the relevance of ER-phagy for human health will be clearly elucidated.

References

Aida, T., Chiyo, K., Usami, T., Ishikubo, H., Imahashi, R., Wada, Y., Tanaka, K.F., Sakuma, T., Yamamoto, T., and Tanaka, K. (2015). Cloning-free CRISPR/Cas system facilitates functional cassette knock-in in mice. Genome Biol. *16*, 87.

Axe, E.L., Walker, S.A., Manifava, M., Chandra, P., Roderick, H.L., Habermann, A., Griffiths, G., and Ktistakis, N.T. (2008). Autophagosome formation from membrane compartments enriched in phosphatidylinositol 3-phosphate and dynamically connected to the endoplasmic reticulum. J. Cell Biol. *182*, 685–701.

Barrangou, R., Fremaux, C., Deveau, H., Richards, M., Boyaval, P., Moineau, S., Romero, D.A., and Horvath, P. (2007). CRISPR provides acquired resistance against viruses in prokaryotes. Science *315*, 1709–1712.

Bhaya, D., Davison, M., and Barrangou, R. (2011). CRISPR-Cas systems in bacteria and archaea: versatile small RNAs for adaptive defense and regulation. Annu. Rev. Genet. *45*, 273–297.

Bingol, B., Tea, J.S., Phu, L., Reichelt, M., Bakalarski, C.E., Song, Q., Foreman, O., Kirkpatrick, D.S., and Sheng, M. (2014). The mitochondrial deubiquitinase USP30 opposes parkin-mediated mitophagy. Nature *510*, 370–375.

Burger, A., Lindsay, H., Felker, A., Hess, C., Anders, C., Chiavacci, E., Zaugg, J., Weber, L.M., Catena, R., Jinek, M., et al. (2016). Maximizing mutagenesis with solubilized CRISPR-Cas9 ribonucleoprotein complexes. Development *143*, 2025–2037.

Chen, S., Lee, B., Lee, A.Y.-F., Modzelewski, A.J., and He, L. (2016). Highly efficient mouse genome editing by CRISPR ribonucleoprotein electroporation of zygotes. J. Biol. Chem. *291*, 14457–14467.

Cho, S.W., Lee, J., Carroll, D., Kim, J.-S., and Lee, J. (2013). Heritable gene knockout in Caenorhabditis elegans by direct injection of Cas9-sgRNA ribonucleoproteins. Genetics *195*, 1177–1180.

Cong, L., Ran, F.A., Cox, D., Lin, S., Barretto, R., Habib, N., Hsu, P.D., Wu, X., Jiang, W., Marraffini, L.A., et al. (2013). Multiplex genome engineering using CRISPR/Cas systems. Science *339*, 819–823.

Cunningham, C.N., Baughman, J.M., Phu, L., Tea, J.S., Yu, C., Coons, M., Kirkpatrick, D.S., Bingol, B., and Corn, J.E. (2015). USP30 and parkin homeostatically regulate atypical ubiquitin chains on mitochondria. Nat. Cell Biol. *17*, 160–169.

Davies, S.P., Helps, N.R., Cohen, P.T., and Hardie, D.G. (1995). 5'-AMP inhibits dephosphorylation, as well as promoting phosphorylation, of the AMP-activated protein kinase. Studies using bacterially expressed human protein phosphatase-2C alpha and native bovine

protein phosphatase-2AC. FEBS Lett. *377*, 421–425.

Deas, E., Plun-Favreau, H., Gandhi, S., Desmond, H., Kjaer, S., Loh, S.H.Y., Renton, A.E.M., Harvey, R.J., Whitworth, A.J., Martins, L.M., et al. (2011). PINK1 cleavage at position A103 by the mitochondrial protease PARL. Hum. Mol. Genet. *20*, 867–879.

Deltcheva, E., Chylinski, K., Sharma, C.M., Gonzales, K., Chao, Y., Pirzada, Z.A., Eckert, M.R., Vogel, J., and Charpentier, E. (2011). CRISPR RNA maturation by trans-encoded small RNA and host factor RNase III. Nature *471*, 602–607.

Ding, W.-X., and Yin, X.-M. (2012). Mitophagy: mechanisms, pathophysiological roles, and analysis. Biol. Chem. *393*, 547–564.

Dooley, H.C., Razi, M., Polson, H.E.J., Girardin, S.E., Wilson, M.I., and Tooze, S.A. (2014). WIPI2 links LC3 conjugation with PI3P, autophagosome formation, and pathogen clearance by recruiting Atg12-5-16L1. Mol. Cell *55*, 238–252.

Faircloth, B.C., and Glenn, T.C. (2014). Protocol: Preparation of an AMPure XP substitute (AKA Serapure).

Fumagalli, F., Noack, J., Bergmann, T.J., Cebollero, E., Pisoni, G.B., Fasana, E., Fregno, I., Galli, C., Loi, M., Soldà, T., et al. (2016). Translocon component Sec62 acts in endoplasmic reticulum turnover during stress recovery. Nat. Cell Biol. *18*, 1173–1184.

Ganley, I.G., Lam, D.H., Wang, J., Ding, X., Chen, S., and Jiang, X. (2009). ULK1.ATG13.FIP200 complex mediates mTOR signaling and is essential for autophagy. J. Biol. Chem. *284*, 12297–12305.

Gegg, M.E., Cooper, J.M., Chau, K.-Y., Rojo, M., Schapira, A.H.V., and Taanman, J.-W. (2010). Mitofusin 1 and mitofusin 2 are ubiquitinated in a PINK1/parkin-dependent manner upon induction of mitophagy. Hum. Mol. Genet. *19*, 4861–4870.

Geng, J., and Klionsky, D.J. (2008). The Atg8 and Atg12 ubiquitin-like conjugation systems in macroautophagy. “Protein modifications: beyond the usual suspects” review series. EMBO Rep. *9*, 859–864.

Gilbert, L.A., Larson, M.H., Morsut, L., Liu, Z., Brar, G.A., Torres, S.E., Stern-Ginossar, N., Brandman, O., Whitehead, E.H., Doudna, J.A., et al. (2013). CRISPR-mediated modular RNA-guided regulation of transcription in eukaryotes. Cell *154*, 442–451.

Gilbert, L.A., Horlbeck, M.A., Adamson, B., Villalta, J.E., Chen, Y., Whitehead, E.H., Guimaraes, C., Panning, B., Ploegh, H.L., Bassik, M.C., et al. (2014). Genome-scale CRISPR-mediated control of gene repression and activation. Cell *159*, 647–661.

Graef, M., Friedman, J.R., Graham, C., Babu, M., and Nunnari, J. (2013). ER exit sites are physical and functional core autophagosome biogenesis components. Mol. Biol. Cell *24*, 2918–

2931.

Greene, A.W., Grenier, K., Aguileta, M.A., Muise, S., Farazifard, R., Haque, M.E., McBride, H.M., Park, D.S., and Fon, E.A. (2012). Mitochondrial processing peptidase regulates PINK1 processing, import and Parkin recruitment. EMBO Rep. *13*, 378–385.

Grumati, P., Morozzi, G., Hölper, S., Mari, M., Harwardt, M.-L.I., Yan, R., Müller, S., Reggiori, F., Heilemann, M., and Dikic, I. (2017). Full length RTN3 regulates turnover of tubular endoplasmic reticulum via selective autophagy. Elife *6*.

Gwinn, D.M., Shackelford, D.B., Egan, D.F., Mihaylova, M.M., Mery, A., Vasquez, D.S., Turk, B.E., and Shaw, R.J. (2008). AMPK phosphorylation of raptor mediates a metabolic checkpoint. Mol. Cell *30*, 214–226.

Hailey, D.W., Rambold, A.S., Satpute-Krishnan, P., Mitra, K., Sougrat, R., Kim, P.K., and Lippincott-Schwartz, J. (2010). Mitochondria supply membranes for autophagosome biogenesis during starvation. Cell *141*, 656–667.

Hamasaki, M., Noda, T., Baba, M., and Ohsumi, Y. (2005). Starvation triggers the delivery of the endoplasmic reticulum to the vacuole via autophagy in yeast. Traffic *6*, 56–65.

Hamasaki, M., Furuta, N., Matsuda, A., Nezu, A., Yamamoto, A., Fujita, N., Oomori, H., Noda, T., Haraguchi, T., Hiraoka, Y., et al. (2013). Autophagosomes form at ER-mitochondria contact sites. Nature *495*, 389–393.

Hanna, R.A., Quinsay, M.N., Orogo, A.M., Giang, K., Rikka, S., and Gustafsson, Å.B. (2012). Microtubule-associated protein 1 light chain 3 (LC3) interacts with Bnip3 protein to selectively remove endoplasmic reticulum and mitochondria via autophagy. J. Biol. Chem. *287*, 19094–19104.

Hara, T., Takamura, A., Kishi, C., Iemura, S.-I., Natsume, T., Guan, J.-L., and Mizushima, N. (2008). FIP200, a ULK-interacting protein, is required for autophagosome formation in mammalian cells. J. Cell Biol. *181*, 497–510.

Hawley, S.A., Davison, M., Woods, A., Davies, S.P., Beri, R.K., Carling, D., and Hardie, D.G. (1996). Characterization of the AMP-activated protein kinase kinase from rat liver and identification of threonine 172 as the major site at which it phosphorylates AMP-activated protein kinase. J. Biol. Chem. *271*, 27879–27887.

Hosokawa, N., Sasaki, T., Iemura, S., Natsume, T., Hara, T., and Mizushima, N. (2009b). Atg101, a novel mammalian autophagy protein interacting with Atg13. Autophagy *5*, 973–979.

Hosokawa, N., Hara, T., Kaizuka, T., Kishi, C., Takamura, A., Miura, Y., Iemura, S., Natsume, T., Takehana, K., Yamada, N., et al. (2009a). Nutrient-dependent mTORC1 association with the ULK1-Atg13-FIP200 complex required for autophagy. Mol. Biol. Cell *20*, 1981–1991.

Huang, J., and Manning, B.D. (2009). A complex interplay between Akt, TSC2 and the two mTOR complexes. Biochem. Soc. Trans. *37*, 217–222.

Ichimura, Y., Kirisako, T., Takao, T., Satomi, Y., Shimonishi, Y., Ishihara, N., Mizushima, N., Tanida, I., Kominami, E., Ohsumi, M., et al. (2000). A ubiquitin-like system mediates protein lipidation. Nature *408*, 488–492.

Inoki, K., Zhu, T., and Guan, K.-L. (2003). TSC2 mediates cellular energy response to control cell growth and survival. Cell *115*, 577–590.

Itakura, E., Kishi, C., Inoue, K., and Mizushima, N. (2008). Beclin 1 forms two distinct phosphatidylinositol 3-kinase complexes with mammalian Atg14 and UVRAG. Mol. Biol. Cell *19*, 5360–5372.

Jin, S.M., and Youle, R.J. (2013). The accumulation of misfolded proteins in the mitochondrial matrix is sensed by PINK1 to induce PARK2/Parkin-mediated mitophagy of polarized mitochondria. Autophagy *9*, 1750–1757.

Jin, S.M., Lazarou, M., Wang, C., Kane, L.A., Narendra, D.P., and Youle, R.J. (2010). Mitochondrial membrane potential regulates PINK1 import and proteolytic destabilization by PARL. J. Cell Biol. *191*, 933–942.

Jinek, M., Chylinski, K., Fonfara, I., Hauer, M., Doudna, J.A., and Charpentier, E. (2012). A programmable dual-RNA-guided DNA endonuclease in adaptive bacterial immunity. Science *337*, 816–821.

Jinek, M., East, A., Cheng, A., Lin, S., Ma, E., and Doudna, J. (2013). RNA-programmed genome editing in human cells. Elife *2*, e00471.

Jung, C.H., Jun, C.B., Ro, S.-H., Kim, Y.-M., Otto, N.M., Cao, J., Kundu, M., and Kim, D.-H. (2009). ULK-Atg13-FIP200 complexes mediate mTOR signaling to the autophagy machinery. Mol. Biol. Cell *20*, 1992–2003.

Kanki, T., Wang, K., Cao, Y., Baba, M., and Klionsky, D.J. (2009). Atg32 is a mitochondrial protein that confers selectivity during mitophagy. Dev. Cell *17*, 98–109.

Khaminets, A., Heinrich, T., Mari, M., Grumati, P., Huebner, A.K., Akutsu, M., Liebmann, L., Stolz, A., Nietzsche, S., Koch, N., et al. (2015). Regulation of endoplasmic reticulum turnover by selective autophagy. Nature *522*, 354–358.

Khaminets, A., Behl, C., and Dikic, I. (2016). Ubiquitin-Dependent And Independent Signals In Selective Autophagy. Trends Cell Biol. *26*, 6–16.

Kim, J., Kundu, M., Viollet, B., and Guan, K.-L. (2011). AMPK and mTOR regulate autophagy through direct phosphorylation of Ulk1. Nat. Cell Biol. *13*, 132–141.

Kim, S., Kim, D., Cho, S.W., Kim, J., and Kim, J.-S. (2014). Highly efficient RNA-guided genome editing in human cells via delivery of purified Cas9 ribonucleoproteins. Genome Res. *24*, 1012–1019.

Kirisako, T., Ichimura, Y., Okada, H., Kabeya, Y., Mizushima, N., Yoshimori, T., Ohsumi, M., Takao, T., Noda, T., and Ohsumi, Y. (2000). The reversible modification regulates the membrane-binding state of Apg8/Aut7 essential for autophagy and the cytoplasm to vacuole targeting pathway. J. Cell Biol. *151*, 263–276.

Kitada, T., Asakawa, S., Hattori, N., Matsumine, H., Yamamura, Y., Minoshima, S., Yokochi, M., Mizuno, Y., and Shimizu, N. (1998). Mutations in the parkin gene cause autosomal recessive juvenile parkinsonism. Nature *392*, 605–608.

Koike-Yusa, H., Li, Y., Tan, E.-P., Velasco-Herrera, M.D.C., and Yusa, K. (2014). Genome-wide recessive genetic screening in mammalian cells with a lentiviral CRISPR-guide RNA library. Nat. Biotechnol. *32*, 267–273.

Kouranova, E., Forbes, K., Zhao, G., Warren, J., Bartels, A., Wu, Y., and Cui, X. (2016). CRISPRs for Optimal Targeting: Delivery of CRISPR Components as DNA, RNA, and Protein into Cultured Cells and Single-Cell Embryos. Hum. Gene Ther. *27*, 464–475.

Koyano, F., Okatsu, K., Kosako, H., Tamura, Y., Go, E., Kimura, M., Kimura, Y., Tsuchiya, H., Yoshihara, H., Hirokawa, T., et al. (2014). Ubiquitin is phosphorylated by PINK1 to activate parkin. Nature *510*, 162–166.

Kuma, A., Mizushima, N., Ishihara, N., and Ohsumi, Y. (2002). Formation of the approximately 350-kDa Apg12-Apg5.Apg16 multimeric complex, mediated by Apg16 oligomerization, is essential for autophagy in yeast. J. Biol. Chem. *277*, 18619–18625.

Lazarou, M., Sliter, D.A., Kane, L.A., Sarraf, S.A., Wang, C., Burman, J.L., Sideris, D.P., Fogel, A.I., and Youle, R.J. (2015). The ubiquitin kinase PINK1 recruits autophagy receptors to induce mitophagy. Nature *524*, 309–314.

Liang, J.-R., Martinez, A., Lane, J.D., Mayor, U., Clague, M.J., and Urbé, S. (2015). USP30 deubiquitylates mitochondrial Parkin substrates and restricts apoptotic cell death. EMBO Rep. *16*, 618–627.

Liang, J.R., Lingeman, E., Ahmed, S., and Corn, J.E. (2018). Atlastins remodel the endoplasmic reticulum for selective autophagy. J. Cell Biol. *217*, 3354–3367.

Lin, M.G., and Hurley, J.H. (2016). Structure and function of the ULK1 complex in autophagy. Curr. Opin. Cell Biol. *39*, 61–68.

Lin, S., Staahl, B.T., Alla, R.K., and Doudna, J.A. (2014). Enhanced homology-directed human genome engineering by controlled timing of CRISPR/Cas9 delivery. Elife *3*, e04766.

Liu, L., Feng, D., Chen, G., Chen, M., Zheng, Q., Song, P., Ma, Q., Zhu, C., Wang, R., Qi, W., et al. (2012). Mitochondrial outer-membrane protein FUNDC1 mediates hypoxia-induced mitophagy in mammalian cells. Nat. Cell Biol. *14*, 177–185.

Makarova, K.S., Grishin, N.V., Shabalina, S.A., Wolf, Y.I., and Koonin, E.V. (2006). A putative RNA-interference-based immune system in prokaryotes: computational analysis of the predicted enzymatic machinery, functional analogies with eukaryotic RNAi, and hypothetical mechanisms of action. Biol. Direct *1*, 7.

Mali, P., Yang, L., Esvelt, K.M., Aach, J., Guell, M., DiCarlo, J.E., Norville, J.E., and Church, G.M. (2013). RNA-guided human genome engineering via Cas9. Science *339*, 823–826.

Marraffini, L.A., and Sontheimer, E.J. (2008). CRISPR interference limits horizontal gene transfer in staphylococci by targeting DNA. Science *322*, 1843–1845.

Matsuda, N., Sato, S., Shiba, K., Okatsu, K., Saisho, K., Gautier, C.A., Sou, Y.-S., Saiki, S., Kawajiri, S., Sato, F., et al. (2010). PINK1 stabilized by mitochondrial depolarization recruits Parkin to damaged mitochondria and activates latent Parkin for mitophagy. J. Cell Biol. *189*, 211–221.

Matsunaga, K., Saitoh, T., Tabata, K., Omori, H., Satoh, T., Kurotori, N., Maejima, I., Shirahama-Noda, K., Ichimura, T., Isobe, T., et al. (2009). Two Beclin 1-binding proteins, Atg14L and Rubicon, reciprocally regulate autophagy at different stages. Nat. Cell Biol. *11*, 385–396.

Meissner, C., Lorenz, H., Weihofen, A., Selkoe, D.J., and Lemberg, M.K. (2011). The mitochondrial intramembrane protease PARL cleaves human Pink1 to regulate Pink1 trafficking. J. Neurochem. *117*, 856–867.

Mercer, C.A., Kaliappan, A., and Dennis, P.B. (2009). A novel, human Atg13 binding protein, Atg101, interacts with ULK1 and is essential for macroautophagy. Autophagy *5*, 649–662.

Mizushima, N., Sugita, H., Yoshimori, T., and Ohsumi, Y. (1998). A new protein conjugation system in human. The counterpart of the yeast Apg12p conjugation system essential for autophagy. J. Biol. Chem. *273*, 33889–33892.

Mochida, K., Oikawa, Y., Kimura, Y., Kirisako, H., Hirano, H., Ohsumi, Y., and Nakatogawa, H. (2015). Receptor-mediated selective autophagy degrades the endoplasmic reticulum and the nucleus. Nature *522*, 359–362.

Narendra, D.P., Jin, S.M., Tanaka, A., Suen, D.-F., Gautier, C.A., Shen, J., Cookson, M.R., and Youle, R.J. (2010). PINK1 is selectively stabilized on impaired mitochondria to activate Parkin. PLoS Biol. *8*, e1000298.

Nascimbeni, A.C., Giordano, F., Dupont, N., Grasso, D., Vaccaro, M.I., Codogno, P., and Morel, E. (2017). ER-plasma membrane contact sites contribute to autophagosome biogenesis by

regulation of local PI3P synthesis. EMBO J. *36*, 2018–2033.

Novak, I., Kirkin, V., McEwan, D.G., Zhang, J., Wild, P., Rozenknop, A., Rogov, V., Löhr, F., Popovic, D., Occhipinti, A., et al. (2010). Nix is a selective autophagy receptor for mitochondrial clearance. EMBO Rep. *11*, 45–51.

Novikoff, A.B. (1956). Electron microscopy of lysosome-rich fractions from rat liver. J. Cell Biol. *2*, 179–184.

Okamoto, K., Kondo-Okamoto, N., and Ohsumi, Y. (2009). Mitochondria-anchored receptor Atg32 mediates degradation of mitochondria via selective autophagy. Dev. Cell *17*, 87–97.

Orsi, A., Razi, M., Dooley, H.C., Robinson, D., Weston, A.E., Collinson, L.M., and Tooze, S.A. (2012). Dynamic and transient interactions of Atg9 with autophagosomes, but not membrane integration, are required for autophagy. Mol. Biol. Cell *23*, 1860–1873.

Otomo, T., and Yoshimori, T. (2017). Lysophagy: A Method for Monitoring Lysosomal Rupture Followed by Autophagy-Dependent Recovery. Methods Mol. Biol. *1594*, 141–149.

Papinski, D., Schuschnig, M., Reiter, W., Wilhelm, L., Barnes, C.A., Maiolica, A., Hansmann, I., Pfaffenwimmer, T., Kijanska, M., Stoffel, I., et al. (2014). Early steps in autophagy depend on direct phosphorylation of Atg9 by the Atg1 kinase. Mol. Cell *53*, 471–483.

Polson, H.E.J., de Lartigue, J., Rigden, D.J., Reedijk, M., Urbé, S., Clague, M.J., and Tooze, S.A. (2010). Mammalian Atg18 (WIPI2) localizes to omegasome-anchored phagophores and positively regulates LC3 lipidation. Autophagy *6*, 506–522.

Puri, C., Renna, M., Bento, C.F., Moreau, K., and Rubinsztein, D.C. (2014). ATG16L1 meets ATG9 in recycling endosomes: additional roles for the plasma membrane and endocytosis in autophagosome biogenesis. Autophagy *10*, 182–184.

Quinsay, M.N., Thomas, R.L., Lee, Y., and Gustafsson, A.B. (2010). Bnip3-mediated mitochondrial autophagy is independent of the mitochondrial permeability transition pore. Autophagy *6*, 855–862.

Rajamohan, F., Reyes, A.R., Frisbie, R.K., Hoth, L.R., Sahasrabudhe, P., Magyar, R., Landro, J.A., Withka, J.M., Caspers, N.L., Calabrese, M.F., et al. (2016). Probing the enzyme kinetics, allosteric modulation and activation of α1- and α2-subunit-containing AMP-activated protein kinase (AMPK) heterotrimeric complexes by pharmacological and physiological activators. Biochem. J. *473*, 581–592.

Richardson, C.D., Ray, G.J., DeWitt, M.A., Curie, G.L., and Corn, J.E. (2016a). Enhancing homology-directed genome editing by catalytically active and inactive CRISPR-Cas9 using asymmetric donor DNA. Nat. Biotechnol. *34*, 339–344.

Richardson, C.D., Ray, G.J., Bray, N.L., and Corn, J.E. (2016b). Non-homologous DNA

increases gene disruption efficiency by altering DNA repair outcomes. Nat. Commun. *7*, 12463.
Rohland, N., and Reich, D. (2012). Cost-effective, high-throughput DNA sequencing libraries for multiplexed target capture. Genome Res. *22*, 939–946.

Ross, F.A., Jensen, T.E., and Hardie, D.G. (2016). Differential regulation by AMP and ADP of AMPK complexes containing different γ subunit isoforms. Biochem. J. *473*, 189–199.

Rostislavleva, K., Soler, N., Ohashi, Y., Zhang, L., Pardon, E., Burke, J.E., Masson, G.R., Johnson, C., Steyaert, J., Ktistakis, N.T., et al. (2015). Structure and flexibility of the endosomal Vps34 complex reveals the basis of its function on membranes. Science *350*, aac7365.

Russell, R.C., Tian, Y., Yuan, H., Park, H.W., Chang, Y.-Y., Kim, J., Kim, H., Neufeld, T.P., Dillin, A., and Guan, K.-L. (2013). ULK1 induces autophagy by phosphorylating Beclin-1 and activating VPS34 lipid kinase. Nat. Cell Biol. *15*, 741–750.

Sanders, M.J., Grondin, P.O., Hegarty, B.D., Snowden, M.A., and Carling, D. (2007). Investigating the mechanism for AMP activation of the AMP-activated protein kinase cascade. Biochem. J. *403*, 139–148.

Sapranauskas, R., Gasiunas, G., Fremaux, C., Barrangou, R., Horvath, P., and Siksnys, V. (2011). The Streptococcus thermophilus CRISPR/Cas system provides immunity in Escherichia coli. Nucleic Acids Res. *39*, 9275–9282.

Saxton, R.A., and Sabatini, D.M. (2017). mTOR Signaling in Growth, Metabolism, and Disease. Cell *168*, 960–976.

Schu, P.V., Takegawa, K., Fry, M.J., Stack, J.H., Waterfield, M.D., and Emr, S.D. (1993). Phosphatidylinositol 3-kinase encoded by yeast VPS34 gene essential for protein sorting. Science *260*, 88–91.

Schwarz, D.S., and Blower, M.D. (2016). The endoplasmic reticulum: structure, function and response to cellular signaling. Cell Mol. Life Sci. *73*, 79–94.

Shalem, O., Sanjana, N.E., Hartenian, E., Shi, X., Scott, D.A., Mikkelson, T., Heckl, D., Ebert, B.L., Root, D.E., Doench, J.G., et al. (2014). Genome-scale CRISPR-Cas9 knockout screening in human cells. Science *343*, 84–87.

Shintani, T., Mizushima, N., Ogawa, Y., Matsuura, A., Noda, T., and Ohsumi, Y. (1999). Apg10p, a novel protein-conjugating enzyme essential for autophagy in yeast. EMBO J. *18*, 5234–5241.

Smith, M.D., Harley, M.E., Kemp, A.J., Wills, J., Lee, M., Arends, M., von Kriegsheim, A., Behrends, C., and Wilkinson, S. (2018). CCPG1 Is a Non-canonical Autophagy Cargo Receptor Essential for ER-Phagy and Pancreatic ER Proteostasis. Dev. Cell *44*, 217–232.e11.

Stack, J.H., Herman, P.K., Schu, P.V., and Emr, S.D. (1993). A membrane-associated complex

containing the Vps15 protein kinase and the Vps34 PI 3-kinase is essential for protein sorting to the yeast lysosome-like vacuole. EMBO J. *12*, 2195–2204.

Sung, Y.H., Kim, J.M., Kim, H.-T., Lee, J., Jeon, J., Jin, Y., Choi, J.-H., Ban, Y.H., Ha, S.-J., Kim, C.-H., et al. (2014). Highly efficient gene knockout in mice and zebrafish with RNA-guided endonucleases. Genome Res. *24*, 125–131.

Suter, M., Riek, U., Tuerk, R., Schlattner, U., Wallimann, T., and Neumann, D. (2006). Dissecting the role of 5'-AMP for allosteric stimulation, activation, and deactivation of AMP-activated protein kinase. J. Biol. Chem. *281*, 32207–32216.

Tanaka, A., Cleland, M.M., Xu, S., Narendra, D.P., Suen, D.-F., Karbowski, M., and Youle, R.J. (2010). Proteasome and p97 mediate mitophagy and degradation of mitofusins induced by Parkin. J. Cell Biol. *191*, 1367–1380.

Terns, M.P., and Terns, R.M. (2011). CRISPR-based adaptive immune systems. Curr. Opin. Microbiol. *14*, 321–327.

Tsukada, M., and Ohsumi, Y. (1993). Isolation and characterization of autophagy-defective mutants of Saccharomyces cerevisiae. FEBS Lett. *333*, 169–174.

van der Vaart, A., and Reggiori, F. (2010). The Golgi complex as a source for yeast autophagosomal membranes. Autophagy *6*, 800–801.

Valente, E.M., Abou-Sleiman, P.M., Caputo, V., Muqit, M.M.K., Harvey, K., Gispert, S., Ali, Z., Del Turco, D., Bentivoglio, A.R., Healy, D.G., et al. (2004). Hereditary early-onset Parkinson's disease caused by mutations in PINK1. Science *304*, 1158–1160.

Wang, T., Wei, J.J., Sabatini, D.M., and Lander, E.S. (2014). Genetic screens in human cells using the CRISPR-Cas9 system. Science *343*, 80–84.

Wiedenheft, B., Sternberg, S.H., and Doudna, J.A. (2012). RNA-guided genetic silencing systems in bacteria and archaea. Nature *482*, 331–338.

Yamamoto, H., Kakuta, S., Watanabe, T.M., Kitamura, A., Sekito, T., Kondo-Kakuta, C., Ichikawa, R., Kinjo, M., and Ohsumi, Y. (2012). Atg9 vesicles are an important membrane source during early steps of autophagosome formation. J. Cell Biol. *198*, 219–233.

Yamano, K., and Youle, R.J. (2013). PINK1 is degraded through the N-end rule pathway. Autophagy *9*, 1758–1769.

Young, A.R.J., Chan, E.Y.W., Hu, X.W., Köchl, R., Crawshaw, S.G., High, S., Hailey, D.W., Lippincott-Schwartz, J., and Tooze, S.A. (2006). Starvation and ULK1-dependent cycling of mammalian Atg9 between the TGN and endosomes. J. Cell Sci. *119*, 3888–3900.

Zeng, X., Overmeyer, J.H., and Maltese, W.A. (2006). Functional specificity of the mammalian

Beclin-Vps34 PI 3-kinase complex in macroautophagy versus endocytosis and lysosomal enzyme trafficking. J. Cell Sci. *119*, 259–270.

Zhong, Y., Wang, Q.J., Li, X., Yan, Y., Backer, J.M., Chait, B.T., Heintz, N., and Yue, Z. (2009). Distinct regulation of autophagic activity by Atg14L and Rubicon associated with Beclin 1-phosphatidylinositol-3-kinase complex. Nat. Cell Biol. *11*, 468–476.

Zhou, Y., Zhu, S., Cai, C., Yuan, P., Li, C., Huang, Y., and Wei, W. (2014). High-throughput screening of a CRISPR/Cas9 library for functional genomics in human cells. Nature *509*, 487–491.

Appendix 1: Ubiquitin and autophagy custom CRISPRi library quality control

This appendix contains quality control data for a custom ubiquitin CRISPRi library. The library is comprised of multiple sub-libraries: autophagy genes, E1 ubiquitin-activating enzymes/E2 ubiquitin-conjugating enzymes, E3 ubiquitin ligases, deubiquitinase genes, and five non-targeting sub-libraries to be used as controls. The autophagy sub-library was used previously in chapter 3, so you can refer to the chapter to see data produced with this library.

The library contains ten sgRNAs for each transcription start site.

Table 8: Number of sgRNAs in each sub-library

Sub-library	# sgRNAs in sub-library
ATG (autophagy genes)	1894
DUB (deubiquitinases)	4897
E1 activating /E2 conjugating enzymes	1835
E3 ubiquitin ligases	30375
Non-targeting 1	2000
Non-targeting 2	2000
Non-targeting 3	2000
Non-targeting 4	2000
Non-targeting 5	2000

This library will be most useful for those looking to gain in-depth data about the ubiquitin and autophagy family proteins, especially considering the depth of coverage of these genes. In each sub-library, 90% or more of reads aligned to a known sgRNA (Figure 16). Greater than 98.5% of sgRNAs are represented with at least one sequencing read (Figure 20 - Figure 28). In addition, the difference in representation between the 90^{th} and 10^{th} percentile is less than 7.5-fold for non-targeting libraries and 10-fold for ubiquitin and autophagy libraries (Figure 17, Figure 18, Figure 19).

The graphs below represent the quality control analysis conducted for these CRISPRi sub-libraries and are intended for future users of this library to refer to in order to understand more about the libraries they are working with.

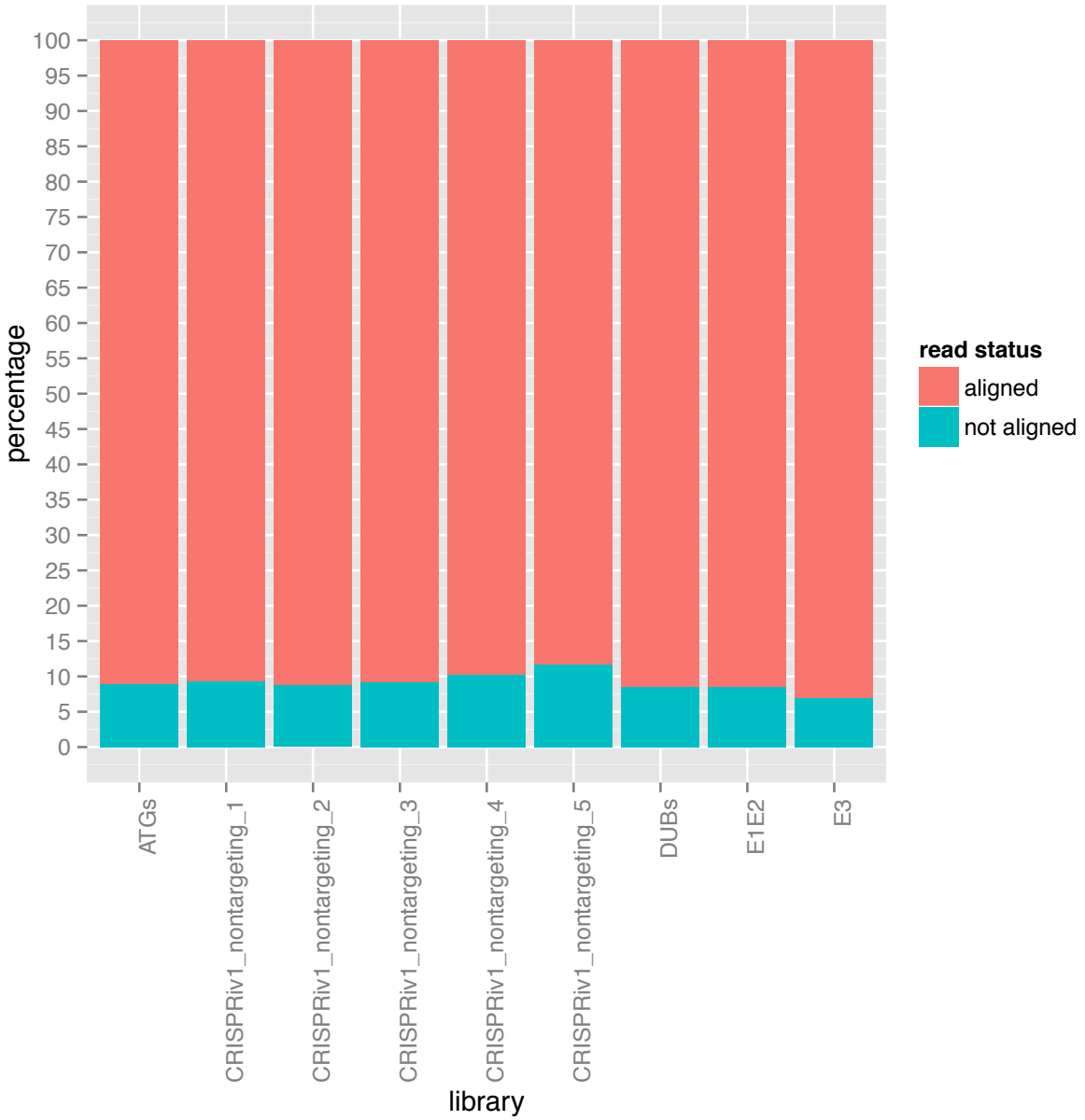

Figure 16: Percentage of aligned reads for each sub-library
The above graph shows the percentage of aligned and not aligned reads for each sub-library. The library was sequenced using the HiSeq2500 and reads were aligned to the file containing all the sgRNAs. Non-targeting sub-library 5 contains more than 10% of not aligned reads, while the rest of the sub-libraries contain less than 10%. This is in-line with other published quality control metrics for CRISPR screens.

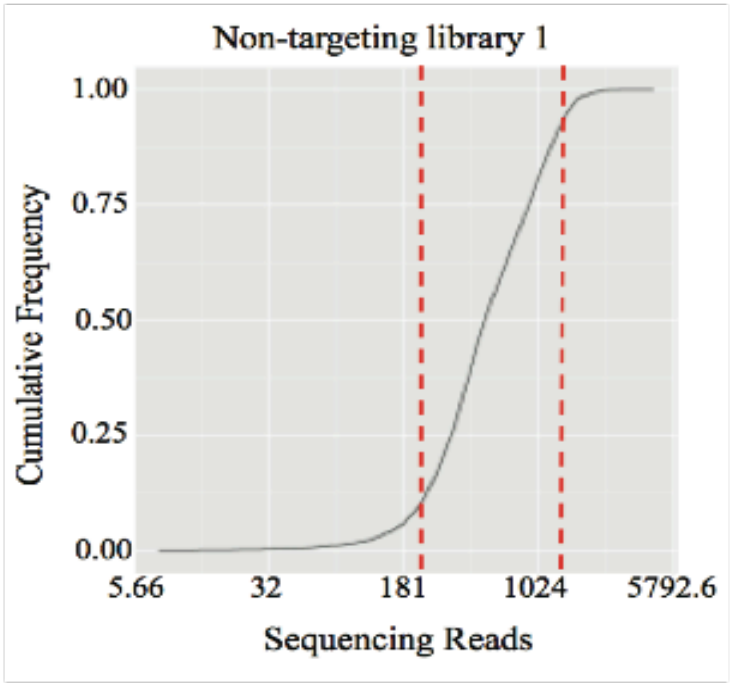

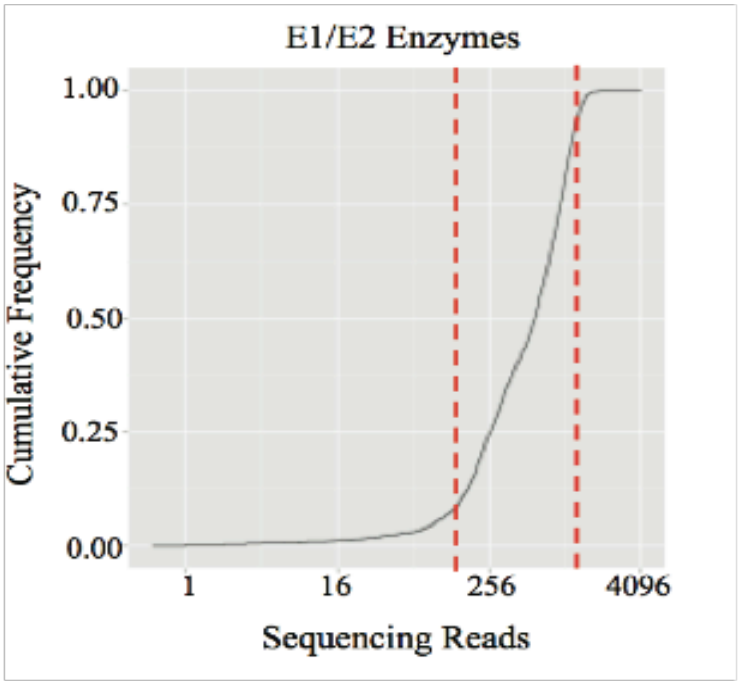

Figure 17: Cumulative frequency of reads for non-targeting sub-library1 and E1/E2 sub-library
The cumulative frequency of sequencing reads for two representative sub-libraries is shown above. The red dashed lines represent the 10th percentile and the 90th percentile of the number of sequencing reads for a given sgRNA. The fold-difference between the 10th and 90th percentiles is one quality control indicator for a library, with a lower fold-difference being better.

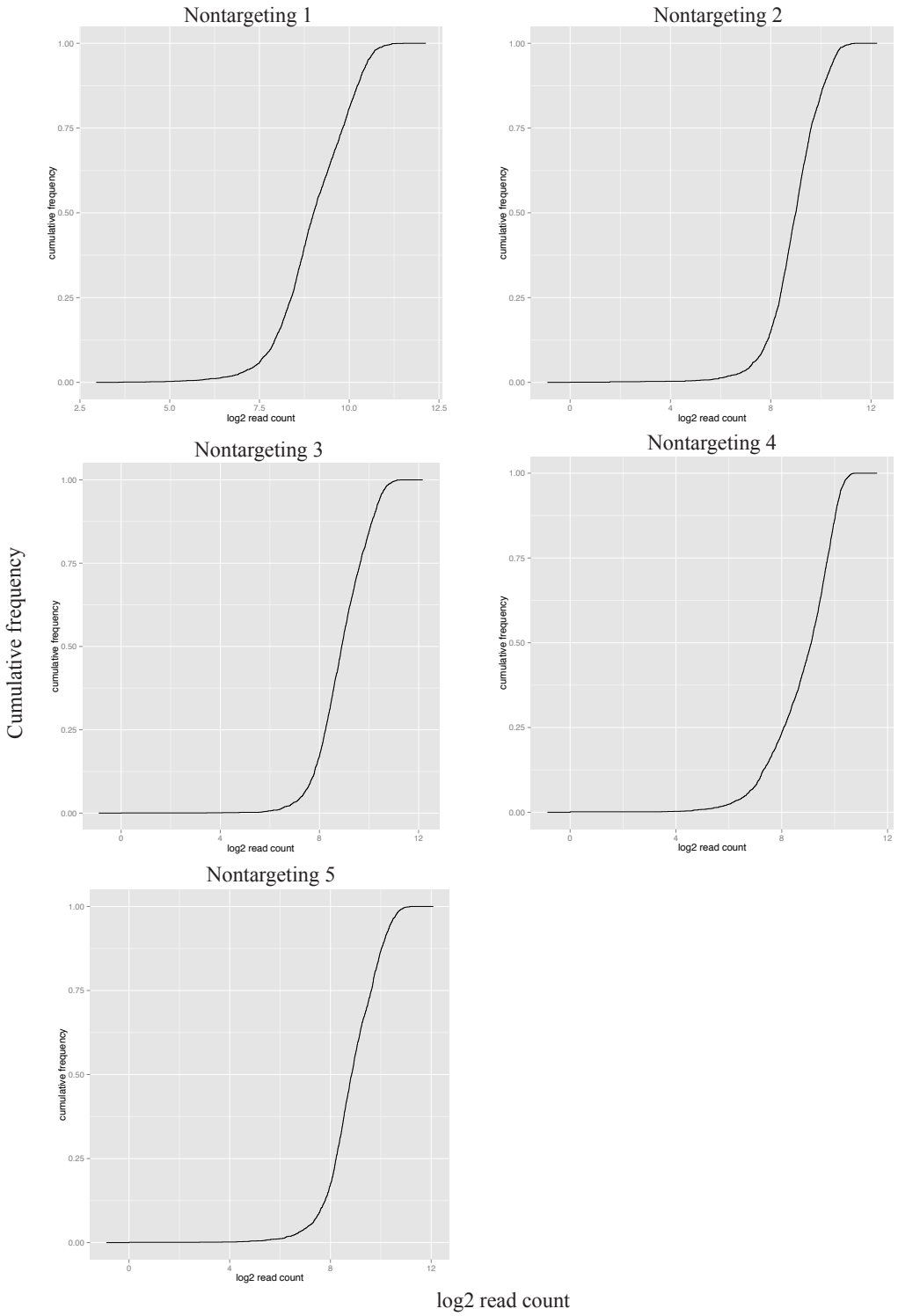

Figure 18: Cumulative frequency of sequencing reads for non-targeting sub-libraries.
The graphs above show the cumulative frequency of sequencing reads for the five non-targeting sub-libraries. The difference in representation of sequencing read counts between the 10th and

90th percentile is 7.5-fold or less for each sub-library.

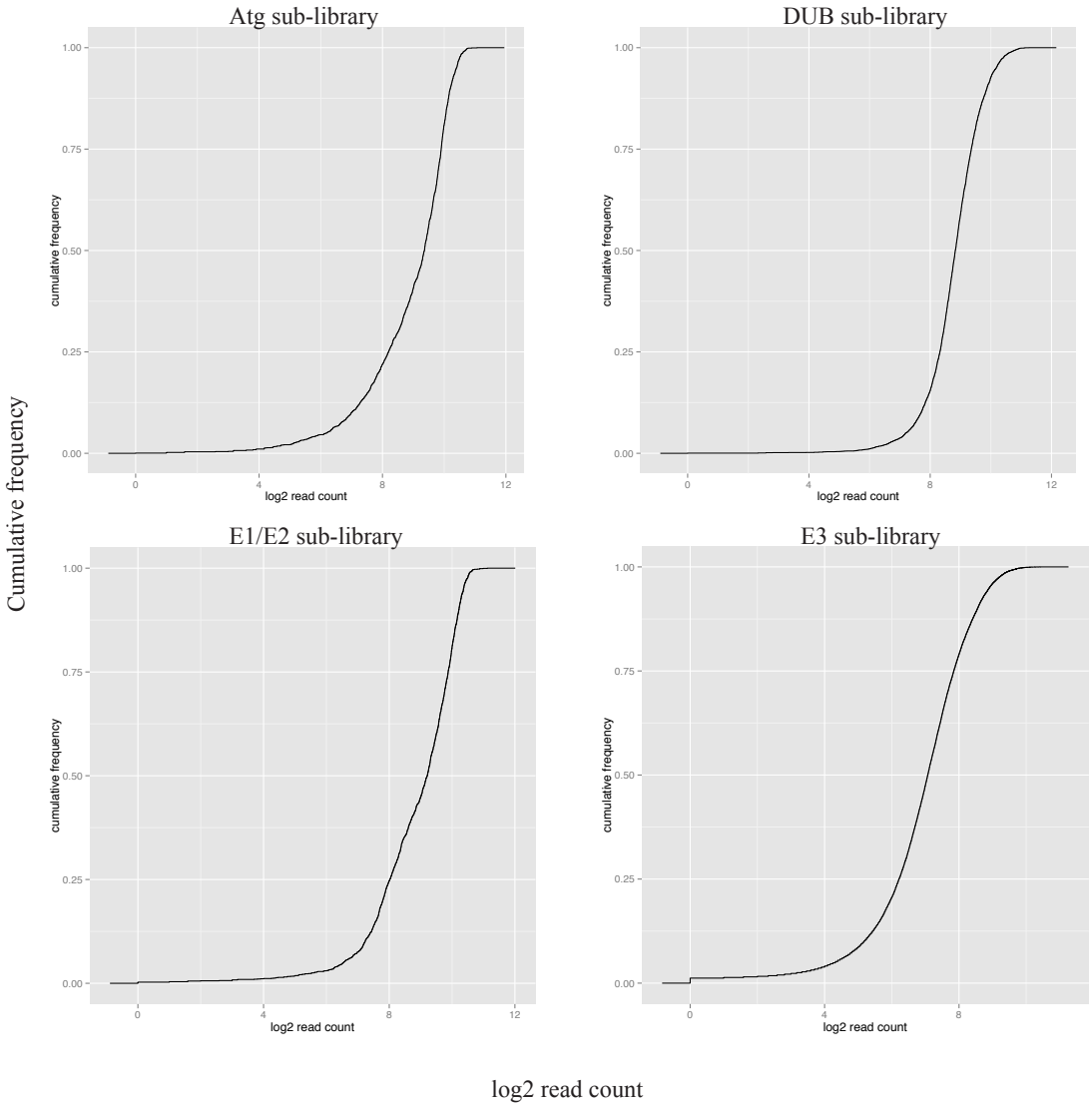

log2 read count

Figure 19: Cumulative frequency of sequencing reads for ubiquitin sub-libraries.
The cumulative frequency of sequencing reads for the ubiquitin/autophagy sub-libraries. The difference in representation of sequencing read counts between the 10th and 90th percentile is 10-fold or less for each sub-library.

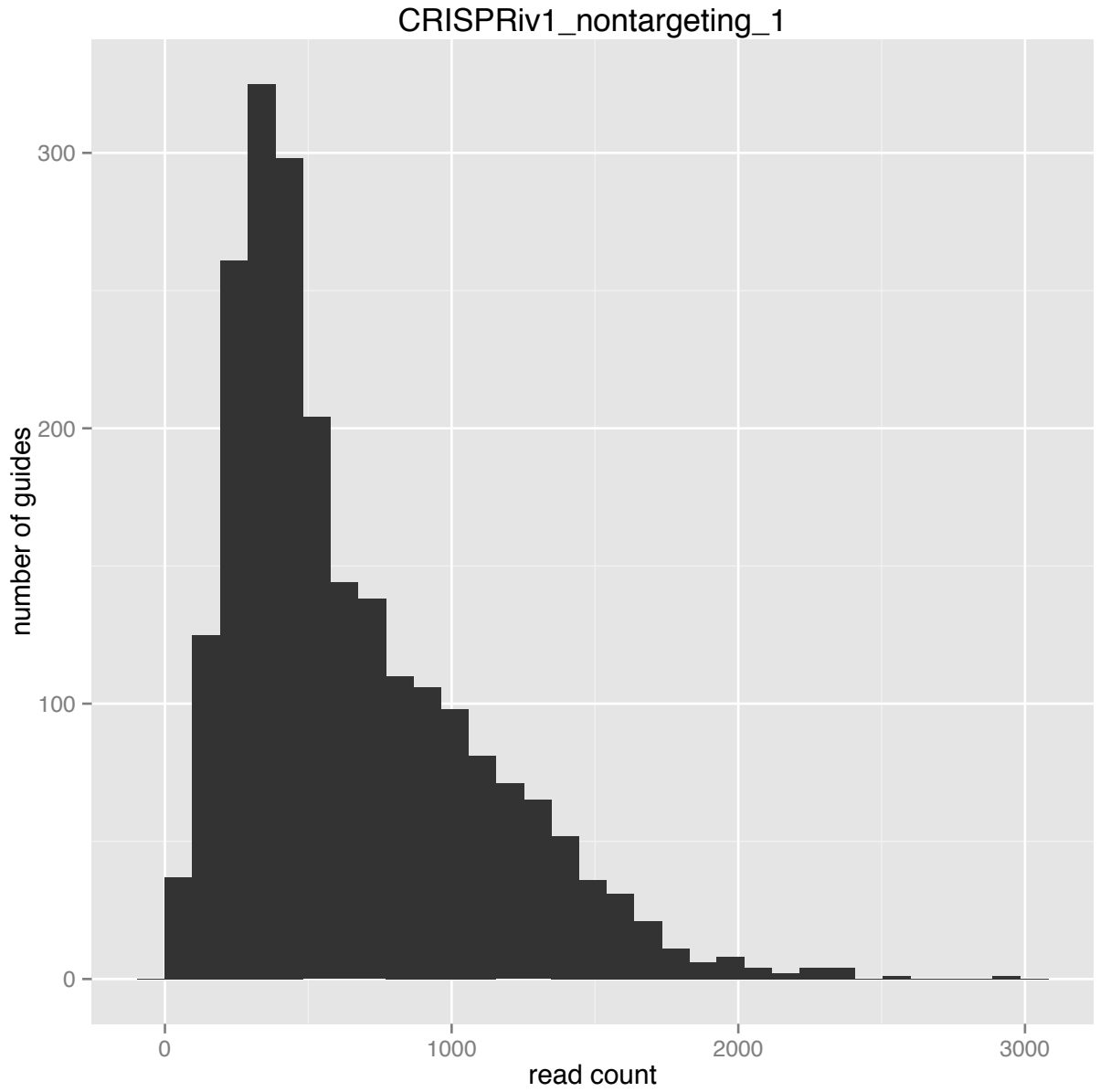

Figure 20: Number of guides and read count for non-targeting sub-library 1
The above graph depicts the number of sgRNAs in this sub-library that are represented by a given read count. Ideally, this graph would be a perfect normal distribution. However, the data is skewed to the right, meaning that a portion of gRNAs are very highly represented in this non-targeting library.

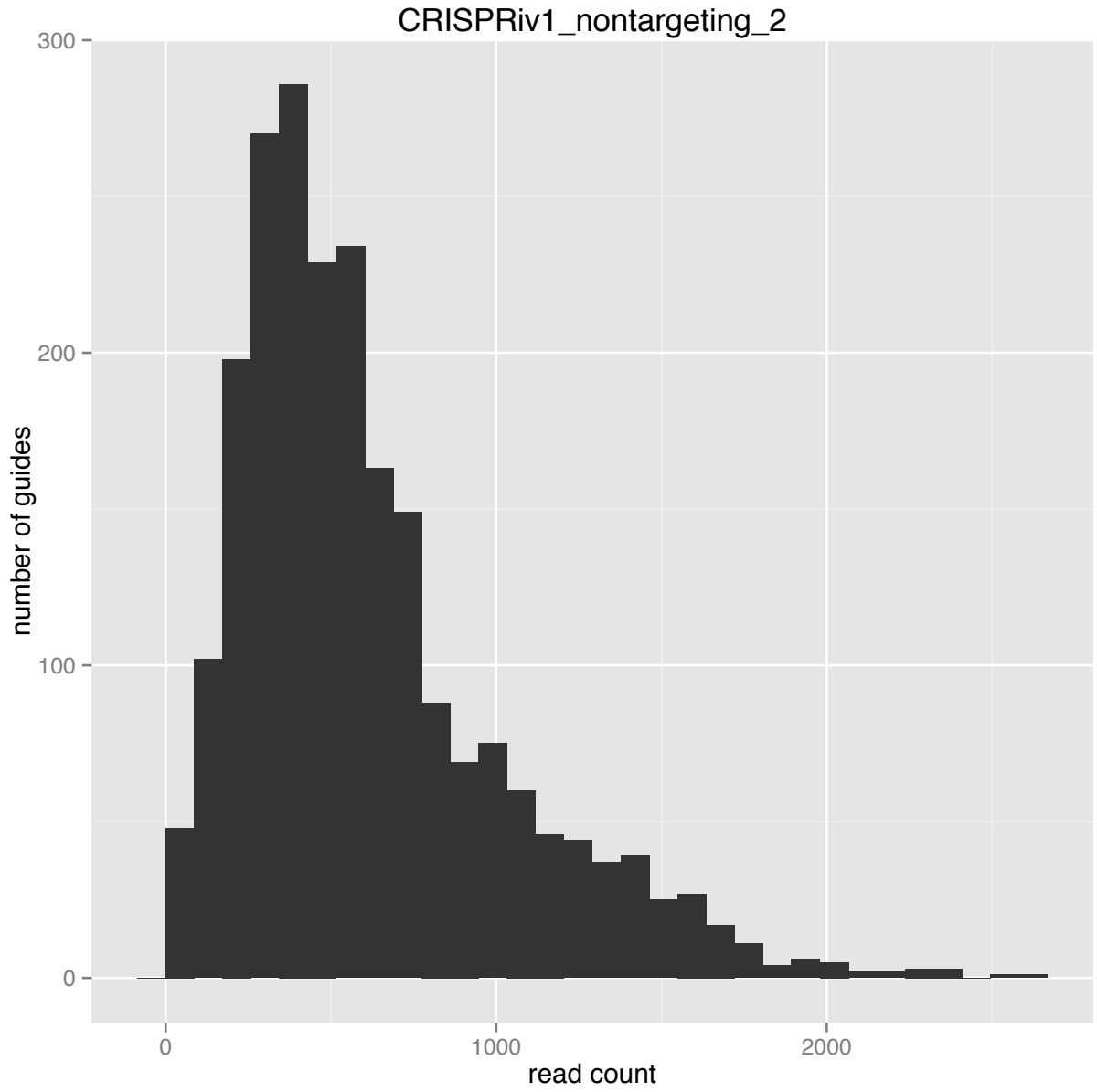

Figure 21: Number of guides and read count for non-targeting sub-library 2
The above graph depicts the number of sgRNAs in this sub-library that are represented by a given read count. Ideally, this graph would be a perfect normal distribution. However, the data is skewed to the right, meaning that a portion of gRNAs is very highly represented in this non-targeting library.

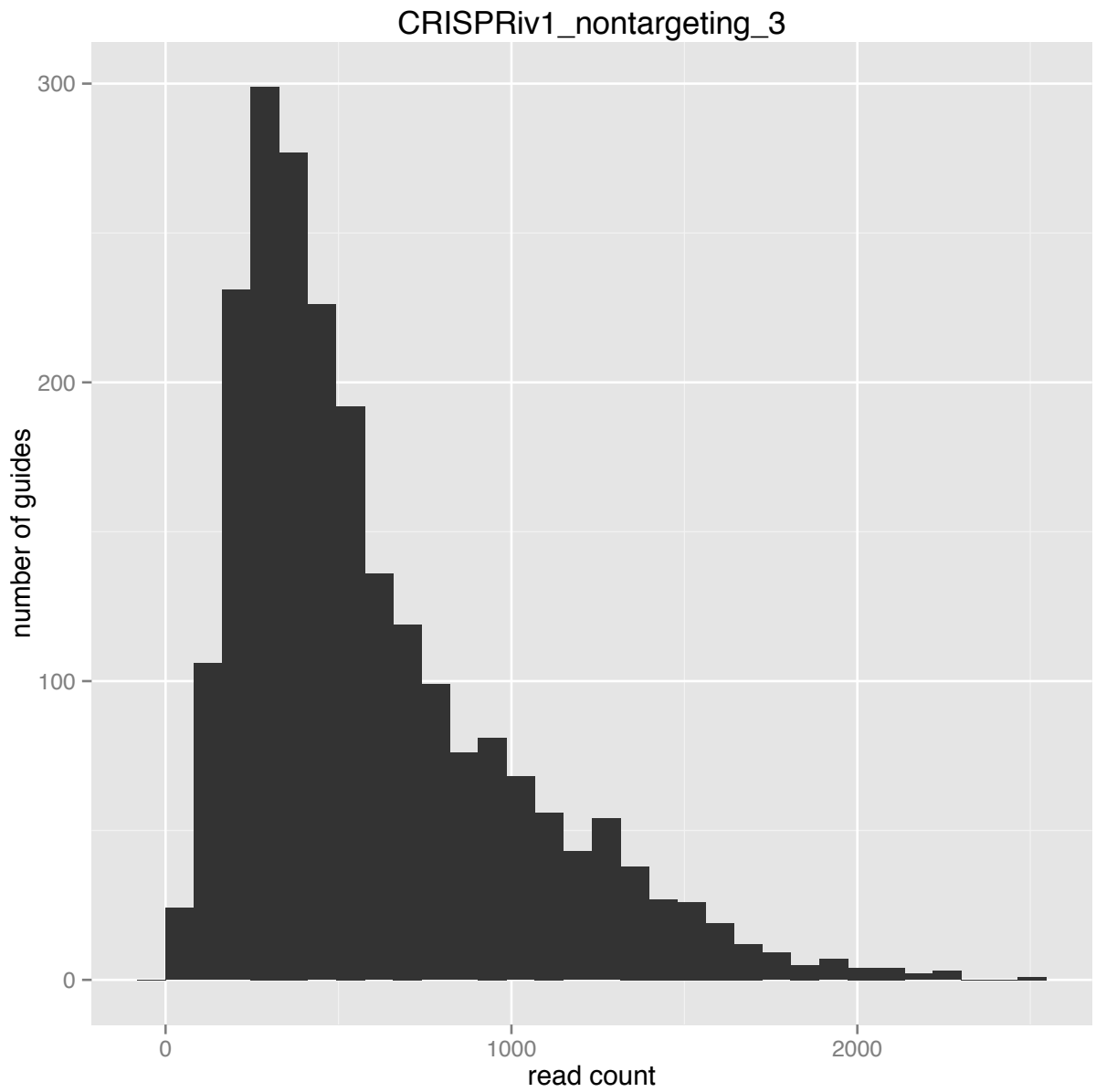

Figure 22: Number of guides and read count for non-targeting sub-library 3
The above graph depicts the number of sgRNAs in this sub-library that are represented by a given read count. Ideally, this graph would be a perfect normal distribution. However, the data is skewed to the right, meaning that a portion of gRNAs is very highly represented in this non-targeting library.

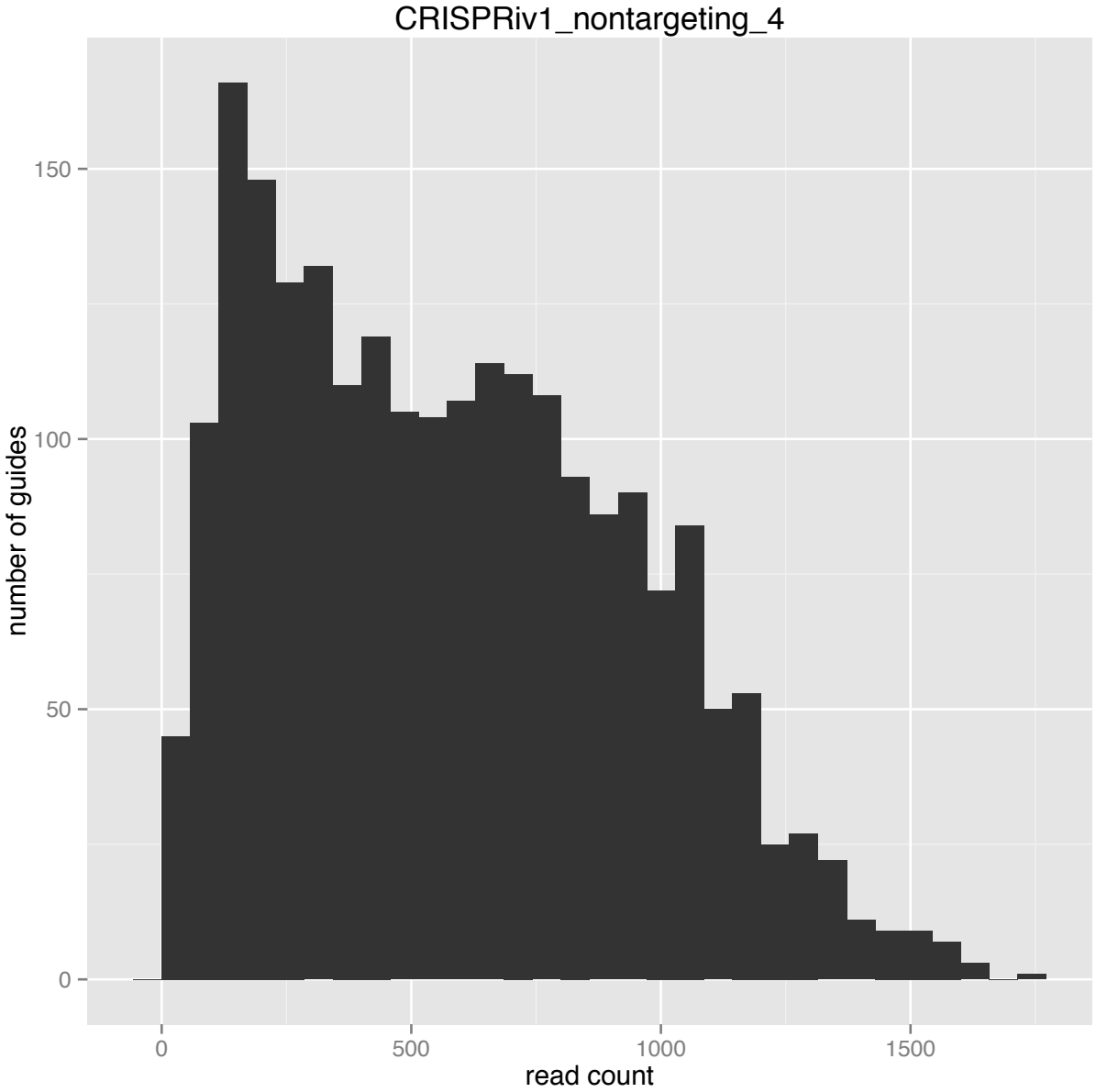

Figure 23: Number of guides and read count for non-targeting sub-library 4
The above graph depicts the number of sgRNAs in this sub-library that are represented by a given read count. Ideally, this graph would be a perfect normal distribution. However, the data is skewed to the right, meaning that a portion of gRNAs is very highly represented in this non-targeting library.

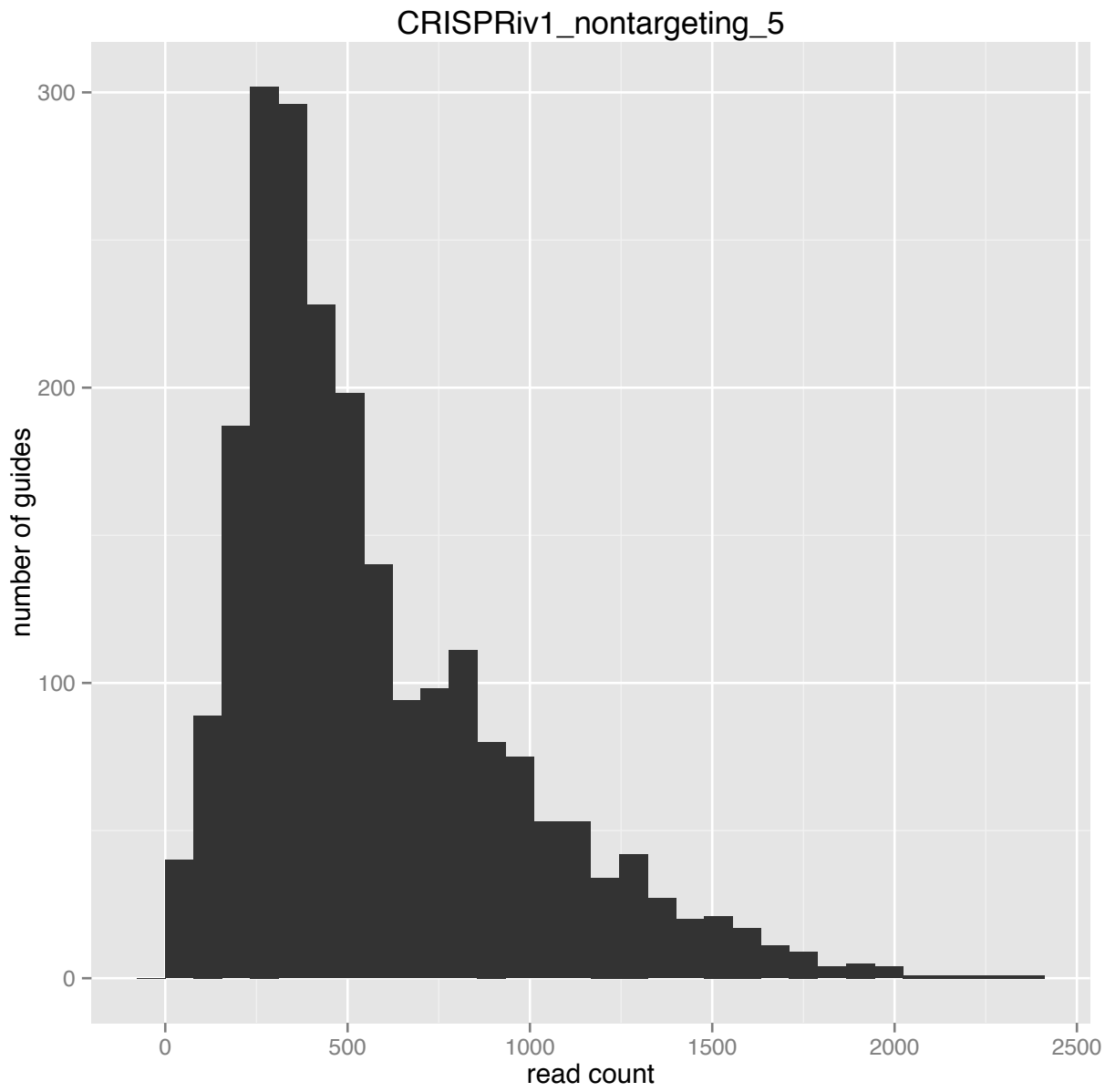

Figure 24: Number of guides and read count for non-targeting sub-library 5
The above graph depicts the number of sgRNAs in this sub-library that are represented by a given read count. Ideally, this graph would be a perfect normal distribution. However, the data is skewed to the right, meaning that a portion of gRNAs is very highly represented in this non-targeting library.

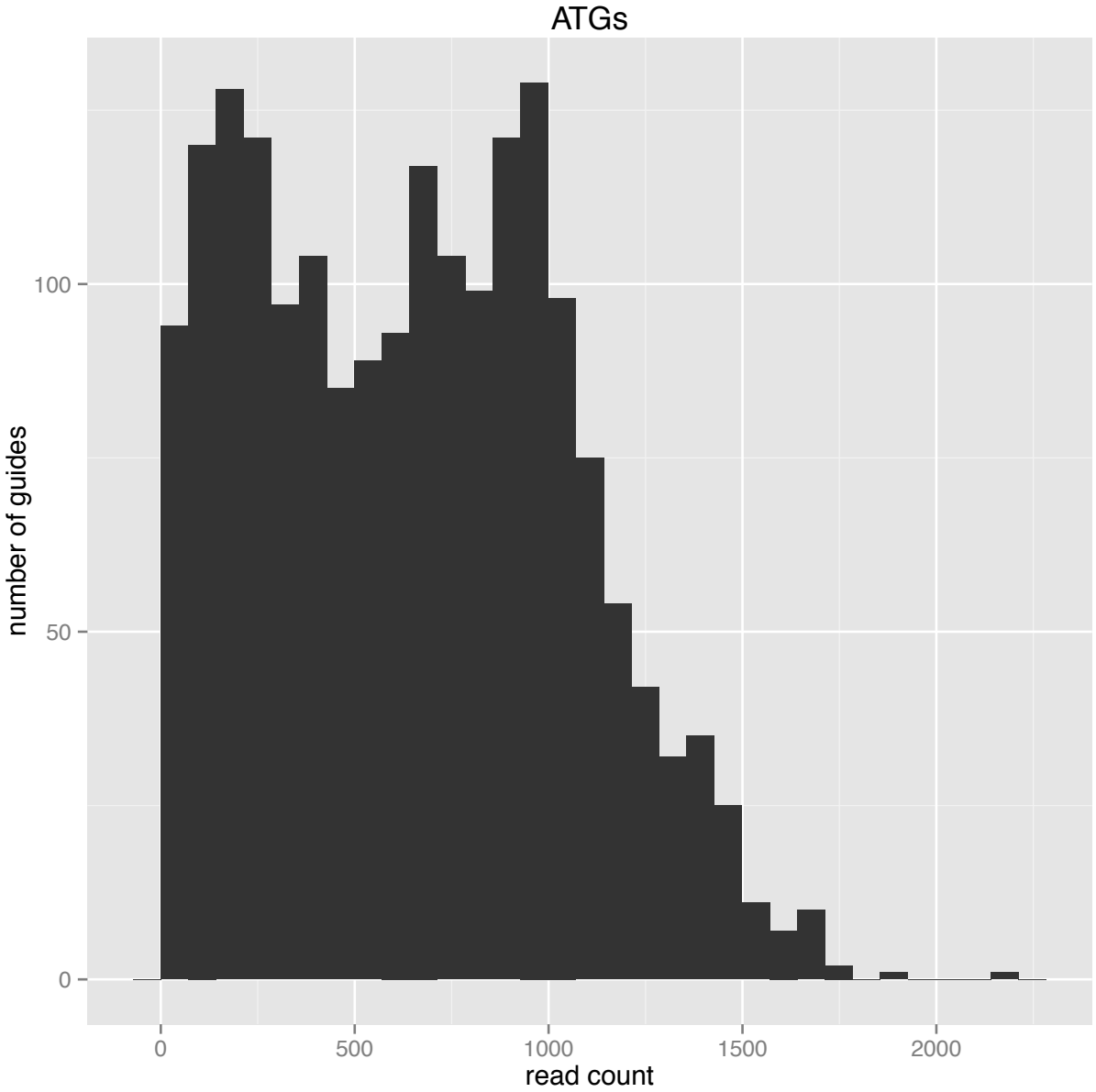

Figure 25: Number of guides and read count for autophagy sub-library
The above graph depicts the number of sgRNAs in this sub-library that are represented by a given read count. Ideally, this graph would be a perfect normal distribution. In this graph, there are a large amount of guides (nearly 100) that are presented at zero read counts.

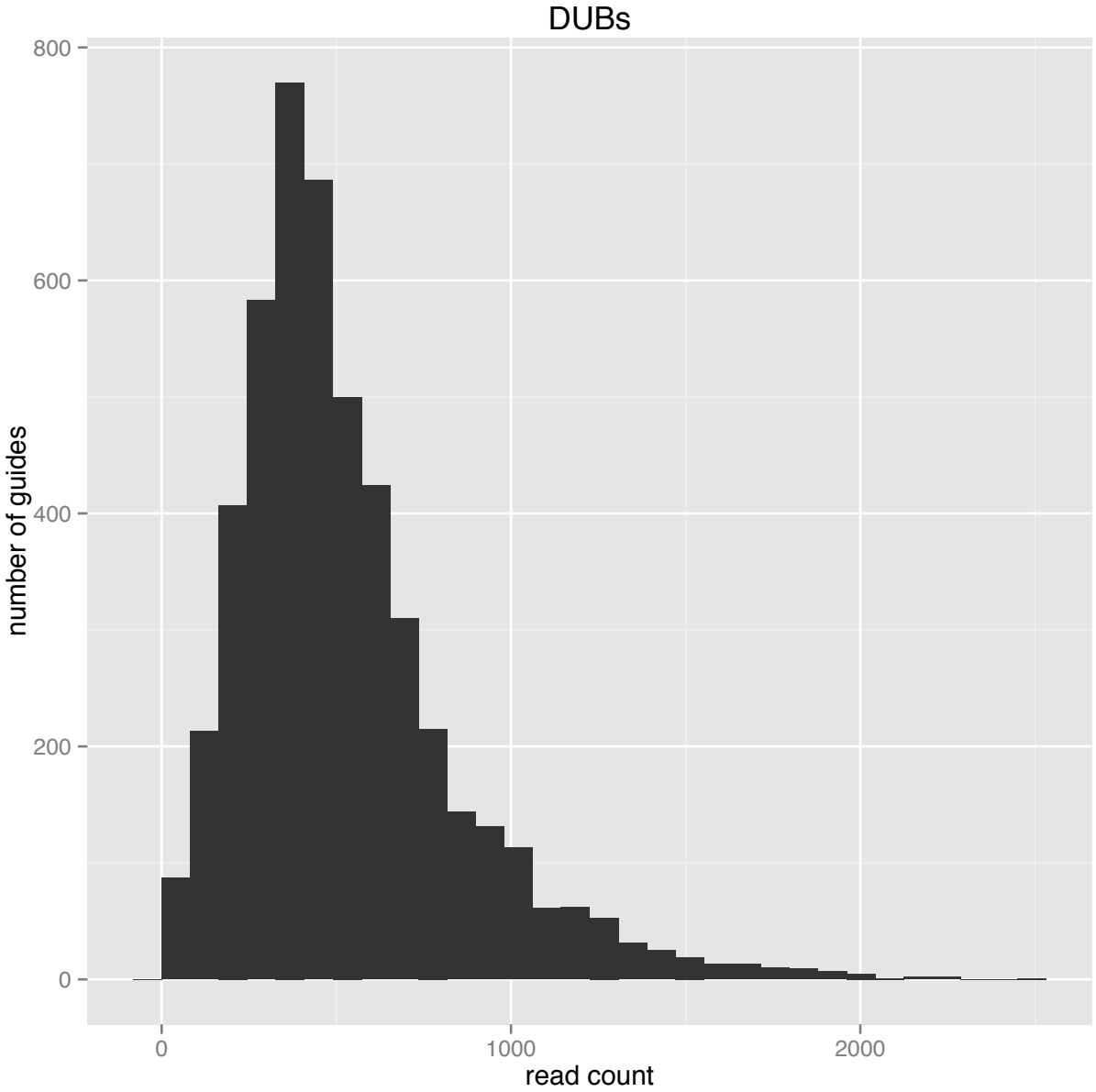

Figure 26: Number of guides and read count for DUB (deubiquitinase) sub-library
The above graph depicts the number of sgRNAs in this sub-library that are represented by a given read count. Ideally, this graph would be a perfect normal distribution. However, the data is skewed to the right, meaning that a portion of gRNAs is very highly represented in this non-targeting library.

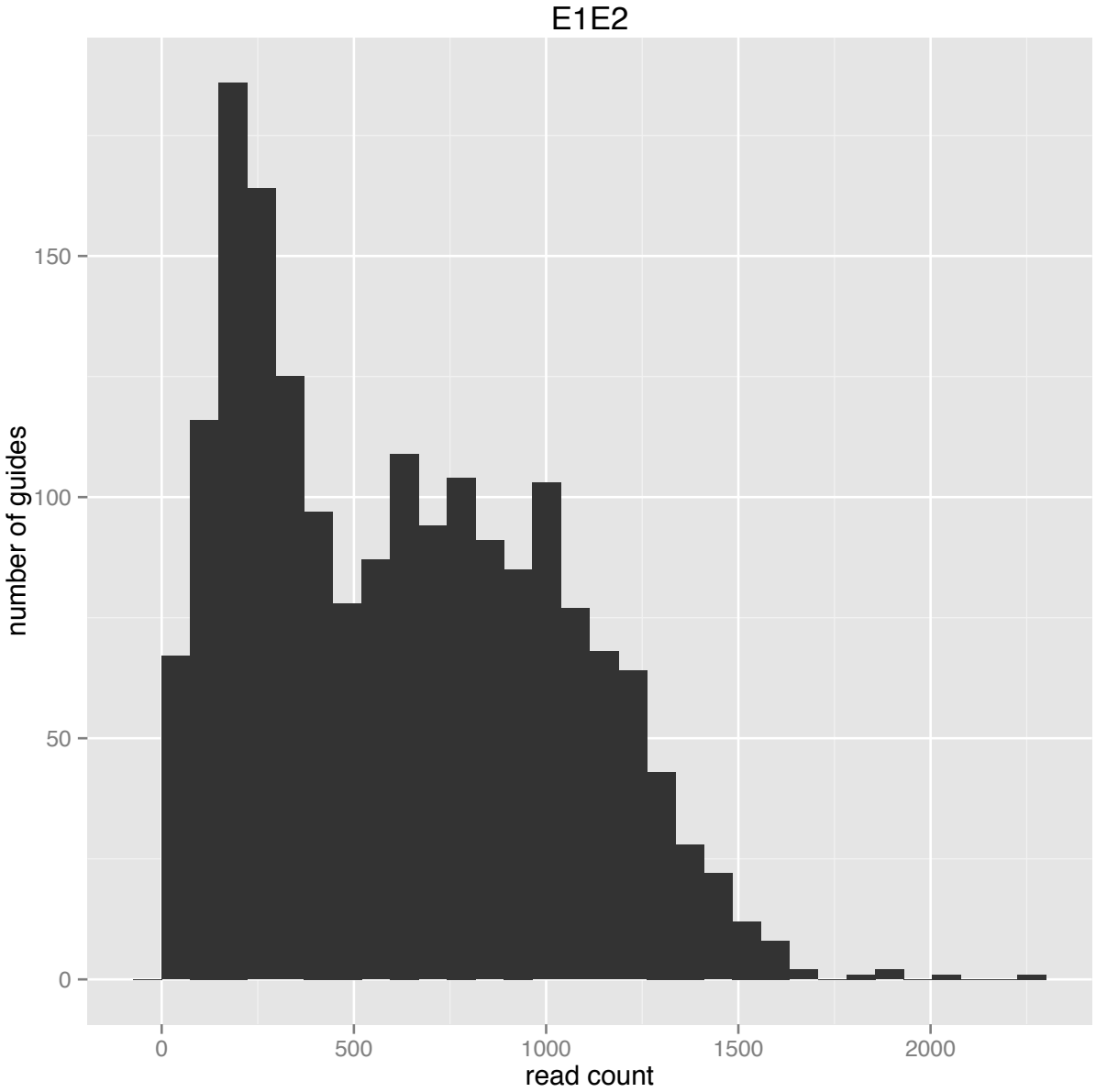

Figure 27: Number of guides and read count for E1 ubiquitin-activating enzymes and E2 ubiquitin-conjugating enzymes sub-library
The above graph depicts the number of sgRNAs in this sub-library that are represented by a given read count. Ideally, this graph would be a perfect normal distribution. However, this sub-library has two peaks. About half the library has guides that are represented at low read counts while another portion of the library is well represented.

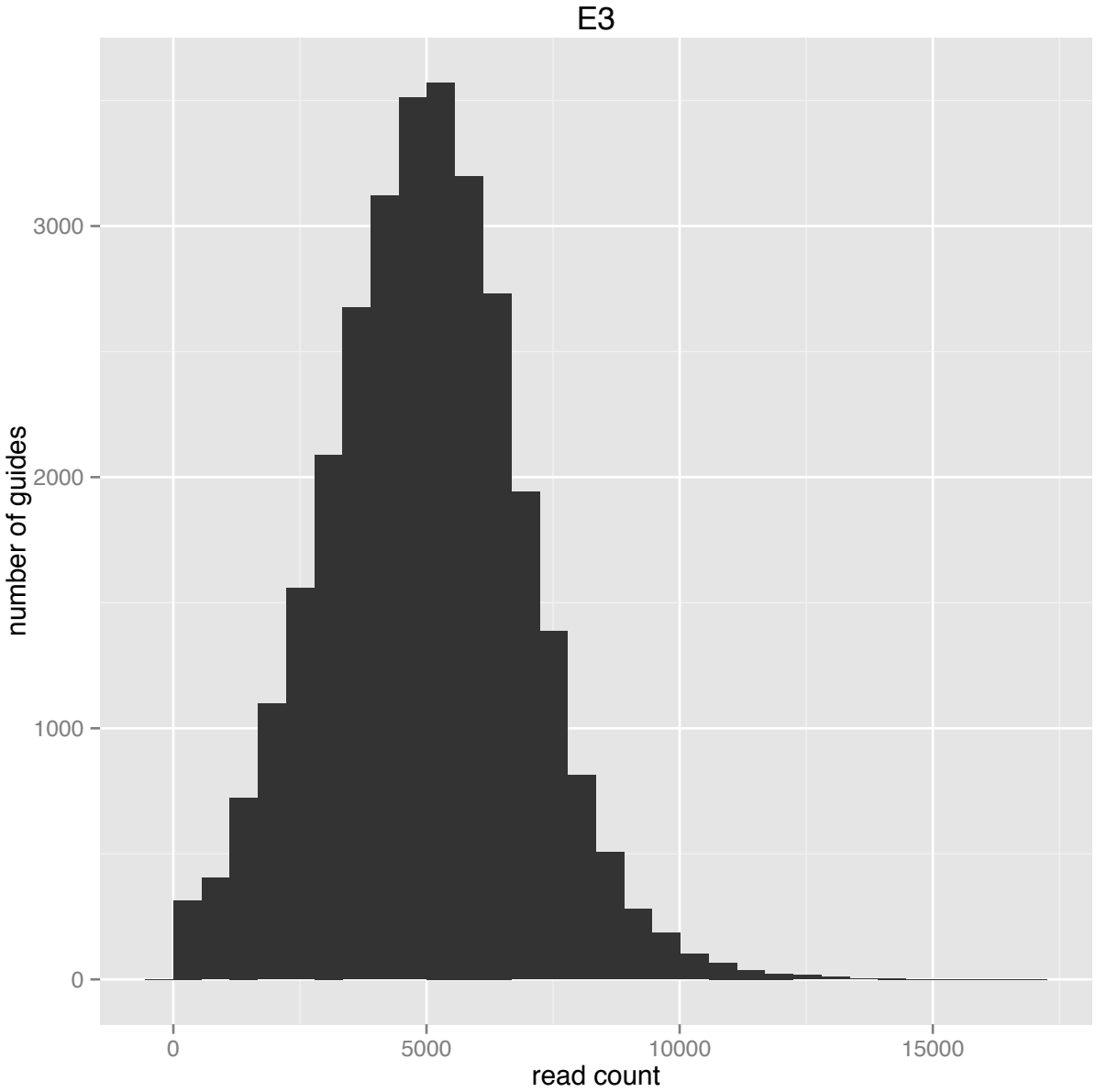

Figure 28: Number of guides and read count for E3 ubiquitin ligase sub-library
The above graph depicts the number of sgRNAs in this sub-library that are represented by a given read count. This sub-library is very close to a normal distribution. Combined with other quality control metrics described above, this sub-library is very high quality.

Appendix 2: Arrayed library to target deubiquitinase proteins active site

Arrayed library screening has long been useful for cell biologists, particularly to observe phenotypic changes via microscopy. Such screening used to be primarily executed by shRNA and siRNAs. With the discovery of CRISPR, there is now a more efficacious and robust way to conduct arrayed screens.

We set out to create an arrayed library targeting the deubiquitinase proteins (DUBs). DUBs remove ubiquitin modification from proteins or organelles within cells. Ubiquitin plays a critical role in cellular homeostasis and DUBs are an integral part of that process. This arrayed library will allow researchers to tackle questions about deubiqutinases and lead to a greater understanding of the important role these enzymes play.

We began by designing two sgRNAs that target the active site of each DUB. We targeted the active site so that these sgRNAs could be used to generate knockout cell lines (where an insertion or deletion is created) or to create a specific point mutation in the active site (by using HDR). For those DUBs where neither of the two initial sgRNAs was efficacious, we ordered subsequent sgRNAs for testing.

Generation of sgRNAs and CasRNP nucleofection was conducted according to the protocol detailed in Chapter 2 Production of CasRNPs for Efficacious Genome Editing.

To determine the best sgRNA for each DUB, we used the T7 endonuclease I assay (T7E1). Briefly, T7E1 works by extracting genomic DNA from the cells of interest, running a PCR with primers that flank the genomic DNA cut site, and re-annealing the PCR fragments. Then, the T7 endonuclease I is added to half of the sample and T7E1 cleaves at mismatched DNA. DNA insertions and deletions (indels) created by CRISPR-Cas9 cutting lead to these eventual mismatched DNA sites. Then you can gain an approximate understanding of CRISRP-Cas9 cleavage with a given sgRNA.

We tested two sgRNAs for all DUBs. For DUBs in which one of the initial sgRNAs was not active, two to four subsequent sgRNAs were tested. The “best” sgRNA was determined as the one that had the most amount of cleaved, smaller DNA fragments in the T7E1 assay. See Figure 29 below for a sample T7E1 assay with select DUBs. As seen in the figure, the sgRNAs work to varying degrees. For future use of the arrayed library, it’s important to keep this in mind and design experiments accordingly.

Effective sgRNAs were determined for all DUBs except three (USP31, USP27X, and USP17L21). The complete list of all sgRNAs is listed in the table below (Table 9) as well as the primers used for the T7E1 assay (Table 10 and Table 11). The sgRNA for each DUB was verified in HEK 293T cells, with the exception of USP9Y. USP9Y is on the Y chromosome, which HEK 293T cells do not have. The sgRNA was verified using A549 cells.

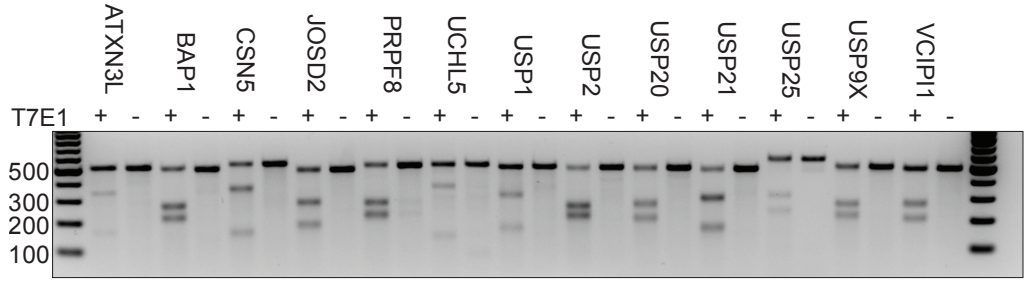

Figure 29: T7E1 assay for select DUB sgRNAs
Agarose gel for select DUBs with and without T7 endonuclease I. The smaller fragments in the lanes with T7E1 show the sgRNA is active, which resulted in indels in the pool of cells.

Table 9: Active sgRNAs that target DUB active sites

DUB	**Best guide**
A20	CTGCATGTAAGACCCAGCAA
AMSH-LP	GCTGTCTTAGCCAAGGCCAT
AMSH	GTCGACACTGGAGAGAAACG
ATXN3L	AGATGTTGTATGCCCAGCTA
ATXN3	ATCAGCTGGATGAGGAGGAG
BAP1	CAGTGAGGGGTGCTGTGTAT
BRCC36	GCCAACCTGTGTGTCTGTCA
CSN5	GCTATGGCTGCTGGCTTTCT
CYLD	AAGGCTTGGAGATAATGATT
JOSD1	TCTACCATGAGAAACAGCGC
JOSD2	CGTGGACAGCACACAGCTCC
MYSM1	ATATCTCGTAAGGAAGGATT
OTUB1	ACTCGTACATCCGCAAGACC
OTUB2	ATCCCCTTTGGTCTTGCGGA
OTUD1	TCTTGCTGACAGCTCGGTAG
OTUD3	GCTTCATGCCAGATCATCCA
OTUD4	GCGGAGCAGGTAATTGCGGG
OTUD5	AGTCTCTGCCTTAGTCCTTA
OTUD6A	CCAGCTGGTCTTGGATGGCG
OTUD6B	CAATGGCTTTATACATACAG
OTUD7A	GACCACCAGTTCAGGCGACC
OTUD7B	GCCCTGTAGAAACAAGATAG
OTULIN	GAGAAACCTCTTCATAGCCC
PRPF8	CTAAGGGTTCCATCTCCTAT
TRABID	ATGACAAGGACTCAGTGCTT

UCHL1	AAGACAAACTGGGATTTGGT
UCHL3	AATAAAGACAAGATGCACTT
UCHL5	CTGATAATGTCTCGCCTAAA
UFSP2	GATGATAGCCATATATGCCC
USP10	CAGTGTCGTTGCAACCCCGT
USP11	GAAGCACGTGTTGCCCAGAT
USP12	AGAGAGAAATTCCCGGTATA
USP13	TCCATGCAGACCAGGGCACG
USP14	GTAAGACTGCAGTCTTTTTT
USP15	CCAAGTTACTTAGGCCACAG
USP16	TGGCAAGGAGAATTCATGGG
USP17L2	AGCAGGTATTTCCCATATTC
USP17L3	AGCAGGTATTTCCCATATTC
USP17L4	AGCAGGTATTTCCCATATTC
USP17L5	AGCAGGTATTTCCCATATTC
USP17L8	AGCAGGTATTTCCCATATTC
USP17L10	AGCAGGTATTTCCCATATTC
USP17L11	AGCAGGTATTTCCCATATTC
USP17L12	AGCAGGTATTTCCCATATTC
USP17L13	AGCAGGTATTTCCCATATTC
USP17L15	AGCAGGTATTTCCCATATTC
USP17L17	AGCAGGTATTTCCCATATTC
USP17L18	AGCAGGTATTTCCCATATTC
USP17L19	AGCAGGTATTTCCCATATTC
USP17L20	AGCAGGTATTTCCCATATTC
USP17L21	no guide
USP17L22	AGCAGGTATTTCCCATATTC
USP17L24	AGCAGGTATTTCCCATATTC
USP17L25	AGCAGGTATTTCCCATATTC
USP17L26	AGCAGGTATTTCCCATATTC
USP17L27	AGCAGGTATTTCCCATATTC
USP17L28	AGCAGGTATTTCCCATATTC
USP17L29	AGCAGGTATTTCCCATATTC
USP17L30	AGCAGGTATTTCCCATATTC
USP18	CTTGTCAACTTCTTTACCCT
USP19	GAACTCCGGGACTTCTTCCA
USP1	CTATCTTAATAGTATACTTC
USP20	TCACGGGCATGAAGAACCTC
USP21	TGAGCAGCACTCGACCTCTT
USP22	TGCGTGGGCTGATCAACCTT
USP24	TGGATAGCAGGTCCAGTTCA

USP25	GGACACCTACAGAAGTTTGG
USP26	GTAAATCATCAGCAAACGAT
USP27X	No guide
USP28	ACCCCAATCCCAATGACTGG
USP29	AATGAGAGTCAAGAGGCACC
USP2	GGTCCCGCATGTAGAGCCTC
USP30	AGTTCACCTCCCAGTACTCC
USP31	No guide
USP32	ATATTACTACAGCTAAGCTT
USP33	ATGCAAAATGACTCAATTTT
USP34	AATCCCATTTATAAGGTGCA
USP35	AGCCCAGAGGAGAGAAGCAA
USP36	TGTGGAGTCCTGCGCCCACG
USP37	TAAAGTATGTTCAGTATAGT
USP38	TCATATAACATGTATTTCCT
USP3	CAGTGGTGCTTCCCTGTAAG
USP41	CCTTGTCAACTTCTTTACCT
USP42	AACAGGTATTGCCCAAATTC
USP43	CCCCATCGCCGGCGGGGAGC
USP44	GTTACACCAGGAGTTACTAT
USP45	CTCTTAATTTATGTAGTCAT
USP46	ACACATTCTCCCGGAATGGA
USP47	TATAATGCATTCCTAAATTC
USP48	AAGTGGCTCCAAGGTTAGTC
USP49	GAGGATGGAGTTCATGTAGC
USP4	ACAGCATCTTGAGGTTTGGG
USP51	CAAGATTGATTAGCCCTCTC
USP5	AGGGCACTACTCACTTCCTC
USP6	Same as USP32 guide
USP7	AAGATCAGTTCAAGGTTGAG
USP8	TATCATCCTGATAACAGTTT
USP9X	GCCCACCCAAAGGATTCGTG
USP9Y	AGAATACTGTTCCTGATAGA
USPL1	AGGAGGAATCTATATTCTGG
VCPIP1	GAGTGTCATGCAAATACAGG
YOD1	CATAGTACACACTAGTAAAG
USP40	TTTAAGCGGAATCAGAAATC
Non-targeting	CGCCAAACGTGCCCTGACGG
Non-targeting	ATGGCAATATGCGTCCCCTA

Table 10: T7E1 forward primers for DUB active sites

DUB	T7E1 PRIMER FORWARD
A20	CCAGGTCACCTAAACTAGTTA
AMSH-LP	AGCAAATTAATTTCCAGCTCT
AMSH	CCTTCAGAGACCAGACTTGGTTGTATGTCAGA
ATXN3L	CCATCAGCTTTTGACTGGATA
ATXN3	TCCTGGCTAACACAGGATGA
BAP1	GGTAGCTACAGAAATCCTCT
BRCC36	GATTCGAGTGATGAAACATCA
CSN5	GATGATTTATATGAAGCAAACTCCA
CYLD	GCAATTTTTATAAGCCAAGTCA
JOSD1	ATTCCAATCTTTTCTCCCAGTGA
JOSD2	GAGCAGAAGAGACAGCGTTT
MYSM1	CAAGTTAAAGGCAACTGTGGT
OTUB1	CTTTAGTGACCCATGCAACT
OTUB2	TGTCTAATTATCCATCTTCCCT
OTUD1	GTGGGGCGAAGAGCACTT
OTUD3	TATCACCGGCTCCACTTG
OTUD4	ATGGAGGCTGCCGTCGGC
OTUD5	CTAAAAGAGTCTCCTACTTCACA
OTUD6A	AGGCCGAGATGGCTCAGAA
OTUD6B	GATGAGTAAGAGAGTAAGGAGCTCACCTTGTAGA
OTUD7A	GTTTCTTAATGCTCATGCTAATTGA
OTUD7B	GTTGTGACATGCAAACATATCTTCAGTCATT
OTULIN	GCCAGTGAGTAAGTGTTAAA
PRPF8	CTCCAACTCTGACCTGGTACTAAGAAGAGT
TRABID	CCGCTTCCTGTTCCAGAAT
UCHL1	AACCTCTCAGAGCCCCACT
UCHL3	CCCATACCTTCACCTTCACT
UCHL5	GGACAAGCTCTGTTGGCTTAATCAGCT
UFSP2	GGAGGCCAGAAGGTAGGT
USP10	GATTAAATGTTGCTATTTGAGGGA
USP11	CCATTAATACCTTTCCTTCTTTCTCT
USP12	CTGGTGACTTTTTCATGTAACGT
USP13	ACCATCACCGTCTCTCAGT
USP14	GGCAAGACTAGTATGATTATTCTCT
USP15	GGAGTATCTTAATTCAGGGTGAGTT
USP16	ATGGGTGGGTGGGTTGGA
USP17L10	ATGGAGGACGACTCACTCTA
USP17L12	GGAGGAAGACTCACTCTACTT
USP17L3	ATGGGGGATGACTCACTCT

USP17L8	ATGGAGGACGACTCACTCTA
USP18	CTTCATGTCCTTAGTAGCTTTAAGA
USP19	GATCTGAGGACACAGGGCT
USP1	GTGGCTTGTTATGTGTAATAATGT
USP20	CCTCTGCTGTATGGTCTGG
USP21	GCATGCTGTTGAAAGGTTAAAGT
USP22	CTGGCCTGTTGTCGTAGAAA
USP24	CACACCTATCTGCCAGGTAT
USP25	GACTATACTTCTCTATGTATTAGCATTGACACTGCTAA
USP26	CAAGAAATCCAAGGCAGATTGT
USP27X	CAACTTAGCAGTAGACCTGTA
USP28	CAGTTGCATTACAGTCTTACAGT
USP29	GATTTAGAAAAAGATAGAGATTTGAAACTCGGGC
USP2	CTGCTCCTCTCCTGGATCAT
USP30	GGAAGAACCAAGCTGTGCT
USP31	TTCAGCAAGCGGCTGTTT
USP32	SAME GUIDE AS USP6
USP33	CACGTAGTCTTAAATGTTAATAGGA
USP34	CTGTAAAAGTAATTTGGGGCCAAGTA
USP35	CTGTTCACACACACCCCA
USP36	GAGCTTTCCAGGAATGTCCT
USP37	GTCATAATGCAGTAGTTCTCAAAGT
USP38	GCCAAGTACTGCCAGTTACT
USP3	GGTGATTTCCTCATAAGCTTTCA
USP40	CAGGGTCACACAGGTAGTTAGGGTCCT
USP41	TGCCCAGAAAGGAGTGCAAT
USP42	CCAGATCATTGAAAATTTCTCATGT
USP43	TGTTCAGCCGCTTCCTGC
USP44	GCAAGAAGAACCATTTCAGGA
USP45	CATCTGCAATTTATTCTGTAATATAGTGTGAGGTG
USP46	CACCAGCAGGTCTCGTTA
USP47	GTTTAAACGTTTAGATTTTGGGGGAAAAAGTTTAT
USP48	CCACTGTTCTAATTTTAGATTTAAGTGG
USP49	GCTCACGGCTCTGTGGTA
USP4	GTAGTGTTTCTTTCCTTAAGGATGT
USP51	GCACCATTTAGCTGTAGACCT
USP5	CCAGAACTTGAACTGGACGAT
USP6	GACATGCTAGAAGAATAATTGTTTGAA
USP7	GTGACAGGAGTGCCACTGT
USP8	GACCTTAGTCGTATGACTAATGTT
USP9X	GGTGATTGGATAAGAAGCTGC

USP9Y	CAGAAGCAGTATCATTAAAAACATCA
USPL1	CCAAAAAGACTAGAAATTATATTGCTATTGACGGT
VCPIP1	GATGGGCCTTTCCAACTATCA
YOD1	CAGTGAACAAAGATTCTTACTGGT

Table 11: T7E1 primers for DUB active sites

DUB	**T7E1 PRIMER REVERSE**
A20	AACCTACCCGAGTATCATAGC
AMSH-LP	GGCGTTGTGTGCTTGCCAAT
AMSH	GAAACACCCAGAACCATGCCCTCTATACT
ATXN3L	GGATTATTGAAATGGATGATCTCT
ATXN3	GTGACTTAGTGAGTTTAAAATCAGT
BAP1	CCTAATAGTACCCAATATCATGTGGT
BRCC36	AACAATCAATATGACATAAATCATTACT
CSN5	GATACCAGAGCAATTTCTCTTTACT
CYLD	AAGGAGTATGTCATAAAAAGCAA
JOSD1	CCTGCTAACGCAATCTAGCT
JOSD2	TGAGCGCGGAGCAGAAGAAA
MYSM1	AAATCCCCAGTATAAAGAATATTAGA
OTUB1	CAGGGCCGAGACAGCACT
OTUB2	CTCTGCCAGGCAGCTCTT
OTUD1	CATTCAGCATCTGCCCCAT
OTUD3	TACCCAATGCATTACTCCTGA
OTUD4	GGAAGGTGAATGCGGAACAA
OTUD5	GTGTCCCAAAGGATATTATTTTCT
OTUD6A	CGTGGTGCGCACGATGTT
OTUD6B	CGCTCAGTGCTGGGAAGCACCT
OTUD7A	TACTTGACAAGAAGGGCCA
OTUD7B	CTAGCAAAGGTAGGGCTCACTCCC
OTULIN	GGTCATTTAACTATGTGAAATCACC
PRPF8	GAGGAACGAGGACAGAGTAACAGCT
TRABID	CCCACCACTACAAGGAAATAAT
UCHL1	GGACTGTGAGTCAGATTAAGTGT
UCHL3	CTTCTAACAGTATATACATTCCCAT
UCHL5	GCTCAGTGCCAAGCCTTTCATCTAAAAT
UFSP2	CAGAAATAAGTCTGCACCATGA
USP10	GGAGATGGACTGGGGTCA
USP11	GAGGCTGATAGTTCAGGAATGA
USP12	GTCATTAATACAGTGGGAAGTAGAA
USP13	CCAGTCTCTGTAGAAGGCA
USP14	AAGCATTAAACACTTTAAAATGCTGA

USP15	GAGAAACATATATTCCACTACCAGT
USP16	CTCAATAATGTAAGTAGCAGATTCTAT
USP17L10	CCTTTCTCATGGCATCCACA
USP17L12	GAACATGAGAAATTCATGGGCA
USP17L3	CATGGCATCCACAGTGAACA
USP17L8	GAACATGAGAAATTCATGGGCA
USP18	CCTGGTGAAGTCCACATTCA
USP19	CACCAGTCCCTAGTGGGTT
USP1	CTCTTACCCCAAAGGAAGTT
USP20	CATTCTGACTGGGAGGATTG
USP21	CAGTGGCAGATGGACCTG
USP22	AACAGAAATGTTCCCCTGCA
USP24	CTTTACACATTTCAGGAGCTACT
USP25	GTGAAAGGCATAAGTAGTGATCTACTGTTAAAAAATACA
USP26	CAGCTGCTGAAATGGCCTT
USP27X	GTATCCACACCAGGTGCA
USP28	GTACTGCCCAACTTAGACATCA
USP29	GCATTTGTGGAGATGAATTTTCATCCC
USP2	GTCTAAGACACAACACCTAGAACA
USP30	CTCTGTCATCTGGACTTCTTTGAA
USP31	AGGTGCGCCAGCTGCTCA
USP32	SAME GUIDE AS USP6
USP33	CTACGGGTATACATAGAGTAACAT
USP34	CTGTACTACAGCATTATGAGTAATCTACTAAAATGTATAACTAT
USP35	CCAGTCCTGACCTGCCTT
USP36	CATCAGTTACTATACATTATGAACTACCCT
USP37	GGCACAGAAAATTTTTGAGTGT
USP38	CTGAGCACTAAAAGCAGTTTCATT
USP3	GGTAGGAACTACTGTCCCCA
USP40	CCAATTTATATCTTATATGTGCAACAATAAACACATACTGTA
USP41	ATCAGCCTGAAGAACAGTCTT
USP42	CCAACTTCTTAGTAATCATAGCACT
USP43	CCTTTCCTGATCGTGCACACA
USP44	CTGTATCTTTTTCCTGACATTCATT
USP45	CCCTGTGTGAAAATAAGGTACATGTATACATATGG
USP46	CTCAGCCTTGAAATGAACTTCT
USP47	GTTATATCTTATGGTGTGAGAAATGCCCCAAA
USP48	CTTGGGAAACAGAGGAAGACT
USP49	GCCGAGCTGTTGGTTGGCTT
USP4	GAAGCCATTCTATACCACCTAGT

USP51	CTGCATGGATCCATATCAGAT
USP5	CAACACACCCAGCCGATA
USP6	GATGTATTCCTTGGCCTATTTCA
USP7	CCAGCACTGGGGAATGAAA
USP8	GCAGCAGAAAACTAATGGACTA
USP9X	CTTAAGAGAGAATAGTATCTGGTATCA
USP9Y	CATGAAAGTATAGTAATCTGAGGGA
USPL1	CAGAATGAGACCCTGACTCCAGATGAA
VCPIP1	CCTCAGGTGGTACAAACAGA
YOD1	AAAATCGATATCTCTATTGCTCCT